



Norwegian University of  
Science and Technology

# CFD Study of a 10 MW Offshore Horizontal Axis Wind Turbine Blade

Jørgen Jensen Tande

Physics

Submission date: May 2011

Supervisor: Jon Andreas Støvneng, IFY

Co-supervisor: Ole Gunnar Dahlhaug, Institutt for Energi- og  
prosesseteknikk







(Photo taken by the author from *La Totoral* wind park, Chile, showing a 2.1 GW wind turbine. Blade length: 43 m.)

## Sammendrag

Denne masteroppgaven er et studie av vindturbin aerodynamikk på et 10 MW havvindturbin blad med en Computational Fluid Dynamics, CFD, tilnærming.

Målene for oppgaven var, (i) lage en Computer Aided Design, CAD, modell fra et sett med koordinater gitt av PhD kandidat Lars Frøyd av et blad som er tilnærmet 70 m langt og designet for en 10 MW havvindturbin, (ii) lage et mesh (et sett av gridpunkter) rundt bladet slik at CFD programmet kan regne på det, (iii) validere ytelsen av rotoren i oppgaven på bakgrunn av tidligere gjennomførte vindturbinsimuleringer utført av CFD og blad element metoden, (iv) lage retningslinjer for tegning av turbinbladet, beskrive meshe prosessen og hvordan man starter CFD simuleringer.

Den første oppgaven var vellykket mens andre og tredje målet viste seg og være mer krevende enn først antatt. Mange mesh ble laget i ANSYS 12.1 og flere valideringsmetoder ble utprøvd. For hvert mesh og hvert valideringsforsøk ble ny viten tilegnet i den krevende prosessen det er og kjøre fluidstrøm analyserende programvare. For å sikre at resultatene oppnådd var fysisk korrekte og validerte ble tre ulike metoder testet. Siden ingen av valideringsmetodene var vellykkede, var ikke CFD resultatene for den 10 MW store havvindturbinen mulig å validere. I vedleggene fines retningslinjene for hvordan man tegner en CAD model av et vindtturbinblad.

Resultatene i denne masteroppgaven kan sees på som en grunnpillars for videre CFD simuleringer på havvindturbinbladet. Forslag for videre strategier av CFD simuleringer på vindturbinbladet er foreslått.

## **Abstract**

This Master thesis is a study of wind turbine aerodynamics on a 10 MW offshore wind turbine blade with a Computational Fluid Dynamics, CFD, approach.

The objectives for the thesis were, (i) make a Computer Aided Design, CAD, model out of a set of coordinates given by PhD candidate Lars Frøyd of a blade of approximately 70 m length and designed for a 10 MW Offshore Wind Turbine, (ii) develop a mesh (a set of grid points) surrounding the blade so that CFD calculations can be performed on the blade, (iii) validate performance of the rotor in question by previously performed wind turbine CFD calculations and Blade Element Method results for the rotor in question, (iv) develop a guideline for drawing a CAD model of the blade, describing the procedure for meshing and how to run CFD calculations.

The first task was successfully completed while the second and third task proved to be more demanding than anticipated. Many meshes were made in ANSYS 12.1 and several validation methods were attempted. For each mesh and validation attempt, new insight was gained in the complexity of fluid flow analysis software. In order to secure that the results obtained are physically correct and viable for the 10 MW wind turbine blade three validation methods were attempted. Because none of the validation methods were successful, the CFD results for the 10 MW offshore wind turbine blade was not possible to validate. In the appendix the guidelines on how to draw a CAD model of a wind turbine blade is described.

The results of the thesis present makes a ground pillar for further CFD simulations on the blade of a wind turbine. Suggestions for further strategies of CFD calculations on the wind turbine blade are suggested.

# Acknowledgements

I would like to thank Prof. Ole Gunnar Dahlhaug for giving me the opportunity to write a Master thesis on the subject closest to my heart, green energy.

I had invaluable software help from many people, amongst them thanks needs to be given to Kari Haugan at DynaVec, Trondheim, for answering many CFD questions, especially in the meshing process. Both the scientific assistant at the Water Power Laboratory of NTNU, Bjørn Winther Solemslie, and PhD candidate Celine Faudot deserves great gratitude. PhD candidate Lars Frøyd also needs thanks for answering any question I might have had about wind energy and letting me play around with his wind turbine blade in Pro Engineer and CFD. Dr. Olimpo from the University of Strathclyde in Scotland, MSc Thomas Hansen from the Institute of Technology in Stockholm, Phd Carlo Enrico Carcangiu from the University of Cagliari in Italy, Prof. Niels N. Sørensen from the Technical University of Denmark, Pricipal Engineer Scott Schreck from National Research Energy Laboratory in th US, Ansys support in Norway, EDR, and Pro Engineer support in Norway, EDR-PLM, also deserves to be mentioned since they have answered many a question.

Finally, I would like to thank my girlfriend, Magdalena, for being so patient with me this whole year when much of my time and many weekends have been spent by my desk at the University.

# Contents

<b>Sammendrag</b> .....	<b>III</b>
<b>Abstract</b> .....	<b>IV</b>
<b>Acknowledgements</b> .....	<b>V</b>
<b>1. Introduction</b> .....	<b>1</b>
1.1. A Brief History of Wind Energy .....	1
1.2. Potential and limitations .....	1
1.3. World Wide Energy Report 2010 .....	2
1.4. Size of wind turbine .....	3
1.5. Motivation and objectives of the thesis .....	4
1.6. Overview of the thesis .....	5
<b>2. State of the art</b> .....	<b>6</b>
2.1. NREL Ames Phase VI Experiment .....	6
2.2. Development and Validation of a CFD Technique for the Aerodynamic Analysis of HAWT .....	7
2.3. CFD-RANS Study of Horizontal Axis Wind Turbines .....	8
2.4. Wind Turbine Simulations Using Navier-Stokes CFD by Thomas Hansen .....	8
2.5. Tidal Turbine Loads: Design and dynamic loads estimation using CFD and Blade Element Momentum Theory [22] .....	9
<b>3. Verification and validation of the CFD calculations</b> .....	<b>10</b>
<b>4. Wind turbines</b> .....	<b>11</b>
4.1. General overview of a Horizontal Axis Wind Turbine .....	11
4.1.1. <i>Power and location</i> .....	11
4.1.2. <i>Power coefficient</i> .....	14
4.1.3. <i>Campbell Diagrams</i> .....	15
4.2. Airfoil theory .....	16
4.3. Functioning of HAWT and Control Systems .....	20
4.3.1. <i>Torque control</i> .....	21
4.3.2. <i>Pitch control</i> .....	23
4.3.3. <i>Stall regulated turbines</i> .....	24
4.3.4. <i>Variable speed operation</i> .....	24
4.4. Dimensionless parameters .....	25



4.4.1.	<i>Reynolds number</i> .....	25
4.5.	Turbulence intensity .....	25
4.6.	Blade Element Method, BEM .....	28
<b>5.</b>	<b>CFD analysis</b> .....	<b>31</b>
5.1.	Fundamental equations .....	31
5.1.1.	<i>Navier Stokes</i> .....	31
5.2.	Turbulence modeling .....	32
5.2.1.	<i>Reynold Averaged Navier Stokes equations (RANS)</i> .....	33
5.2.3.	<i>SST k-<math>\omega</math> model</i> .....	35
5.3.	Boundary layer theory .....	36
5.3.1.	<i>Turbulent Boundary Layer and Near Surface Modeling</i> .....	38
5.3.2.	<i>Near wall meshing</i> .....	40
5.3.3.	<i>Automated near-wall treatment for <math>\omega</math> – based models [42].</i> .....	40
5.3.4.	<i>How to determine a target <math>y^+</math> in the CFX 12.1 mesher</i> .....	41
5.4.	Discretization schemes .....	42
5.5.	Meshing .....	43
5.6.	Test cases .....	44
5.6.1.	<i>Grid construction</i> .....	47
5.6.2.	<i>Grid quality</i> .....	49
<b>6.</b>	<b>Method</b> .....	<b>51</b>
6.1.	Wind turbine simulations/setup .....	51
<b>7.</b>	<b>Results and discussion</b> .....	<b>53</b>
7.1.	Validation .....	53
7.2.	Validation runs .....	55
7.2.1.	<i>Grid Quality case 3</i> .....	62
7.2.2.	<i>Grid Quality case 1</i> .....	64
<b>8.</b>	<b>Further strategy</b> .....	<b>67</b>
<b>9.</b>	<b>References</b> .....	<b>69</b>
A.1.	Appendix From Matlab through Pro Engineering .....	1
A.1.1.	<i>Introduction</i> .....	1

<i>A.1.2. From Matlab to Pro Engineering</i> .....	1
<i>A.1.3. How to draw the object in Pro Engineer</i> .....	3
<i>A.1.4. Accuracy and units</i> .....	3
<i>A.1.5. How to connect points</i> .....	3
<i>A.1.6. Tangency for two meeting lines</i> .....	5
<i>A.1.7. Splitting lines using "Trim tool"</i> .....	6
<i>A.1.8. Boundary blend</i> .....	6
<i>A.1.9. Solid ends</i> .....	7
<i>A.1.10. Merge</i> .....	8
<i>A.1.11. Smoothing of surfaces</i> .....	9
<i>A.1.12. Solidify</i> .....	9
<i>A.1.13. Cutting of sharp edges</i> .....	9
<i>A.1.14. Making the cake</i> .....	11
<i>A.1.15. Assembling cake and blade</i> .....	13
<i>A.1.16. Tunnel</i> .....	14
<b>A.2. Appendix From Pro Engineer to CFX</b> .....	16
<i>A.2.1. Workflow in a CFX analysis</i> .....	16
<i>A.2.2. Importing objects to ANSYS from ProE</i> .....	16
<i>A.2.3. Installing quick buttons in your work window</i> .....	16
<i>A.2.4. Regions</i> .....	18
<i>A.2.5. Face spacing and Edge spacing</i> .....	20
<i>A.2.6. Inflation</i> .....	22
<i>A.2.7. Meshing the tunnel</i> .....	22
<i>A.2.8. Sweep</i> .....	22
<i>A.2.9. Edge sizing</i> .....	23
<i>A.2.10. CFX Pre</i> .....	24
<i>A.2.11. Rotor Domain – tidal turbin</i> .....	25

<i>A.2.12. Rotor Domain – wind turbine</i> .....	25
<i>A.2.13. Stator Domain – tidal turbine</i> .....	25
<i>A.2.14. Stator domain – wind turbine</i> .....	25
<i>A.2.15. Inlet and Outlet</i> .....	25
<i>A.2.16. Domain Interface</i> .....	26
<i>A.2.17. Periodicity, only in the rotational run</i> .....	27
<i>A.2.18. The run</i> .....	27
<i>A.2.19. Post Processing</i> .....	28
A.3. Appendix, Different formulas used in the thesis .....	29

## Figures

Figure 1: Size evolution of wind turbines over time [8] .....	4
Figure 2: NREL Ames Phase VI Experiments wind turbine [13].....	6
Figure 3: Pressure transducer distribution on the airfoil, upper part of figure, and span wise placement of the pressure transducers on blade, lower part of figure [13]. .....	7
Figure 4: Wind Turbine with the basic elements marked [26].....	11
Figure 5: Weibull distribution in red and energy in wind in blue [25]. .....	13
Figure 6: Vertical view of a HAWT [25]. .....	13
Figure 7: Power coefficient vs tip speed ratio [29]. .....	15
Figure 8: Example of a Campbell diagram for a wind turbine [2].....	16
Figure 9: Airfoil. ....	16
Figure 10: Vortices superimposed on a uniform flow.....	17
Figure 11: Airfoil with different parameters. ....	18
Figure 12: Optimal torque curve [23]. ....	21
Figure 13: A simple scheme of a DFIG wind turbine [24]. ....	22
Figure 14: Torque-slip curves showing the effect of rotor circuit resistance [23].....	22
Figure 15: 90-percentiles of measured turbulence depending on wind speed at different heights compared to turbulence intensity given by the International Design Standard for Offshore Wind Turbines IEC 61400-3, [34]. ....	27
Figure 16: Research platform FINO1.....	27
Figure 17: Boundary layer at a flat plate at zero incidence, [52]. .....	37
Figure 18: Displacement thickness, [52]. .....	37
Figure 19: The three sub divisions of the <i>near wall region</i> [42]. .....	38
Figure 20: A detailed description of the three regions of the near wall region [41]. .....	39
Figure 21: Difference between cell centered- and vertex centered scheme [53]. ....	42
Figure 22: 3D shapes which a grid can contain [54]. .....	43
Figure 23: This figure shows the different entities associated with the grid [54]. .....	44
Figure 24: The blade for the 10 MW wind turbine. The blade to the right shows the pressure side, e.g. underside of the blade. ....	44

Figure 25: The cake in case 1 with the carved out 10 MW blade highlighted.....	44
Figure 26: The tunnel in case 1 resembling the surrounding of the wind turbine.....	45
Figure 27: Short blade, case 2, medium blade, case 3, large blade, case 1.....	45
Figure 28: Tunnel for the tidal turbine.....	47
Figure 29: Example of how the blade in case 1 is divided into regions.....	48
Figure 30: Close up of blade in case 1 with regions marked.....	48
Figure 31: Here the difference between in size of the surface mesh on the LE and the surface mesh on the suction side is visible.....	49
Figure 32: Example of <i>Expansion Factor</i> [55].....	50
Figure 33: Example of <i>Aspect Ratio</i> [55].....	50
Figure 34: Example of <i>Orthogonality</i> [55].....	50
Figure 35: Different regions of stator in case 3.....	51
Figure 36: Different regions of rotor in case 3.....	52
Figure 37: Reynolds number as a function of relative blade length for case 1 and case 3.....	55
Figure 38: Angle of attack from CFD and BEM.....	57
Figure 39: Streamlines for 10 MW wind turbine run a, suction side of blade.....	58
Figure 40: Streamlines of rated power for 1 MW tidal turbine.....	62

## **Tables**

Table 1: Turbulence intensity at different wind speeds 90 m above sea level.....	28
Table 2: List of RANS turbulence models sorted by number of additional transport equations, [41]. .....	34
Table 3: This table shows the dimensions of the different parts of each case. ....	46
Table 4: Different interfaces in stator and rotor. ....	52
Table 5: Parameters for the inflation layers of case 1 run a and run b. ....	58
Table 6: Meshes used in run a (mesh 1) and run b (mesh 2) of case 1. ....	59
Table 7: Inflation parameters for case 3. ....	60
Table 8: Tunnel dimensions case 3. ....	60
Table 9: The different meshes tested in case 3. ....	61
Table 10: Mesh statistics for case 3. ....	63
Table 11: Mesh statistics for case 1 run a. ....	65
Table 12: Mesh statistics for case 1 run b. ....	66

## Nomenclature

$C_p$	power coefficient [-]
$C_D$	drag coefficient [-]
$C_L$	lift coefficient [-]
$F_D$	drag force [N]
$F_L$	lift force [N]
$g$	acceleration of gravity [ $\text{m}\cdot\text{s}^{-2}$ ]
$Q$	shaft torque [Nm]
$T$	thrust force on the rotor [N]
$TSR$	tip speed ratio [-]
$U_\infty$	incoming velocity [ $\text{m}\cdot\text{s}^{-1}$ ]
$U_{rel}$	relative velocity [ $\text{m}\cdot\text{s}^{-1}$ ]
$\alpha$	angle of attack [rd]
$\varphi$	flow angle [rd]
$\theta$	twist angle [rd]
$\rho$	air density [ $\text{kg}\cdot\text{m}^{-3}$ ]

# 1. Introduction

## 1.1. A Brief History of Wind Energy

The energy of the wind has been utilized since early recorded history all across the world. There are certain proofs that wind energy propelled boats along the river Nile around 5000 B.C. The Europeans got the idea of using wind power from the Persians who introduced it into the Roman Empire by 250 A.D. However, the first practical windmills were made in Afghanistan around 7<sup>th</sup> century of our era. Since then, technology has been improving so by the end of the 11<sup>th</sup> century people in the Middle East were using windmills extensively for food production. Returning merchants and crusaders carried this idea back to Europe where the Dutch refined the windmill and adapted it for draining lakes and marshes in the 1300's.

One of the first larger windmills was built in Scotland in 1887 by Professor James Blyth from Glasgow. Blyth's 10 m high, cloth-sailed wind turbine was installed in the garden of his holiday cottage and was used to charge accumulators that powered the lighting in the cottage electricity. The industrialization led to a gradual decline in the use of wind for such purposes. In Denmark, wind power has played an important role since the first quarter of the 20<sup>th</sup> century. In 1956 a 24 m diameter wind turbine was installed at Gedser, where it ran until 1967. This was a three bladed, horizontal axis, upwind, stall regulated turbine similar to those used nowadays for commercial wind energy development.

The popularity of using wind energy has always fluctuated with the price of fossil fuels. When fuel prices fell in the late 1940's, interest in wind generators decreased. But when the price of oil went up in the 1970's the worldwide interest in wind turbine generators went up again. These first three parts in this chapter is derived from [1] and [2].

## 1.2. Potential and limitations

One of the main advantages of wind energy is that it is renewable and clean. Using wind energy means less smog, less acid rain and fewer green house gas emissions. This in turn benefits society, both healthcare and environmental costs will be reduced. Since the fuel (wind) is free, it can generate a stable long term price for power production than any other conventional power plant such as coal or gas driven power plants.

The cost of producing wind energy has been reduced by 80% since the 1980s. The more wind turbines that are made and the more governments invest in this area, the more the prices will drop. One other advantage of wind energy is that it is readily available around the globe, and therefore many countries that are today dependent on energy import, might be able to minimize this import.

However, one of the main disadvantages with wind turbines is that they are susceptible to a varying wind regime. For this reason one cannot use wind directly as a dependable source of base load power. Cities, where the energy is most needed, tend to have less wind than open land or sea because the buildings deflect wind and also because many cities have been built in



areas of more stable weather. If wind turbines were moved offshore one could produce more electricity and also achieve a more stable power generation due to the fact that the wind is both stronger and more stable offshore compared to onshore. This would result in longer distances for the transmission of electricity, but large efforts are being made internationally, especially at Dogger Bank, a shallow area off the east coast of England, to build offshore windmill parks [3]. So it would seem that the possibility of higher and more stable wind overcomes the drawbacks of having to transport the electricity over a larger distance.

There is also something called “Smart Grids” that researchers have their eye on nowadays. This is the electrical grid of tomorrow making it possible for both the consumer and the power plant to communicate [4]. Today’s grid generally “broadcasts” electricity from a few central power generators to a large number of users. One of the ideas behind “Smart Grids” are that they should be more capable of routing power in better ways to respond to a very wide range of conditions. This means that “Smart Grids” should be able to respond to for example clouds blocking the sun or the wind not blowing. Or if consumers turn off their lights to save money during peak hours, the grid should be able to track this and reroute power elsewhere. Combining this with going offshore to more steady winds this could help the implementations of wind energy to the base load power.

Other limitations is that one cannot get more than about 59% of the power available in the wind; this will be explained in more detail in chapter 4.1.2. Bird mortality are also an environmental factor that has obtained some attention. This sets limitations as to where one can place a windmill park. This problem can be circumvented to some degree by placing the windmills offshore and away from certain birds’ migrating path. But then by placing windmills at sea it will affect the fisheries. But there are no sources of energy that comes without any disadvantages. In this aspect wind energy is one of the best alternatives today.

### **1.3. World Wide Energy Report 2010**

How much installed wind power capacity does the earth have today? In this section some key elements from the World Wide Energy Report 2010, [5], prepared by The World Wind Energy Association (WWEA), will be presented. The WWEA is a non-profit organization which works for a world energy system fully based on the various renewable energy technologies, with wind energy as one of the cornerstone. WWEA acts as a communication platform for all wind energy actors worldwide. The organization also advises national governments and international organizations on favorable policies for wind energy implementation.

Key elements from their report from the 10<sup>th</sup> World Wind Energy Conference and Renewable Energy Exhibition in Cairo, Egypt from the 31<sup>st</sup> of October to the 2<sup>nd</sup> of November 2010:

- As of 2010 the world wide wind capacity reached 197 GW with a slight decrease in new capacity.
- China has become the world leader in installed wind energy, installing 18.9 GW, more than 50% of the world market.

- Of the total world capacity of 197 GW installed wind power, 37 GW was added in 2010, slightly less than in 2009.
- Wind power showed a growth rate of 23.6%, the lowest growth since 2004 and the second lowest the past decade. One of the likely causes of this was the aftermath of the global economical recession.
- All wind turbines installed by the end of 2010 worldwide can generate 430 Terrawatthours per annum, more than the total electricity demand of the United Kingdom, the sixth largest economy of the world and equaling 2.5% of the global electricity consumption.
- Many Western European countries stagnation in installation of wind turbines, whereas there is a strong growth in this area in Eastern European countries.
- Germany keeps its number one position in Europe with 27215 MW of installed effect, followed by Spain with 20676 MW.
- The highest shares of wind power can be found in three European countries: Denmark (21%), Portugal (18%) and Spain (16%).
- Asia accounted for the largest share of new installations (54.6%) followed by Europe (27%).
- Latin America (1.2%) and Africa (0.4%) still played only a marginal role in new installations.
- WWEA sees a global capacity of 600'000 MW, 600 GW, as possible by the year 2015 and more than 1500 GW by the year 2020.

#### **1.4. Size of wind turbine**

The issue of what size of turbine produces energy at minimum cost has been debated for a long time. Spokesmen for large machines cite economics of scale and the increase in wind speed with height in their favor [6]. Opponents of this camp think about the “square-cube law”, whereby energy capture increases as the square of the diameter while rotor mass increases with the cube and thus is governing the costs. In reality, both arguments are correct, and there is a trade-off between economies of scale and a variant of the “square-cube law” which takes into account the wind shear effect. This trade-off can be examined with the help of simple cost modeling, but this will not be considered in this thesis. Further information on this subject can be found in *Wind Energy Handbook*, [6].

The European Wind Energy Association, EWEA, has the opinion that 20 MW wind turbines are technically feasible and could be the most cost efficient option for expanding Europe’s offshore wind energy capacity. This is according to the recently published results of “UpWind”, the largest EU-funded wind energy project ever, [7]. Today one can find offshore wind turbines up to 6 MW. Although there is a clear desire to build 20 MW turbines, one should rather do a stepwise scale-up in order to understand what is feasible with today’s technology and what needs to be improved in order to build a wind turbine of this magnitude. A very problematic area even on turbines of today’s size is the large weight of the nacelle at the top of the turbine. For a 20 MW turbine this weight would be immense, so new technology will be needed to keep this weight at a reasonable level.

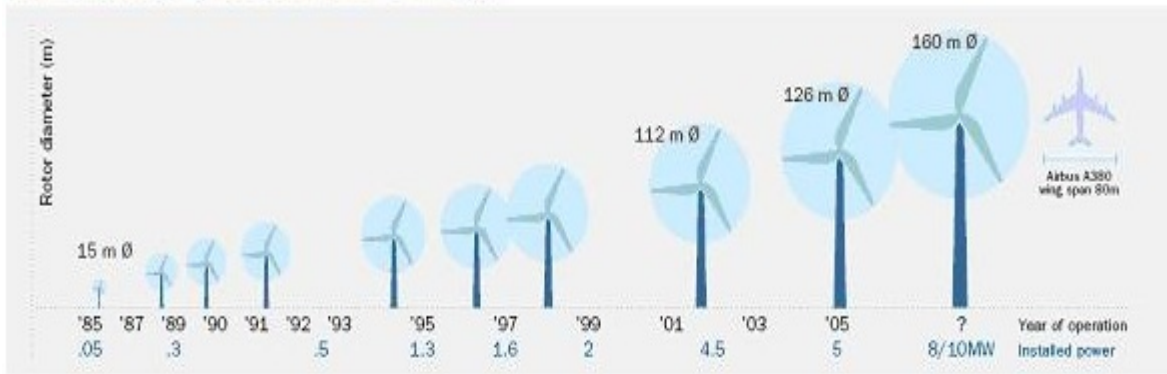


**Figure 1: Size evolution of wind turbines over time [8]**

The aerodynamic research for wind turbines has made a substantial contribution to the fast development of modern wind energy, being the exploring techniques rather primitive just a few decades ago. Although wind turbines are green energy machines and benefits humanity in many ways, they have met quite a lot of resistance from local communities which do not want them in their backyard because of noise issues and claims of them polluting the scenery. Actually has quite a few windmill projects stopped in the early planning phases due to resistance from the local community. To circumvent problems like this considerable research effort is now being made into moving the wind turbines offshore. Here one can make larger turbines because of higher wind speeds offshore and without worrying about noise or any scenery pollution. It looks like the future for wind turbines lies at the sea, where size only is determined by what's actually physical and structurally feasible. Other benefits of moving the wind turbines offshore are that the wind is less affected by the surrounding terrain and therefore will have a more uniform velocity profile than a wind turbine onshore would have.

### **1.5. Motivation and objectives of the thesis**

According to [9] if the earth was to have a network of land based 2.5 MW turbines restricted to non-forested, ice-free, non-urban areas operating at as little as 20% of their rated capacity, they could supply >40 times the current worldwide consumption of electricity and >5 times total global use of energy in all forms. So the access of wind energy is large, but how do we tap into this resources in a more extensive way? One way of doing this is making larger wind turbines and taking them offshore.

To make wind power economically feasible, it is important to maximize the efficiency of converting wind energy into mechanical energy. Among the different aspects involved rotor dynamics is a key determinant for achieving this goal. Today's increase in diameter of modern Horizontal Axis Wind Turbine, HAWT, mainly for offshore use can tolerate higher tip speeds due to lesser noise restrictions. As a result, flow compressibility near the tip may affect their performance and, in addition, machines may now operate closer to stall, [10]. For this reason, accurate Computational Fluid Dynamics, CFD, methods are necessary and several works documenting the applications of CFD for wind turbine appear frequently in literature. For these large diameter machines, the flow near the tip is further accelerated over the suction side and can raise mildly compressible conditions of local Mach numbers approaching 0.4 for an 80 m/s tip speed; this may result in poorer performing wind turbines.

The objectives for this Master Thesis are:

- i. Firstly make a Computer Aided Design, CAD, model out of a set of coordinates given by PhD candidate Lars Frøyd to fit a blade of approximately 70 m length and designed for a 10 MW Offshore Wind Turbine.
- ii. Secondly, develop a mesh (a set of grid points) surrounding the blade so that CFD calculations can be performed on the blade.
- iii. Thirdly, validate performance of the rotor in question by previously performed wind turbine CFD calculations and Blade Element Method, BEM, results for the rotor in question.
- iv. Fourthly, develop a guideline for drawing a CAD model of the blade, describing the procedure for meshing and how to run CFD calculations.

## **1.6. Overview of the thesis**

This Master thesis consists of 8 main chapters. The first chapter gives a short introduction on where wind energy stands today along with potential, limitations and other general aspects of wind energy. The second chapter consists of how far CFD analyses on wind turbines have come today. A short presentation of issues concerning the verification and validation of CFD calculations will then follow in chapter three. Many aspects concerning wind turbine technology will be presented in chapter 4 along with how the blade element method works. This method forms the basis of the making of the wind turbine blade used in the present thesis. In chapter five some background theory for CFD is given, along with boundary layer theory and grid construction. The simulation setup is presented in chapter six. Grid quality and validation methods are discussed in chapter seven. Finally some further strategies are given in chapter eight.

## 2. State of the art

Three approaches are available to analyze the flow around a wind turbine. Firstly, field or wind tunnel testing provides accurate results but is highly complex, expensive and cannot be applied for the large wind turbines available today. Secondly, analytical and semi-empirical models exist, which adopt simplifying assumptions and are thus not universally reliable. Thirdly, CFD probably offers the best support or alternative to direct measurements [11] and it is CFD measurements of the rotor blades of a 10 MW Offshore Wind Turbine that are the preferred approach.

During the past decade there has been a substantial amount of papers published on the basis of a wind turbine experiment in the largest wind tunnel in the world, namely the NREL Ames Phase VI Experiments in the U.S. This experiment was finished on the 17th of May in the year 2000. There has been a more recent and equally large experiment performed in Europe called The MEXICO Project, this experiment finished late 2006. The MEXICO Project focused more on the wake behind the turbine than the former experiment that had its focus on the flow over the rotor and the turbine itself and the loads the turbine experienced. Because the NREL experiment took place some years before the MEXICO Project, there has been many more papers published based on data from the NREL experiments.

In the following the most updated base of knowledge with regard to validation are being outlined.

### 2.1. NREL Ames Phase VI Experiment

The turbine used for the NREL Phase VI experiments is a double bladed, 10 meters in diameter, stall regulated turbine with a power rating of about 20 kW. The wind tunnel experiment setup is shown in Figure 2. The twisted and tapered blades are optimized by P. Giguère and M. Selig at the department of Aeronautical and Astronautical Engineering at the University of Illinois [12]. The turbine is extensively instrumented and both aerodynamic and aeroelastic measurements are available from the large database of tested configurations. Tests were made both upwind and downwind, parked experiments and wake measurements were also performed.



**Figure 2: NREL Ames Phase VI Experiments wind turbine [13].**

The NASA Ames wind tunnel is a 24.4 by 36.6 meter wind tunnel. This tunnel is known as the largest wind tunnel in the world and it is powered by six 18.000 horse power fans capable of producing wind velocities of up to 50 m/s [14]. The S sequence is considered to be the cleanest configuration during the test campaign and extra equipment like flow probes was dismantled and sealed. Here, the turbine is run in an upwind configuration with 0° cone angle, the rotor is rotated at 72 rpm and the blade pitch is set to 3° at the tip. Wind speeds ranging from 5 m/s to 25 m/s and yaw angles from 0° to 180° are tested.

The NREL Phase VI campaign has been extensively used by many researches [10]. The main measured quantity was the chord wise pressure distribution at five span wise blade sections. A total of 22 pressure transducers were placed in each chord wise section, see Figure 3. The S809 airfoil was used from 25% of the blade radius to the tip. Unfortunately, there were not any wake measurements, which could further enhance the values of these experiments and the fidelity of the CFD validation. There is a project called the MEXICO project [15] which looks promising for wake validation purposes since they offer particle image velocimetry (PIV) measurements of the wake.

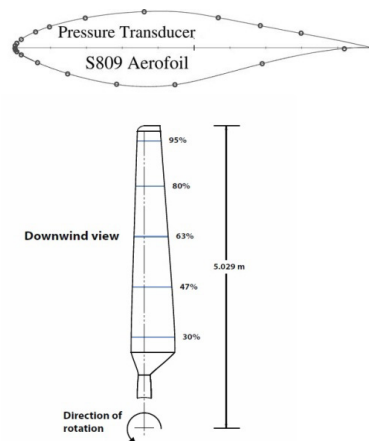


**Figure 3: Pressure transducer distribution on the airfoil, upper part of figure, and span wise placement of the pressure transducers on blade, lower part of figure [13].**

## **2.2. Development and Validation of a CFD Technique for the Aerodynamic Analysis of HAWT**

This paper [10] demonstrates the potential of a compressible Navier – Stokes CFD method for the analysis of horizontal axis wind turbines. The method was first validated against experimental data of the NREL/NASA – Ames Phase VI at 7 m/s, 10 m/s and 20 m/s free streams for a zero degree yawed isolated rotor. Comparisons are shown for the surface pressure distribution at several stations along the blade as well as for the integrated thrust and torque values. For attached and moderately stalled flow conditions the thrust and torque predictions are fair, though improvements in the stalled flow regime are necessary to avoid over prediction of torque. The obtained results suggest that the present method can cope well with the flows encountered around wind turbines providing useful results for their aerodynamic performance and revealing flow details near and off the blades and tower.

The typical wind conditions which CFD calculations are performed at are 7 m/s, 10 m/s and 20 m/s with blade rotating at 72 rpm. Several comparisons between CFD and experiments have been reported obtaining various levels of agreement. Duque et al. [16] demonstrated good agreement between experiments and computed CFD results with the OVERFLOW-D2V1.5D solver, developed by NASA, and the Baldwin-Barth turbulence model. Furthermore, Sørensen et al. [17] obtained good predictions using the ELIPSYS3D incompressible solver, a solver developed at Risø National Laboratory and Danmarks Tekniske Univeristet (DTU), and the  $k-\omega$  shear stress transport (SST) turbulence model for the 7 m/s case. The 10 m/s case was also computed but results were sensitive to the employed turbulence model. The 20 m/s case was well predicted despite the fact that the torque was underestimated. Le Pape et al. [18] also computed this case for the three wind speeds mentioned before using ELSA compressible solver, developed by ONERA and CERFACS, and the  $k-\omega$  SST turbulence model. For 7 m/s the agreement was good but at 10 m/s there were discrepancies between CFD and measurements and this was also the case for the 20 m/s computations. The thrust was well predicted but the torque was under predicted. Later, Le Pape and Gleize revisited the problem with a low Mach number preconditioning technique, the ELSA solver, and the  $k-\omega$  SST turbulence model. The agreement at 7 m/s was still good, and the 10 m/s run was improved but at 20 m/s the torque was still under predicted.

### **2.3. CFD-RANS Study of Horizontal Axis Wind Turbines**

This doctoral thesis [19] has studied the wind turbine aerodynamics with a CFD-RANS approach. He modeled the whole rotor of a wind turbine by means of periodicity and in a moving reference system. For the meshing process GAMBIT software was used. The finite-volume solution package Fluent was used and as validation of the computational methods used a comparison of the overall power production of a BEM-designed turbine was performed. The purpose of proving the capabilities of full 3D CFD-RANS for the study of wind turbine aerodynamics was achieved. The aim of this thesis was to get a better understanding of the physical behavior of the flow field past wind turbine rotors, including the boundary layer flow as well as the wake region. The most important features of the investigated machines were captured with CFD, so that a broad review of wind turbines aerodynamics was given, through the post processing of the computed solutions. A study on the blade root and tip was carried out, demonstrating the advantages of some recent improvements in rotor blade design, and showing the capabilities for CFD as an optimization method.

### **2.4. Wind Turbine Simulations Using Navier-Stokes CFD by Thomas Hansen**

In this thesis [13] the blade used in the NREL AMES Phase VI experiments was simulated with the computational fluid dynamics (CFD) code STAR-CCM+. The calculations were made by solving the incompressible Navier-Stokes equations considering the flow as steady. The turbulent flow was calculated using the  $k-\omega$  SST turbulence model. He used 2D calculations to check the codes ability to simulate the performance of the airfoil used on the wind turbine, and the quality of the mesh was investigated. The rotating aspect was modeled using a moving reference frame and the effects on the flow field due to the rotation are

studied. The results were verified by comparing them to measurements from the Unsteady Aerodynamic Experiment performed in the NASA Ames wind tunnel. In other words, the pressure measurements from five different span wise locations on the instrumented wing was used [13] for validating the CFD simulations. By comparing the pressure distribution to the experimental values the accuracy of the CFD simulation was determined. The validity of these results was then used to determine the accuracy of the three dimensional flow field. In this thesis, CFD simulations are compared with the so called S sequence experiments [14].

The data sets for 7, 10, 13, 15, 20 and 25 m/s are collected from the NREL database for validating the CFD simulations. These specific velocities were selected for comparison because the all correspond to distinct flow field states that target pertinent flow field phenomena. The data sets were also used for the “blind comparison” study and the results from these wind speeds are depicted by Sørensen [17] and others.

It was found that CCM+ was able to predict the aerodynamic properties of the wind turbine well, in both two and three dimensions. The simulations from [20] using  $\gamma - Re_\theta$  transition model are found to improve the results compared to the fully turbulent simulations, except for the predictions of the stall. The  $\gamma - Re_\theta$  transition model were introduced by Menter [21] to enhance the CFD codes ability for the prediction of the onset of transition in flow. For the 3D simulations both the pressure coefficients and the normal force coefficients predictions compare well to the experimental results. To look at the angle of attack for lift and drag it was found to be sufficient to use steady calculations.

## **2.5. Tidal Turbine Loads: Design and dynamic loads estimation using CFD and Blade Element Momentum Theory [22]**

This paper [22] describes a way of designing the blades for a tidal turbine. The blades made have been subjected to CFD computations and a theoretical analysis of the loads in a non-uniform stream. The CFD calculations were validated against a small-scaled model tested in the towing tank at Marintek Laboratory (Trondheim, Norway).

Before performing CFD calculations a mesh needed to be made. The surroundings of the blade were divided in two, one domain close to the blade with rotating flow and on larger domain with unidirectional flow. The CFD study was performed with a steady state analysis and a shear stress transport (SST) turbulence model. To validate that CFD simulations are correct, the rotor efficiency calculated by the CFD simulations were compared to the rotor efficiency calculated by the BEM and the shaft torque and thrust force from the pool trials were also used. The CFD calculated shaft torque matched the pool trial torque well, only 1.4% error was recorded. The  $C_p$  obtained through CFD was 0.421; the highest  $C_p$  obtained in the experiments was 0.427. The BEM results gave a  $C_p$  of 0.426.



### **3. Verification and validation of the CFD calculations**

The verification process consists of checking the iterative convergence, e.g. residual values and the number of iterations. This is done by checking that quantities like drag and boundary layer profile do not change as the number of iterations increases. Consistency checks are important, e.g. see if mass is conserved. Also grid dependency needs to be looked at, e.g. does lift, drag or other measurements change as the amount of grid nodes is increased or decreased. In other words the verification process is needed to ensure that the program solves the equations correctly.

The quality of a CFD simulation can depend on a great number of elements. Errors can occur in the numerical model used, e.g. round-off errors, discretization errors, iterative and grid errors, the code embedded in the software and human error, e.g. incorrect use of the software. Uncertainties are mainly concerned in the input, e.g. the geometry, boundary conditions, fluid properties and such, or in the models used such as turbulence models, assumptions and simplification.

The validation process consists of checking that the method in use agrees with earlier experiments. This tests, amongst other things, the ability of the turbulence model used to represent reality. The methods chosen to validate the thesis' simulations will be discussed in chapter 7.

## 4. Wind turbines

After reading a fair bit of literature on wind turbines, the author have noticed that there are very few papers or books that give the reader a short and understandable introduction on how wind turbines operate (control systems) and important issues in the making of the turbine such as Campbell diagrams and the Weibull distribution. This will be mentioned among the more standard aspects of wind turbines such as power coefficient and tip speed ratio. Also a small taste of airfoil theory will be given along with a section on turbulence intensity in the air that is surrounding us.

This knowledge is fundamental for understanding the challenges detected in responding to the objectives outlined in the present study, and the overview presented here is mainly compiled from [23], [6], [24], [25] and [2].

### 4.1. General overview of a Horizontal Axis Wind Turbine

There are two main types of wind turbines, the horizontal axis and the vertical axis. The horizontal axis machine has the main rotor and the electrical generator at the top of a tower and is normally pointed into the wind (Figure 4). Vertical axis machines have the main rotor shaft arranged vertically. Key advantages of this arrangement are that the turbine does not need to be pointed into the wind in order to be effective. Key disadvantages includes low power coefficient, highly dynamical loading due to the  $360^0$  rotation, difficulty modeling the wind flow and a pulsating torque.

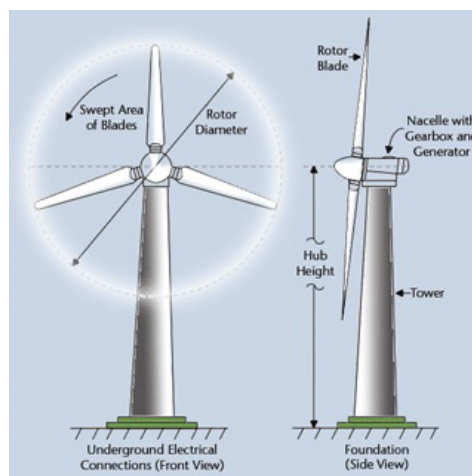


Figure 4: Wind Turbine with the basic elements marked [26].

The most popular wind turbine today and the design which has been taken in by the companies producing windmills is the horizontal one. This mainly due to a higher efficiency and a better overall economic profile than what the vertical axis wind turbine can show for.

#### 4.1.1. Power and location

The power available in the wind is given by

$$P = \frac{1}{2} \rho A U^3 \quad [\text{W}] \quad (4.1)$$

Where  $\rho$  is the density of air ( $1.225 \text{ kg/m}^3$ ),  $A$  is the rotor swept area and  $U$  is the wind speed. The dimension of power is Watt [ $\text{W}=\text{Nm/s}$ ]. The energy equals the power multiplied with time,  $\text{Energy} = \text{Power} \cdot \text{Time}$ . The Dimension for energy is Joule [ $\text{J}=\text{Nm}$ ].

$$E = PT \quad [\text{J}] \quad (4.2)$$

Before choosing a location to set up a windmill the wind conditions in that specific area needs to be investigated. During this process the normal procedures is to use the Weibull distribution and wind roses. A wind rose is a diagram showing the direction and speed of the wind over some period of time. Due to its similarities with a flower it gets its name, wind rose. The Weibull distribution is a two-parameter function used to fit the wind speed frequency distribution [27]. This family of curves has been shown to give a good fit to measured wind speed data. The Weibull function provides a convenient representation of the wind speed data for wind energy calculation purposes. In wind analysis it is used to represent the wind speed probability density function, PDF, commonly referred to as the wind speed distribution. The relation between the probability density function and the cumulative density function is

$$CDF(U) = P(U \leq u) = \int_{0, -\infty}^u PDF(u) \quad (4.3)$$

The PDF of the wind is the likelihood of a certain wind speed  $U$  occurring at any given time. The CDF of a certain wind speed  $U$  is the probability that  $U$  is the maximum wind speed one will observe at any given time.

The Weibull distribution function as a cumulative density function [28] is given by

$$F(U) = 1 - e^{-\left(\frac{U}{c}\right)^k} \quad [-] \quad (4.4)$$

$F$  is the wind speed probability,  $k$  is the shape factor,  $c$  is called the Weibull parameter or scale factor and  $U$  is the wind velocity. The shape factor is related to the width of the distribution. A low shape factor indicates that the deviation from the average wind occurs more often than if one had a high shape factor. In an area with a high shape factor the observed wind lays closer to the average wind speed and the wind conditions are therefore more stabile. A low shape factor can be a sign of areas that are more prone to storms or that have long periods of little wind. A high shape factor will produce a narrow and high graph. The Weibull parameter,  $c$ , is the weighted average speed. A large  $c$  generally means stronger wind.

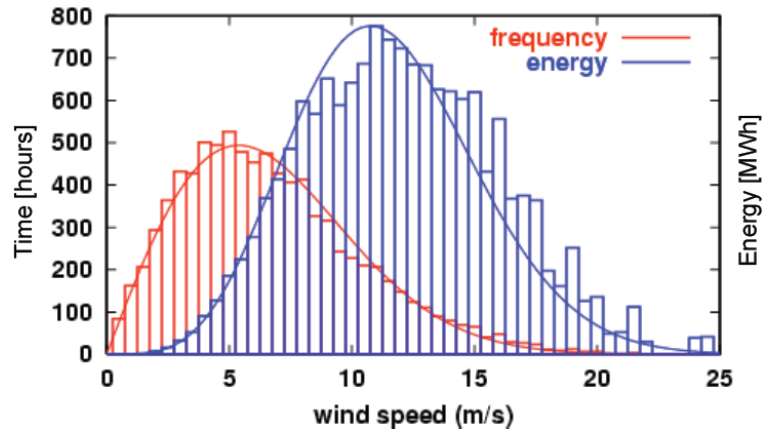


Figure 5: Weibull distribution in red and energy in wind in blue [25].

The energy varies with wind velocity to the power of 3, see Figure 5, and the maximum energy in the wind weighted with how often a certain wind speed occur gives a maximum at a higher wind speed than the winds that are most often occurring. Because of this windmills are designed to achieve maximum torque at a higher wind speed than the average wind speed at a given location.

Unfortunately we are not available to extract all the energy available in the wind. To investigate this a little closer we write eq. (4.1) as

$$P = \frac{1}{2} \dot{m} (U_1^2 - U_4^2) \quad [\text{W}] \quad (4.5)$$

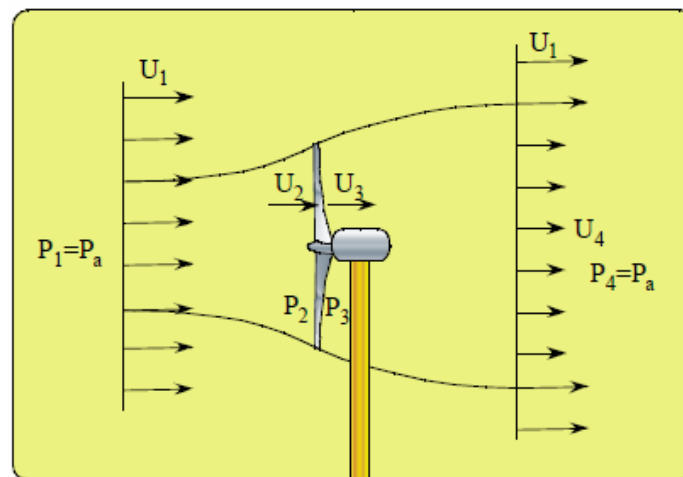


Figure 6: Vertical view of a HAWT [25].

From eq. (4.5) we clearly see that if the wind is not reduced, no power is extracted. But then again if there is no wind behind the rotor, e.g. the mass flux is brought to rest; no power will be extracted because the mass flux is zero. Due to *continuity*

$$\dot{m} = \rho U_1 A_1 = \rho U_2 A_2 = \rho U_3 A_3 = \rho U_4 A_4 = \text{const} \quad [\text{kg/s}] \quad (4.6)$$

this is clearly not possible, so one actually needs movement behind the rotor in order to extract energy from the wind.

#### 4.1.2. Power coefficient

Now, if the maximum energy output is not a 100%, what is it? A power coefficient,  $C_p$ , needs to be introduced into equation (1.1).

$$P = \frac{1}{2} \rho A U^3 C_p \quad [\text{W}] \quad (4.7)$$

Eq. (4.7) must have some theoretical maximum value. According to *Betz Theorem* [6] the limit is 0.5926. This limit is based on *Momentum theory* and uses global control volume analysis to provide information on how much energy can be captured from the wind. A manufacturer of wind turbines will have this limit as a “mission impossible”, e.g. their ultimate goal in regards to the power capture of their windmill. But because there always are losses in a wind turbine operation such as in the gearbox, generators, electric wiring and aerodynamic losses this limit remains only theoretical. Some examples of aerodynamic losses are

- Contamination of bugs; when the blade is contaminated with bugs and insects it will cause the maximum lift to fall.
- At times, the wind turbine might operate in the wake of another turbine; this will cause the turbine to lose power production.
- The larger the turbine, the more the incoming wind deviates in speed, direction and turbulence intensity along the blade.
- Drag, stall and 3D effects like tip losses will obstruct the quest in reaching Betz limit.

A well performing machine will today have value for  $C_p$  around 0.45.

The power coefficient of a rotor varies with the *tip speed ratio*,

$$\lambda = \frac{\omega R}{U} \quad [-] \quad (4.8)$$

The tip speed ratio says something about the relationship between incoming velocity,  $U$ , the length of the blade,  $R$ , and the rotational speed of the rotor,  $\omega$ . The  $C_p$  is only a maximum for a unique tip speed ratio.

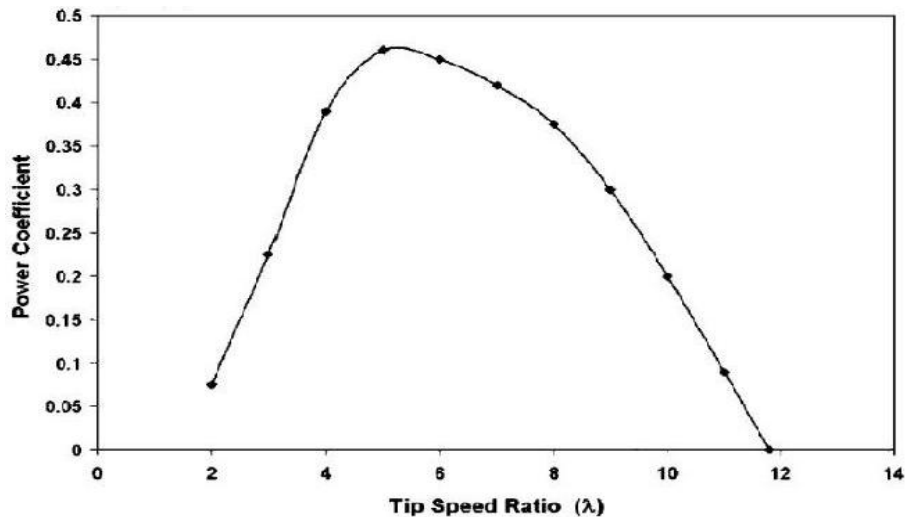


**Figure 7: Power coefficient vs tip speed ratio [29].**

In eq. (4.8) the only parameter one has control over is the rotational speed. As the wind varies, different control systems come into action in order to change the rotational speed in such a way that a maximum power coefficient is maintained. For more information on control systems, read chapter 4.3.

#### **4.1.3. Campbell Diagrams**

The Campbell diagram illustrates the most important natural frequencies of a wind turbine, (Figure 8). 1P and 3P shows the frequencies of the rotor and each rotor blade, respectively. The critical areas in are found when the dotted lines and whole lines meet. These frequencies have to be paid special attention to since resonant movement at these frequencies can be a major concern. This diagram is used in the industry as an aid to see to what areas of the wind turbine extra care is needed at the development stage. Sometimes operation at or near a natural frequency cannot be completely avoided. This may occur during start up or shut down or at some distinct rotor speeds. Effects of operation under such conditions must be considered. The most important considerations when designing a wind turbine are expected events during normal operation, extreme events and fatigue. The Campbell diagram is most helpful in regards to the first category, expected events during normal operation.

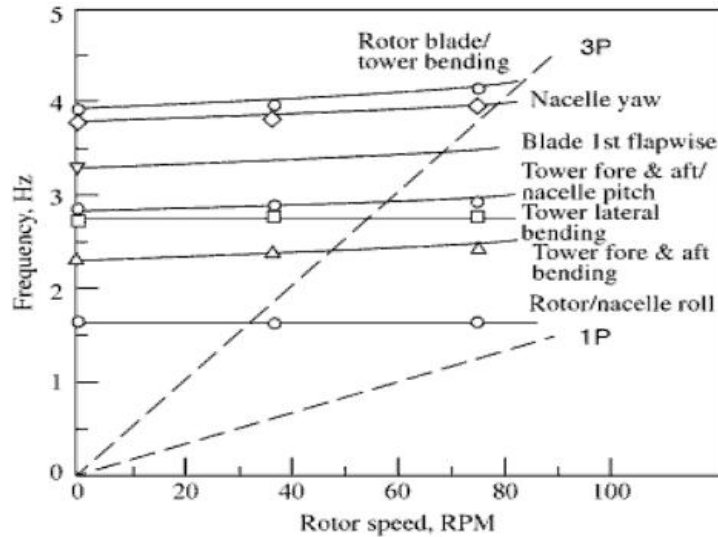


Figure 8: Example of a Campbell diagram for a wind turbine [2].

## 4.2. Airfoil theory

In order to understand the main driving force behind the wind turbine one has to know a little bit about how an airfoil is shaped. The rotor blade for the turbine in this thesis is based upon six different airfoils, five of which all have been made by the Wind Energy Research Group of Delft University, namely the profiles DU 99-W-405, DU 99-W-350, DU 97-W-300, DU 91-W2-250, DU 93-W-210 and NACA 64(3)-618.

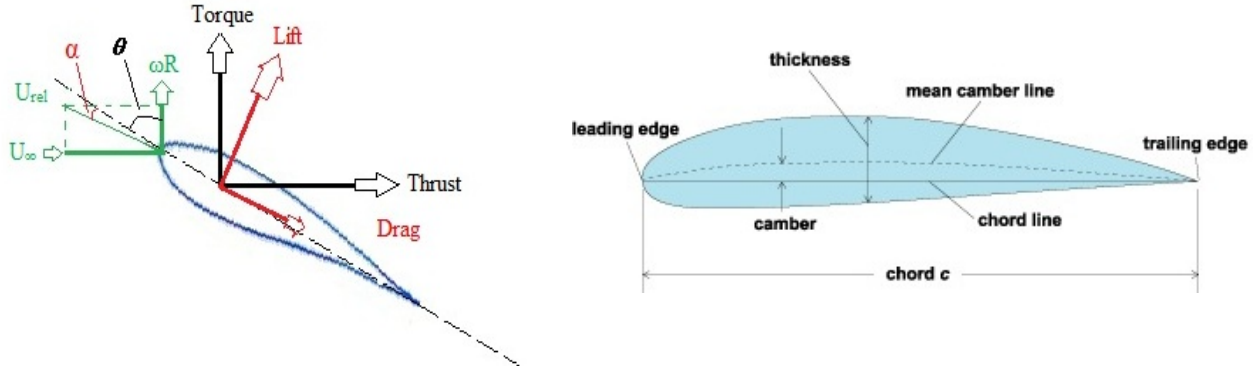


Figure 9: Airfoil.

On the airfoil to the left in Figure 9: Airfoil  $U_{\infty}$  is the incoming wind,  $\omega R$  is the rotational speed of the wing relative to the hub and  $U_{rel}$  is the relative wind that blade experiences. The  $\alpha$  is called the angle of attack and is the angle between the relative wind and the chord line. When the wind turbine operates, the blade is subjected to all of the forces like, torque, thrust, lift and drag (Figure 9). The airfoil to the right, taken from *Encyclopedia of Science and Technology* [30], serves as an example of what the leading edge, trailing edge, chord line and camber is. The mean camber line is mid way between the upper and lower side of the airfoil at all times.

A wing is shaped such that when the airflow meets the leading edge, it splits into two separate streams, one over and one under the wing. The distance over the upper surface is longer than the distance along the lower surface. This causes the flow to experience a difference in speed which results in faster air, and therefore lower pressure, over the wing than under the wing. Therefore the upper side of the airfoil is named suction side and the lower side is called pressure side. The pressure difference between suction and pressure side is what in turn gives rise to the wing being forced upwards. This is the simplified and basic principle of an airfoil.

We will now look in a little bit more detail how aerodynamic lift is created since this is the main driving force of the wind turbine. For full details on this matter see *Aerodynamics for Engineers*, [31]. Lift  $L$  is defined as the force acting on the airfoil in a direction normal to the free stream direction. Drag  $D$  is defined as the force along the free stream direction. Lift will only be present if the flow incorporates a circulatory flow about the body.

Before calculating lift on an airfoil we need to introduce thin airfoil theory. Basic assumptions for this theory are:

- Lifting characteristics are negligibly affected by viscosity
- Resulting pressure forces are only slightly influenced by airfoil thickness
- Airfoil operates at small angle of attack

Since lift is associated with potential vortex flow, a continuous distribution of vortices superimposed upon a uniform flow is considered. The *potential vortex* is a flow with circular paths around a central point where the fluid particles do not rotate themselves but instead simply move on a circular path. The airfoil surface is presented as a uniform flow. This derivation of lift is taken from [32]:

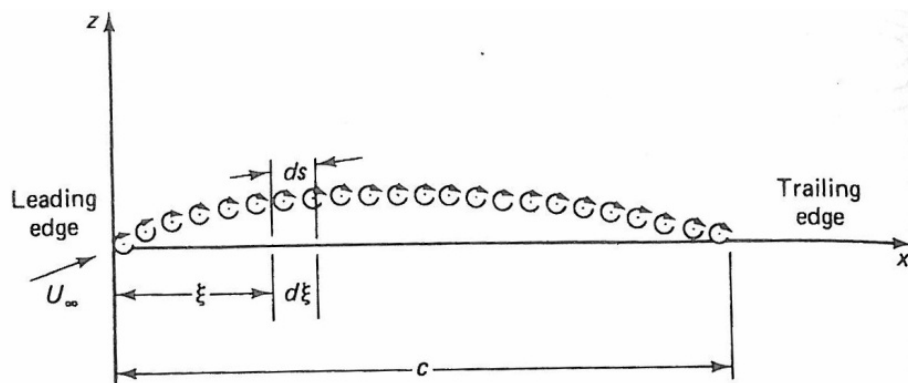


**Figure 10: Vortices superimposed on a uniform flow.**

The total circulation is the sum of the circulations from all the imposed vortex filaments

$$\Gamma = \int_0^c \gamma(s) ds \quad (4.9)$$

where  $\gamma(s)$  is the distribution of line vortices. This distribution includes all the velocities that are tangential to the path  $s$ .



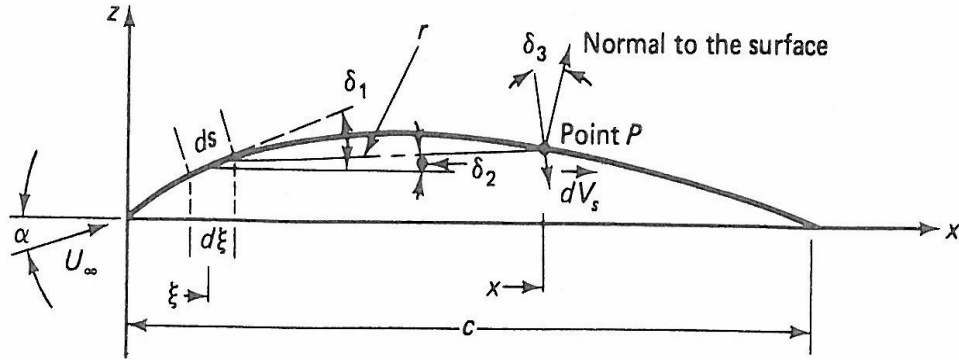


**Figure 11: Airfoil with different parameters.**

Induced velocity component normal to the camber line at point P, see Figure 11, due to vortex element  $\gamma(s)ds$  is

$$dV_n = -\frac{\gamma \cos \delta_3}{2\pi r} ds \quad (4.10)$$

The negative sign is due to the fact that  $\gamma > 0$  in the clockwise direction. Furthermore, we define

$$\cos \delta_2 = \frac{x - \xi}{r} \quad (4.11)$$

and

$$ds = \frac{d\xi}{\cos \delta_1} \quad (4.12)$$

By introducing (4.11) and (4.12) into (4.10) we obtain

$$V_n(x) = \frac{1}{2\pi} \int_0^c \frac{\gamma(\xi) \cos \delta_3 \cos \delta_2 d\xi}{(x - \xi) \cos \delta_1} \quad (4.13)$$

Component of free-stream velocity normal to the camber line at P in Figure 11

$$U_{\infty,n}(x) = U_{\infty} \sin(\alpha - \delta_p) \quad (4.14)$$

With  $\delta_p$  the slope of camber line at P, we have

$$\delta_p = \tan^{-1} \frac{dz}{dx} \quad (4.15)$$

From eq. (4.14) and (4.15) we get

$$U_{\infty,n}(x) = U_{\infty} \sin\left(\alpha - \tan^{-1} \frac{dz}{dx}\right) \quad (4.16)$$

The sum of eq. (4.13) and (4.16) gives zero (normal velocity on solid wall):

$$V_n(x) = \frac{1}{2\pi} \int_0^c \frac{\gamma(\xi) \cos \delta_3 \cos \delta_2 d\xi}{(x-\xi) \cos \delta_1} = U_\infty \sin(\alpha - \tan^{-1} \frac{dz}{dx}) \quad (4.17)$$

Within the assumptions of thin airfoil theory, the angles  $\delta_1$ ,  $\delta_2$ ,  $\delta_3$  and  $\alpha$  are small. Using appropriate trigonometric relations, eq. (4.17) becomes

$$\frac{1}{2\pi} \int_0^c \frac{\gamma(\xi) d\xi}{x-\xi} = U_\infty (\alpha - \frac{dz}{dx}) \quad (4.18)$$

For the camber line of symmetric airfoil,  $\frac{dz}{dx}$  is everywhere zero. Thus, eq. (4.18) becomes

$$\frac{1}{2\pi} \int_0^c \frac{\gamma(\xi) d\xi}{x-\xi} = U_\infty \alpha \quad (4.19)$$

This integral equation is solved with the coordinate transformations

$$\xi = \frac{c}{2}(1 - \cos \theta) \quad (4.20)$$

and

$$\xi = \frac{c}{2}(1 - \cos \theta_0) \quad (4.21)$$

With the limits of integration set to  $\xi = 0$ ,  $\theta = 0$  and  $\xi = c$ ,  $\theta = \pi$  the equation becomes

$$\frac{1}{2\pi} \int_0^\pi \frac{\gamma(\theta) d\theta}{\cos \theta - \cos \theta_0} = U_\infty \alpha \quad (4.22)$$

Using the Kutta condition  $\gamma(\pi) = 0$  the solution of eq.(4.22) yields

$$\gamma(\theta) = 2\alpha U_\infty \frac{1 + \cos \theta}{\sin \theta} \quad (4.23)$$

From a circular cylinder we have that the force in y direction

$$F_y = -\rho U \Gamma \quad (4.24)$$

This is defined as the line integral of the velocity around any closed curve

$$\Gamma = \int \vec{v} dl \quad (4.25)$$

With positive clockwise circulation  $\Gamma$  we get lift as

$$L = \rho U_\infty \Gamma \quad (4.26)$$

The lift on a flat plate airfoil can be calculated as follows

$$L = \int_0^c \rho_\infty U_\infty \gamma(\xi) d\xi \quad (4.27)$$

We now use the distribution given in eq. (4.23) with the transformations (4.20) and (4.21), this gives

$$L = \rho_\infty U_\infty^2 \alpha c \int_0^\pi (1 + \cos \theta) d\theta = \pi \rho_\infty U_\infty^2 \alpha c \quad (4.28)$$

The lift coefficient for a thin plate is

$$C_L = \frac{L}{\frac{1}{2} \rho_\infty U_\infty^2 c} = 2\pi\alpha \quad (4.29)$$

We see here that the lift coefficient can be determined directly from the angle of attack if the assumption for thin airfoil theory applies and we are operating with just a thin plate. For an airfoil the lift coefficient is determined as

$$C_L = \frac{L}{\frac{1}{2} \rho_\infty U_\infty^2 c} \quad (4.30)$$

### 4.3. Functioning of HAWT and Control Systems

In this section the basics functioning of modern HAWT are briefly summarized. This first section is taken from [19]. Wind turbine blades are affected by a force distribution, which makes the rotor rotate and thus generates a mechanical torque at the rotor shaft. The shaft transfers the torque from the blades to the generator, but this passage can be achieved in different ways. The most commonly applied wind turbine set-ups are:

- A Classical turbine with a gearbox, i.e. the so called *Danish concept*. A gearbox with typically three steps connects the rotor shaft, the slow turning one, to the generator shaft, the fast turning one. The generator shaft is directly connected to the electrical grid and therefore has a fixed rotational speed. Usually, in old types, those configurations do not present an active aerodynamic control, but blades are stall regulated while the wind changes.
- A turbine without a gearbox, with the axle directly connected to the generator. It is a newer concept, where a large multi pole generator allows the unique shaft to rotate with the low speed of the rotor.

- A hybrid concept, which combines the previous two. It is made by adopting a smaller generator and a smaller, usually 1-step, gearbox for matching the requested angular speed.

There are two main ways of controlling the wind turbine under varying wind conditions and ensuring that it delivers a certain amount of constant power to the net, i.e. *Pitch regulation* and *Torque control*. In *Pitch control* the blades are physically rotated about their longitudinal axis. In *Torque regulation* the current and resistance in the rotor of the generator can be manipulated in different ways to achieve a constant torque. The following sections are based on [23], [6] and [2].

#### 4.3.1. Torque control

Nowadays, most HAWT are variable speed operating devices, e.g. DFIG turbines Doubly Fed Induction Generators. This means that they will try to follow a rated torque curve,

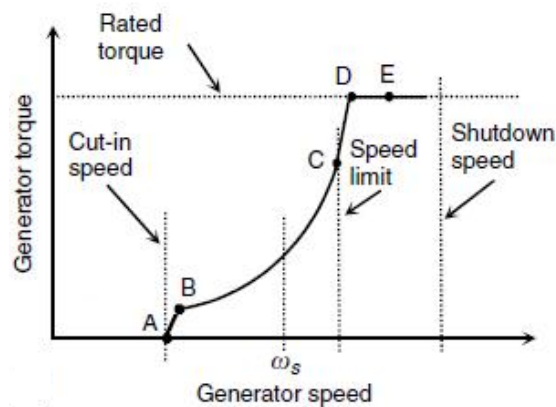


**Figure 12: Optimal torque curve [23].**

In varying wind conditions, section B-C corresponds to the optimal torque-speed curve in under rated wind speed conditions (Figure 12). For very low wind speeds the model operates at almost constant rotational speed (A-B). Rotational speed is also limited, for example, by aerodynamic noise constraint, and at point C the controller allows the torque to increase, at essentially constant speed, to rated torque (C-D). If the wind speed increases further the control objective follows D-E, where pitch regulation, see chapter 4.3.2 Pitch control, limits aerodynamic input power. For very high wind speeds, the pitch control will regulate input power until the wind shutdown speed limit is reached [23].

The equation of the torque of an induction generator is:

$$T = \frac{3 P_f R_r I_r^2}{2 s \omega_s} \quad [\text{kNm}] \quad (4.31)$$

$R_r$  is the rotor resistance,  $I_r$  is the rotor current,  $P_f$  is the number of poles in the generator,  $s$  is the slip speed and  $\omega_s$  is the rotational speed of the stator. We can only change  $P_f$ ,  $I_r$  or  $R_r$ , under normal operation the usual procedure is to change the latter two. In order to change the number of poles you will need an extra generator inside the turbine. By changing the voltage in the rotor windings the Torque in the generator can be altered. Another possibility is that if

we have external resistor banks, we can change the resistance in the rotor windings by shifting between different rotor banks connected to the rotor resistance. This is not the exact equation the torque of a wind turbine generator follows; that equation is much more complicated. But eq. (4.31) gives a good picture of what areas of the generator that is open for alteration during operation.

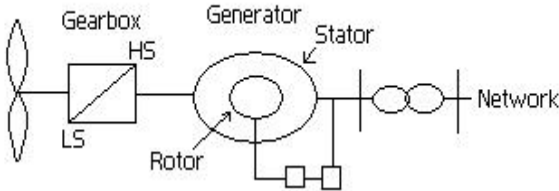


**Figure 13: A simple scheme of a DFIG wind turbine [24].**

Figure 13 shows a simple scheme of a DFIG wind turbine. The slow movement of the shaft passes first through the gearbox so the rotational speed is increased; it then enters the generator where the electricity is made before it passes through a transformer and onto the grid. The two small squares midway on the lower side of the scheme are the power converters. Their function can be to efficiently convert the variable frequency output of an induction generator, driven by a variable speed wind turbine, to a fixed frequency appropriate for the grid or a load.

The slip speed,  $s = \frac{n_s - n_r}{n_s}$ , gives us information on the ratio between rotational speed of the stator and the rotational speed of the rotor.  $n_s$  and  $n_r$  are given in revolutions/minute. If the slip is positive it means that the rotor runs below synchronous speed and if the slip is negative the rotor runs above synchronous speed.  $\omega_s$  in (4.31) is given in rad/s, so is also  $\omega_r$ , the rotational speed of the rotor. If  $\omega_r > \omega_s$  the generator delivers power to the net.

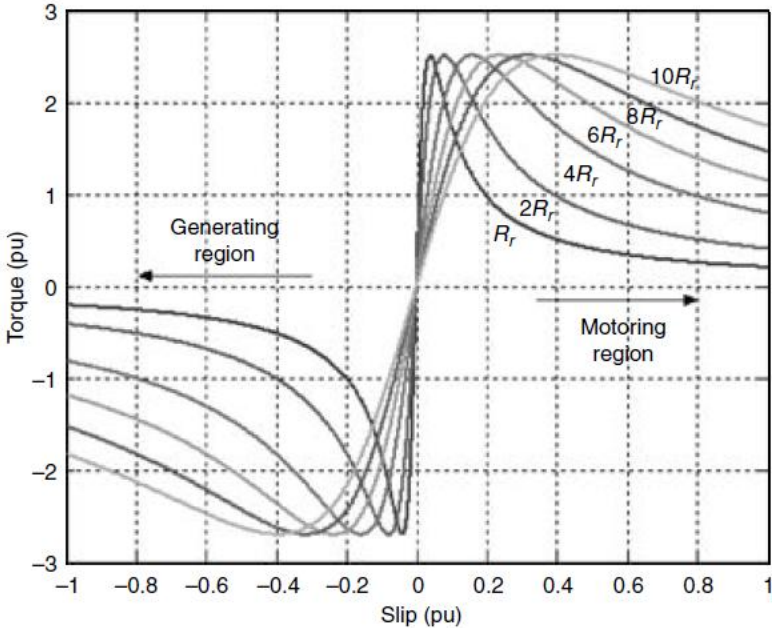


**Figure 14: Torque-slip curves showing the effect of rotor circuit resistance [23]**

The effect of varying the rotor resistance on the torque of the induction machine illustrates that between zero and synchronous speed, the machine performs as a motor (Figure 13). Beyond synchronous speed the machine performs as a generator. One way of controlling the rotor resistance, and therefore the slip and speed of the generator, is to use a wound rotor connected to external variable resistors [23]. One way to connect the wound rotor to the external variable resistors is through the use of brushes and slip rings.

Torque for a fixed speed, directly connected to grid, induction generator is determined only by slip speed. If aerodynamic torque varies, rotor speed  $n_r$ , also varies by a very small amount such that the generator torque changes to match the aerodynamic torque, therefore the generator torque cannot be actively controlled in a fixed speed wind turbine. The aerodynamic torque is the torque acting on the blade as a result of the thrust, lift and drag created by the wind. If a frequency converter interposed between generator and network, the generator speed would be able to vary. A frequency converter can be actively controlled to maintain constant generator torque or power output above rated wind speed. Below rated wind speed, torque can be controlled to any desired value, e.g. with the aim of varying rotor speed to maintain max aerodynamic efficiency.

#### 4.3.2. Pitch control

The second main way to control a wind turbine is to change the pitch angle. The pitch is the angle which the blade makes with the rotor plane. When the pitch is changed, the pressure distribution over the blade is altered, this leads to a change in the induction factors,  $a$  and  $a'$  which in turn changes the angle of attack. The axial induction factor,  $a$ , is a measure of how much the rotor retards the flow.

$$a = \frac{U_1 - U_2}{U_1} \quad (4.32)$$

The rotational induction factor,  $a'$ , is a measure of how much the incoming wind is set in rotation. If one thinks of the incoming wind on the turbine as smooth and uniform the wind will have no rotation before the wind turbine, but after it has gone through the turbine the wind, now called the wake, will have a rotation in opposite direction compared to the turning of the blades.

Pitch control regulate loads produced by the rotor, such as thrust force, torque and aerodynamic power. These loads have strong interaction with the tower. When the blades pitch to regulate torque, thrust on the rotor blades also changes, all these changes feed into tower motion.

In region III (Figure 12), from D to E, the turbine is in the above rated wind speed region, a reduction or an increase in pitch will here result in reduction in torque. In below rated wind speed the turbine, generally speaking, seeks to achieve a maximum power of the available wind, therefore the pitch angle is kept nearly constant. The loads are lower below rated than above rated wind speed and there is no need to pitch the blades heavily. Above rated wind speed pitch control is effective in regulating aerodynamic power and loads produced by the rotor. In this region changing the pitch interacts with the tower. There are two ways to alter

the pitch, either the pitch is increased or it is decreased. Either way a reduction in torque will be obtained.

An increase in pitch, i.e. pitching towards feather, means turning the leading edge into the wind will reduce torque by decreasing  $\alpha$  and hence decreasing the lift. This technique requires more dynamic pitch activity than pitching towards stall. A decrease in pitch, i.e. pitching towards stall, means turning the leading edge downwind reduces the torque by increasing  $\alpha$  towards stall where the lift starts to decrease and drag increases. A pro for active stall regulation is that once a large part of blade is in stall, very small pitch movements suffice for further regulation if wind speed augments, but pitching to stall results in greater thrust loads because of increased drag.

#### **4.3.3. Stall regulated turbines**

There is a third way to control wind turbines called stall regulation. This type of control is not extremely widespread but is worth mentioning. Passive stall turbines have blades that are bolted in place. Blades are designed to stall at high wind speeds to prevent generator from being overpowered. Synchronous generator connected to grid runs at a fixed speed, a gust of wind will cause large stresses on the wind turbines drive train because torque goes up and the magnetic forces will resist an increase in speed. A synchronous generator allows for a limited amount of slip or variation in generator RPM. There is less technical devices in a fixed speed machine than in a variable speed machine, this is to the fixed speed machine's advantage. In a variable speed generator the power must be rectified, in order to do this there is a need for more advanced power electronics, this increases cost and is not a 100% efficient.

The lift curve slope at start of stall region is negative, this means that  $C_L$  decreases with increasing  $\alpha$ , resulting in negative aerodynamic damping which in turn might lead to instability of the blades bending modes in plane and out of plane. What this means is that a small disturbance can result in an even greater disturbance. This is one of the drawbacks of stall regulation.

#### **4.3.4. Variable speed operation**

There are different ways to achieve variable speed operation, following are a few examples of how.

- The stator of the generator can be connected to the network through a frequency converter. Here one must be aware that the converter needs to be rated for the full power output of the turbine.
- A wound rotor induction generator with the stator directly connected to the network and its rotor connected to the network through slip rings and a frequency converter. This means that the frequency converter need only be rated to handle a fraction of the total power, all though the larger this fraction is the larger the available speed range will be.
- A special case of variable speed operation is a variable slip induction generator. This type of turbine has an active control of resistances in series with rotor windings that allows the torque/speed relationship to be modified. This can happen because the closed loop control is based on measured currents and this makes it possible to maintain constant torque above

rated efficiency allowing variable speed operation in this region. Below rated wind speed it behaves just like a normal induction generator.

To summarize some of what is mentioned in this chapter there are four main concepts for the rotor-generator-grid coupling [19]:

- Type A – *fixed speed wind turbine concepts*.  
It corresponds to the *Danish concept*, where there is a squirrel cage induction generator directly connected to the grid through a transformer.
- Type B – *variable speed wind turbine concept with variable rotor resistance*.  
This generator variant is called *Optislip* induction generator, where the rotor winding of the generator is connected with an optically, no need for slip rings, controlled resistance. By changing the resistance the slip changes and thus the power output can vary in a range of 0-10% of the synchronous speed.
- Type C – *variable speed wind turbine concept with partial scale power converter*  
This configuration denotes the variable speed controlled wind turbine with doubly fed induction generator, DFIG, and pitch control. The stator is directly connected to the grid, while the rotor is connected through a partial scale power converter. The variable speed range is +/- 30% around the synchronous speed.
- Type D – *variable speed wind turbine concept with full scale power converter*  
This configuration corresponds to the full variable speed, pitch controlled wind turbine with the generator connected to the grid through a full scale power converter. The generator can be excited electrically, WRSG or WRIG, permanent magnet excited type, PMSG, or squirrel cage induction generator, SCIG. Typically, a direct driven, multi pole synchronous generator, no gearbox, is used. This concept has full control of the speed range from 0 to 100% of the synchronous speed. However, it has a higher power loss in the power electronics compared to the Type C concept, since all the generated power has to pass through the power converter.

## 4.4. Dimensionless parameters

### 4.4.1. Reynolds number

The Reynolds number gives a measure of the relative importance of inertia forces and viscous forces; for a wing it is defined as:

$$\text{Re} = \frac{L_C U_\infty}{\nu} \quad (4.33)$$

where  $\nu$  is the kinematic viscosity [ $\text{kg} \cdot \text{m}^2$ ] defined as the ratio of the absolute viscosity to the fluid density,  $L$  the length of the airfoils chord line and  $U_\infty$  is the incoming speed. See [33] or any other fluid mechanics textbook for more information about the Reynolds number.

### 4.5. Turbulence intensity

This section is mainly derived from [34] and [35]. Turbulence intensity is mentioned in this thesis because, among other things, it has role to play in regards to what loads the wind



turbine should be dimensioned for and one can also define the value itself in CFD. The turbulence intensity depends on roughness length and is therefore a function of wind speed. The knowledge of the turbulence intensity over the open sea is relevant for a better general understanding of the marine boundary layer as well as for the construction and operation of offshore wind turbines, loads on the structure of the turbines and power output both increase with increasing turbulence intensity. It is normally barely mentioned when one reads standard literature on wind energy. An in depth analysis indicate that this is a highly important parameter in regards to the loads experienced by a wind turbine and is anticipated to play a larger and larger role in design as the size of wind turbines are growing. In a CFD simulation TI is a boundary condition set at the inlet which, together with the turbulence models applied, will calculate the force acting on the blade.

Determining the turbulent intensity in the air affecting the wind turbine is a challenging matter. The rotation needs for instance to be accounted for. In real life, the rotating blades experience an effective turbulent intensity that decreases toward the tip due to rotation. The measured turbulent intensity of 0.5 % found in the test section of the NREL Ames tunnel can therefore not be used because it is measured indoors in a closed environment. According to Sørensen [20], when using a turbulent intensity of 1.5 % having a rotation of 72 rpm and a wind speed of 10 m/s, the turbulent intensity will vary from 1.2 % at 1 m radius to 0.38 % at 5 m radius. Parametric studies made by Sørensen on the effect of changing the inflow turbulent intensity reveal a large deviation in the result between 7 m/s and 20 m/s. His studies show that the best results obtained in CFD for the 7 m/s and 10 m/s inlet velocity cases are achieved by using a turbulent intensity of 1.25 %, [36].

Turbulence can be thought of as fluctuations in air flow. A steady flow of air would have low turbulence. An unsteady flow of air would have higher turbulence. But what does it mean “low” and “higher”, when talking about turbulence? A uniform measurement scale is needed and Turbulence Intensity (I) is that measurement scale.

Turbulence Intensity is a scale characterizing turbulence expressed as a percent. An idealized flow of air with absolutely no fluctuations in air speed or direction would have a turbulence intensity value of 0%. This idealized case never occurs on earth. However, due to how turbulence intensity is calculated, values greater than 100% are possible. This can happen when, for example, the average air speed is small and there are large fluctuations present.

The turbulence intensity is a function of the height (z), defined as the ratio of the magnitude of the RMS value of the wind speed fluctuations (  $\langle \sigma \rangle$  ) and the mean wind speed (U), [37]:

$$I(z) = \frac{\langle \sigma \rangle}{U} \quad (4.34)$$

In contrast to land surfaces the roughness of the sea surface is not constant but depends strongly on wind speed because wave height and consequently surface roughness length increase with increasing wind speed [34].

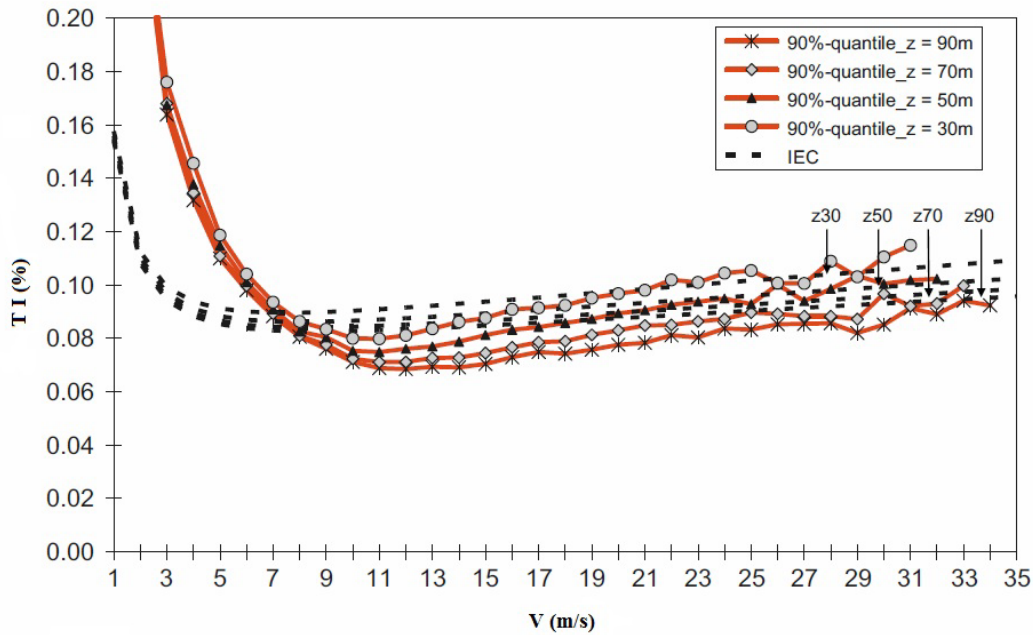


**Figure 15: 90-percentiles of measured turbulence depending on wind speed at different heights compared to turbulence intensity given by the International Design Standard for Offshore Wind Turbines IEC 61400-3, [34].**

It is clearly visible that the turbulence intensity is dependent on the wind speed (Figure 15). For low wind speeds the turbulence intensity is high, for medium wind speeds the turbulence intensity decreases to its minimum, whereas for high wind speeds the turbulence intensity increases steadily. Apparently, stability effects cause higher average turbulence intensity at lower wind speeds. The steadily increasing turbulence intensity at higher wind speeds can be explained by the fact that the roughness of the sea surface increases with increasing wind speeds [37].



**Figure 16: Research platform FINO1.**

For the choice of the turbulence intensity in this thesis processed data from the offshore measurement platform FINO1 which is located 45 km north of the island of Borkum in the German Bight will be used. The water is here 30 m deep so it resembles quite well conditions that might be seen by a future full size version of the 10 MW.

The standard IEC 64100-3 for the design of offshore wind turbines uses the 90% quantiles of the turbulence intensity to describe the wind loads on wind turbines. The 90% quantiles of measured turbulence intensity depending on wind speed at different heights for the period (Figure 15). This thesis uses the results for 90 m above sea level; this will nearly correspond to the hub height of the reference turbine which is a 100 m above sea level. The value used will be 7.4 which corresponds to the rated wind speed for the 10 MW wind turbine (Table 1).

**Table 1: Turbulence intensity at different wind speeds 90 m above sea level.**

U, wind speed at 90 m above sea level	Turbulence Intensity in %
7,5	8,5
10	7,75
12	7,5
13	7,4

#### **4.6. Blade Element Method, BEM**

The method used to design the blades of the 10 MW wind turbine was the “Blade Element Momentum Theory”, BEM. This design process is explained in details by Hansen, [38]. This section is taken from [22] and [19]. The BEM method is a combination of the blade element theory and the momentum theory. The blade element theory splits the rotor blades into elemental sections in order to calculate the thrust and torque on each section. The BEM method uses the axial and rotational induction factors from the momentum theory, these factors were introduced in chapter 4.3.2.

The rotor induces a velocity in the negative axial direction, i.e. against the wind, which is proportional to the far upstream velocity. The proportionality factor  $a$  is called the axial induction factor. It is assumed that the stream upstream from the rotor has no rotational velocity, but because of viscosity and continuity in the fluid, the flow starts rotating upstream from the rotor, though very close to the blades. A rotational induction factor  $a'$  is then introduced. This factor is proportional to the angular speed of the blades. The velocities in the rotor region in the axial and ortho-radial directions are defined in equations and respectively

$$U_{\infty} = (1 - a)U \quad [\text{m/s}] \quad (4.35)$$

$$U_{rot} = (1 + a')\omega r \quad [\text{m/s}] \quad (4.36)$$

The combination of  $U_{\infty}$  and  $U_{rot}$  gives the relative velocity  $W$  seen by a section of the blade. The flow angle  $\phi$  is defined on Figure 9 on page 16 as the angle between rotational velocity  $U_{rot} = \omega R$  and  $U_{rel}$ .  $U$  is here the incoming speed felt by the turbine blade which is a little lower than  $U_{\infty}$ . While designing the blade, the angle of attack can be modified by twisting the section with a certain twist angle  $\theta$ .

The design method BEM is an iterative approach which determines, for a given output power and for each section, the optimal angle of attack and chord length of the airfoils that have been selected to form the basis of the rotor blade. It calculates the lift and drag forces of each section, sums them over the whole blade and compares the obtained power with the wanted power. If the convergence criterion is not fulfilled, the angles of attack are slightly changed until the nominal power is obtained.

The lift and drag forces are obtained through the lift and drag coefficients, which can be given by a software such as X-Foil [39]. The elementary forces acting on each section of elementary span  $dr$  are then defined as:

$$F_L = \frac{1}{2} \rho \frac{\pi D_t^2}{4} W^2 C_L dr \quad [\text{N}] \quad (4.37)$$

$$F_D = \frac{1}{2} \rho \frac{\pi D_t^2}{4} W^2 C_D dr \quad [\text{N}] \quad (4.38)$$

Where  $C_L$  and  $C_D$  are the lift and drag coefficients of the local airfoil for the corresponding angle of attack. It is therefore important to choose an airfoil which minimizes the drag force and optimizes the lift force in the range of the angle of attacks of interest. This will increase the shaft torque and reduce the thrust force acting on the rotor.

Near the tip and root of the blade the equations used by the BEM are not correct because of three dimensional effects, i.e. tip loss and flow separation at root. The loss of lift at the root is often neglected because of the small contribution to the moment from this region. Multiplying the aerodynamic forces obtained with the BEM by the Prandtl's tip loss factor, [38], gives a more realistic distribution over the blade.

The BEM can be written as an algorithm in MATLAB and will therefore automatically determine the optimal design of the blade. This was done when designing the 10 MW wind turbine blade made by PhD candidate Lars Frøyd [40], see Figure 24. The blade is designed for a rated speed of 13 m/s with a tip speed ratio of 6.9. The maximum power coefficient obtained while designing the blade was  $C_p = 0.49$ . This efficiency will be compared CFD computations. Already now the author can state that the efficiency found by CFD will not be as high as the efficiency given the BEM, this is due to the fact that no 3D effects are considered in BEM. The BEM routine does not take into account any variations in the inflow. A constant value of the thrust force  $T$  and torque  $Q$  can therefore be directly calculated;  $Q = 7745.5$  [kNm] and  $T = 1187.4$  [kN].

The torque is the mechanical energy extracted from the flow that can be converted into electricity. The  $C_p$  is the coefficient between the power available in the wind and the torque on the blade

$$C_p = \frac{P}{\frac{1}{2} \rho U_\infty^3 A} = \frac{\text{Power}(\text{rotor})}{\text{Power}(\text{wind})} \quad (4.39)$$

The power generated by the blade is given as

$$P = Q\omega \quad [\text{W}] \quad (4.40)$$

with  $\omega$  being the rotational speed of the turbine given.

This chapter has clearly demonstrated how a wind turbine is controlled under operation with regards to pitch or torque control, some key elements on how to investigate wind conditions and the nature of turbulence relevant for this system. Furthermore the outline gives the functioning of an airfoil as well as the power coefficient, the Campbell Diagrams, tip speed ratio, the Weibull Distribution and the blade element method.

## 5. CFD analysis

The flow of fluid can be mathematically described by the equations for conservation of mass, momentum and energy. These partial differential equations (PDEs) are based on the assumption that the fluid can be described as a continuous medium. The techniques used to solve the problem replace the PDEs by a set of algebraic equations by dividing the physical domain into a large number of discrete control volumes, called elements or cells. Within these cells algebraic relationships describe how the flow variables, such as velocity, temperature or pressure, vary locally with the space coordinates. This is the general idea behind *Computational Fluid Dynamics*, also known as *CFD*. The layout and contents of these chapters are taken much from [41], supplied with knowledge from [35], [42] and [43].

### 5.1. Fundamental equations

The governing equations of fluid flow represent mathematical statements of the conservation laws of physics:

- The mass of a fluid is conserved, in laymen terms this means that all that all mass that comes in, must go out.
- The rate of change of momentum equals the sum of forces on a fluid particle (Newton's second law).
- The rate of change of energy is equal to the sum of the heat rate added to a fluid particle and the work done on it (first law of thermodynamics).

These conservation laws are applied to a small fluid element, or control volume, by the Navier Stokes equations. These equations will from now on be abbreviated as NS in this thesis.

#### 5.1.1. Navier Stokes

$$\text{Conservation of mass} \quad \frac{\partial \rho}{\partial t} + \nabla \cdot (\rho \bar{U}) = 0 \quad (5.1)$$

$$\text{Conservation of momentum} \quad \frac{\partial(\rho \bar{U})}{\partial t} + \rho(\bar{U} \cdot \nabla) \bar{U} = -\nabla p + \nabla \cdot \bar{\bar{\sigma}} + \rho \bar{f}_b \quad (5.2)$$

Here  $\bar{\bar{\sigma}}$  is the stress tensor for Newtonian viscous fluid,  $\bar{f}_b$  are body forces, i.e. gravity. The bar over for example  $\bar{U}$  means that  $U$  is a vector.

Equation (5.1) is the unsteady, three-dimensional mass conservation or continuity equation at a point in a compressible fluid. The first term on the left hand side is the rate of change in time of the density (mass per unit volume). The second term describes the net flow of mass out of the element across its boundaries and is called the convective term, [44].

All flows in the present thesis are considered incompressible, i.e. the density is constant. Also temperature effects are neglected, and the conservation of internal energy has been left out of the NS equations as well in this chapter.

For an incompressible fluid the density  $\rho$  is constant and equation (5.1) becomes

$$\nabla(\rho\bar{U}) = 0 \quad (5.3)$$

or in Cartesian notation

$$\frac{\partial u}{\partial x} + \frac{\partial v}{\partial y} + \frac{\partial w}{\partial z} = 0 \quad (5.4)$$

By using equation (5.3) the viscous term in equation (5.2) is simplified, reducing the momentum equation to, [45]:

$$\frac{\partial(\rho\bar{U})}{\partial t} + \rho(\bar{U} \cdot \nabla)\bar{U} = -\nabla p + \mu\nabla^2\bar{U} + \rho\bar{f}_b \quad (5.5)$$

If the flow is steady state, the first term is equal to zero. There is now four variables and four equations; one equation for continuity and three equations for momentum balance, with three velocity components and pressure as unknowns.

## 5.2. Turbulence modeling

All flows encountered in engineering practice become unstable above a certain Reynolds number and are eventually observed to be turbulent. In the turbulent state of a fluid flow the flow behavior is random and chaotic and the velocity and pressure change continuously with time. Turbulence is always a three dimensional phenomena, even if mean velocities and pressure only vary in one or two dimensions [45]. Visualizations of turbulent flow reveal rotational flow structures, so called turbulent eddies, with a wide range of length scales [44]. In order to solve the NS equations numerically the discretization must account for the same range of scales, meaning that the grid must be smaller than the specific micro scales of the flow. To solve the Navier Stokes equations in such a way is called *Direct Numerical Simulation* (DNS).

DNS means solving the NS equations numerically and without any modeling. Performing a DNS simulation with today's computer technology is both time consuming and can only be performed on simple geometries and simple flows. Since this is too costly in computer power the next step of choosing a simulating method would be the Large Eddie Simulation (LES).

LES calculates large scales of the flow field solution directly and models the small scale effects. This allows better fidelity than alternative approaches that do not resolve any scales of the solution but models all scales, such as the Reynolds Averaged Navier Stokes (RANS). This makes the computational cost for LES for practical engineering systems with complex geometry or flow configurations, such as turbulent jets, pumps, vehicles, and landing gear, attainable using supercomputers. Because of the length of the blade in this thesis, and the fact that one needs to obtain a certain amount of the wake in order to see the flow correctly on the blade, rules out the possibility of using LES as an approach. With the high number of nodes needed to represent this geometry correctly the computational cost of DNS or LES is impossible to meet in this thesis. Nor does the author have access to any super computer so this thesis will use RANS modeling.

### 5.2.1. Reynold Averaged Navier Stokes equations (RANS)

The RANS equations are time-averaged equations of motion for fluid flow. The idea behind the equations is Reynolds decomposition, whereby an instantaneous quantity is decomposed into its time averaged and fluctuating quantities. These equations are used based on knowledge of the properties of flow turbulence to give an approximate time averaged solutions to the NS equations.

RANS are turbulence models that are used to predict the effects of turbulence in fluid flow without resolving all scales of the smallest turbulent fluctuations [42]. A number of models have been developed that can be used to approximate turbulence based on the RANS equations. The models can be classified as either eddy-viscosity or Reynolds stress models. This thesis will use the k- $\omega$  based Shear Stress Transport, k- $\omega$  SST, model which is classified as an eddy-viscosity model.

For most engineering purposes it is unnecessary to resolve the details of the turbulent fluctuations. Therefore, RANS modeling is the most widely used CFD approach in many industries today. The basis for RANS modeling is *Reynolds decomposition*. Reynolds decomposition is a mathematical technique used to separate the average and fluctuating parts of a quantity [45]. For example if we examine the instantaneous incoming speed on a wind turbine  $U_\infty$ :

$$U_\infty = \tilde{U}_\infty + U_\infty' \quad (5.6)$$

$\tilde{U}_\infty$  is the steady component of the time averaged  $U_\infty$  and  $U_\infty'$  is the fluctuating part of the incoming wind.  $U_\infty'$  is defined in such a way that its average is zero.

Instantaneous pressure

$$P = \tilde{P} + P' \quad (5.7)$$

Mean velocity

$$\tilde{U}_\infty = \frac{1}{T} \int_{t_0}^{t_0+T} U_\infty dt \quad (5.8)$$

Reynolds decomposition allows us to simplify NS by substituting in the sum of the steady component and the fluctuating parts of, for example, the incoming wind and then taking the mean value. The resulting equation contains a non-linear part known as the *Reynolds stress* which gives us the turbulence part of NS.

For further use in this section we will write the instantaneous velocity in an arbitrary direction as

$$U_i = \tilde{U}_i + U_i' \quad (5.9)$$

The letter  $i$  can be the x, y or z – direction.



When inserting (5.9) into (5.2) and averaging, one obtains an equation expressing momentum conservation of the averaged motion. This equation is often referred to as the RANS equation, [45] and [41]:

$$\frac{\partial \tilde{U}_i}{\partial t} + \tilde{U}_j \frac{\partial \tilde{U}_i}{\partial x_j} = \frac{1}{\rho} \frac{\partial}{\partial x_j} \left[ -P \delta_{ij} + \mu \left( \frac{\partial \tilde{U}_i}{\partial x_j} + \frac{\partial \tilde{U}_j}{\partial x_i} \right) - \overline{\rho U'_i U'_j} \right] \quad (5.10)$$

P stands for pressure, the  $\mu \left( \frac{\partial \tilde{U}_i}{\partial x_j} + \frac{\partial \tilde{U}_j}{\partial x_i} \right)$  term are the viscous stresses,  $\tilde{U}$  is the averaged velocity,  $\rho$  is the density and  $\overline{\rho U'_i U'_j} = -\tau_{ij}$  are the turbulent stresses, or sometimes called the Reynolds stresses. This latter term represents the effect of the turbulent fluctuations on the mean flow. The  $\delta_{ij}$  is the Kronecjer delta. The Kronecker delta can take the values  $\delta_{ij} = 1$  if  $i = j$  or 0 if  $i \neq j$ . The Reynolds stresses introduce six new unknowns related to turbulence, three normal stresses,  $\overline{U_1'^2}, \overline{U_2'^2}, \overline{U_3'^2}$  and three shear stresses,  $\overline{U_1' U_2'}, \overline{U_1' U_3'}, \overline{U_2' U_3'}$ .

The most common RANS turbulence models are classified by the number of extra transport equations needed in order to provide closure for the RANS flow equations. Closure implies that there are a sufficient number of equations for all the unknowns, including the Reynolds-Stress tensor resulting from the averaging procedure. The equations used to close the system define the type of turbulence model. The following models form the basis of current turbulence calculation procedures:

**Table 2: List of RANS turbulence models sorted by number of additional transport equations, [41].**

Number of extra transport equations	Name
Zero	Mixing length model
One	Spalart Allmaras model
Two	k - ε model
	k - ω model
	SST model
Seven	Reynolds stress model (RMS)

### 5.2.2. The general eddy viscosity hypothesis

One way of closing the RANS equations is to introduce an eddy viscosity term,  $\nu_t$ . In 1877 Boussinesq postulated that the momentum transfer caused by fully turbulent eddies can be modeled with an eddy viscosity [46]. In other words he ment that the Reynolds stresses are proportional to the mean rates of deformation:

$$\tau_{ij} = -\overline{\rho U'_i U'_j} = 2\nu_t S_{ij}^* - \frac{2}{3} \rho k \delta_{ij} \quad (5.11)$$

Where  $\nu_t$  is a scalar property called the *eddy viscosity*. The turbulent kinetic energy per unit mass is here  $k$  and  $S_{ij}^*$  are the mean strain rates, [41].

$$S_{ij}^* = \frac{1}{2} \left[ \frac{\partial \tilde{U}_i}{\partial x_j} + \frac{\partial \tilde{U}_j}{\partial x_i} \right] \quad (5.12)$$

$$k = \frac{1}{2} (\overline{U_1^2} + \overline{U_2^2} + \overline{U_3^2}) \quad (5.13)$$

The hypothesis is reasonable for simple turbulent shear flows such as boundary layers, mixing layers, round jets, channel flows etc. If equation (5.11) into the Reynolds averaged momentum equation (5.10) and rearrange, the resulting equation becomes, [41]:

$$\frac{\partial \tilde{U}_i}{\partial t} + \tilde{U}_j \frac{\partial \tilde{U}_i}{\partial x_j} = \frac{\partial}{\partial x_i} \left[ -\frac{P}{\rho} \delta_{ij} + \frac{2}{3} k \right] + \frac{\partial}{\partial x_j} \left[ 2(\nu + \nu_t) S_{ij}^* \right] \quad (5.14)$$

The effective viscosity is the sum of molecular and turbulent (eddy) viscosities. The convenience of the eddy viscosity concept is coupled with the mathematical convenience of retaining the same form of the governing equations in both turbulent and laminar cases, which allows the same solution procedure for both cases.

When it comes to the values  $k$ ,  $\varepsilon$  and  $\omega$  they are normally not known, but most commercial solvers allow for rough approximations based on the already mentioned turbulence intensity and some characteristic length scale.

### 5.2.3. SST k- $\omega$ model

For prediction of wind turbine aerodynamics the k- $\omega$  based SST model in CFX is the most preferred models of all the available. This is a well tested method within the wind turbine industry and has been used by many researchers around the globe, for example in [10], [19] and [47].

Currently, the most used two-equation models in aerodynamics are the k- $\omega$  based models of Menter [48]. The k- $\omega$  based SST model accounts for the transport of the turbulent shear stress and gives highly accurate predictions of the onset and the amount of flow separation under adverse pressure gradients [35]. The transport equation of the turbulent kinetic energy is solved together with the equation of the specific rate of dissipation of turbulent kinetic energy, defined as  $\omega = \varepsilon/k$  [ $s^{-1}$ ]. To benefit from this model, a resolution of the boundary layer of more than 10 points, 10 inflation layers, is required, more on this in chapter 5.3.1.

This following section is mainly derived from [42]. One of the main problems in turbulence modeling is the accurate prediction of flow separation from a smooth surface. The standard two-equation turbulence model  $k - \varepsilon$  often fails to predict the onset and the amount of flow separation under adverse pressure gradient conditions. This is an important phenomenon in many technical applications, particularly for airplane aerodynamics since the stall characteristics of a plane are controlled by the flow separation from the wing. For this reason,

the aerodynamic community has developed a number of advanced turbulence models for this application, like the  $k-\omega$  model. In general, turbulence models based on the  $\varepsilon$ -equation predicts the onset of separation too late and under-predict the amount of separation later on. This behavior gives an overly optimistic performance characteristic for an airfoil.

The shear stress transport formulation combines the better of two worlds. The shear stress transport (SST)  $k-\omega$  model was developed to effectively blend the robust and accurate formulation of the  $k-\omega$  model in the near wall region with the free stream independence of the  $k-\varepsilon$  model in the far field [19]. The SST  $k-\omega$  model is similar to the standard  $k-\omega$  model, but it includes a number of features that makes the SST  $k-\omega$  model more accurate and reliable for a wider class of flows than the standard  $k-\omega$  model. The SST  $k-\omega$  model does produce a bit too large turbulence levels in regions with large normal strain, like stagnation regions with strong acceleration.

One of the main differences between the  $k-\varepsilon$  model and the  $k-\omega$  based SST model is the eddy viscosity,

- $k-\varepsilon$  model

$$\nu_t = \rho C_v \frac{k^2}{\varepsilon} \quad (5.15)$$

$\varepsilon$  is the rate of energy dissipation caused by the smallest eddies working against viscous stresses. As listed in Table 2, the turbulence model uses two extra transport equations, one for  $k$  and one for  $\varepsilon$ .

- SST  $k-\omega$  model

$$\nu_t = \frac{a_1 k}{\max(a_1 \omega, SF_2)} \quad (5.16)$$

$a_1$  is a coefficient used for closure and is normally set to 5/9. The turbulent kinetic energy is  $k$ ,  $\omega$  is the specific dissipation rate,  $S$  is an invariant measure of strain rate and  $F_2$  is the second blending function. For more details of the differences between these different models and the mathematics behind them, the reader is requested to investigate [49], [50] and [51].

### 5.3. Boundary layer theory

Near a no-slip wall, represented by for example an airplane wing, wind turbine blade or ship hull, there are strong gradients in the dependent variables. In addition, viscous effects on the transport processes are large and it is in this area that the highest gradients of velocity and pressure occur. This makes the modeling of these variables of utter importance in CFD calculations. How this is done will be highlighted in chapter 5.3.1. The region where all this happens is called the *boundary layer*.

The aerodynamic boundary layer was first defined by Ludwig Prandtl in 1904. It allows us to simplify the equations of fluid flow by dividing the flow into two areas, one inside the

boundary layer and one outside the boundary layer. Inside the layer viscosity is dominant and the majority of the drag experienced is created. Outside the layer viscosity can be neglected without significant effects on the solution of the NS equations.

There is no unique boundary layer thickness, since the effect of the viscosity in the boundary layer decreases asymptotically as one move outwards from the wall.

According to [52] two of the main definitions of boundary layer thickness in laminar flow are,

- 99% thickness
- Displacement thickness

99% thickness:

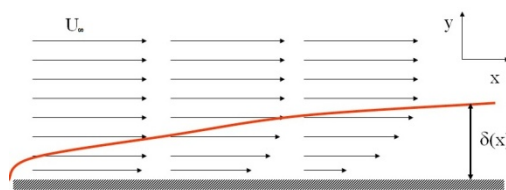


**Figure 17: Boundary layer at a flat plate at zero incidence, [52].**

Let  $U_\infty$  be the free stream velocity, i.e. the incoming wind on a rotor blade.  $\delta(x)$  is the displacement thickness. Let  $u$  be the wind velocity close to the surface of the rotor blade. The thickness of the boundary layer starts from the surface of the rotor blade and ends when  $u = 0.99U_\infty$ , that is when  $u$  is 99% of the value of  $U_\infty$ . The boundary layer thickness can be defined in this way as

$$\delta_{99} \approx 5.0 \sqrt{\frac{\nu x}{U_\infty}} \quad (5.17)$$

Displacement thickness,  $\delta_1$  :

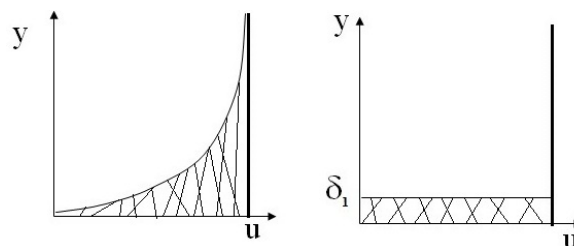


**Figure 18: Displacement thickness, [52].**

There is a reduction in the flow due to the presence of the boundary layer (Figure 18, left panel). To the right is the equivalent to having a theoretical boundary layer with zero flow.

$$U_\infty \delta_1(x) = \int_{y=0}^{\infty} (U_\infty - u) dy \quad (5.18)$$

$U_\infty$  is the velocity on the outer edge of the boundary layer at position  $x$ . From this, the two shaded areas in Figure 18 must be equal. The displacement thickness tells us how far the streamlines of the outer flow are displaced by the boundary layer.

### 5.3.1. Turbulent Boundary Layer and Near Surface Modeling

The treatment of turbulent boundary layers is far more difficult than looking at laminar flow. This is due to the time dependent variation of the flow properties. The following sections will give the reader an insight into:

- How to account for viscous effects at the wind turbine blade in the turbulent boundary layer.
- How to resolve the rapid variation of flow variables which occurs within the turbulent boundary layer region.

This section is mainly taken from [41] and [42]. A great number of experiments have shown that the near wall region, or inner layer, can generally be divided into three regions where different modeling laws apply.

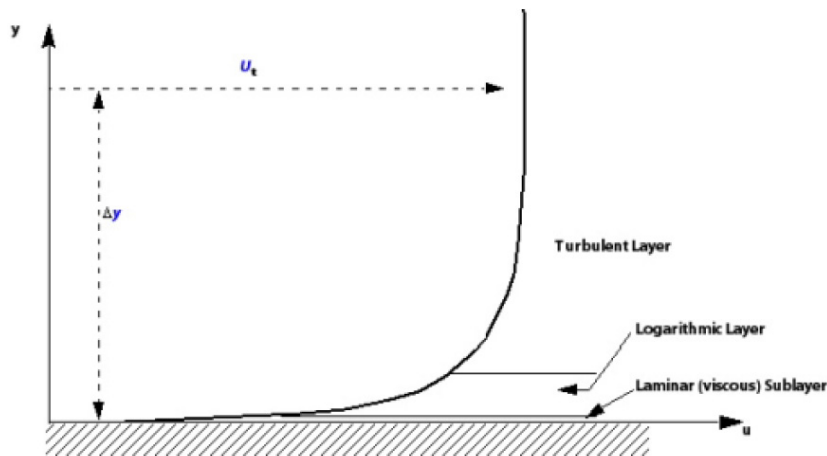


Figure 19: The three sub divisions of the *near wall region* [42].

The innermost layer is called the *viscous sub layer*, here the flow is almost laminar like and the molecular viscosity plays a dominant role in momentum and heat transfer. In this region one assumes that the shear stress is constant and equal to the wall shear stress  $\tau_w$ . A linear relationship can be obtained between the mean velocity  $\tilde{U}$  and the distance from the wall  $y$  by integrating  $\tau_w = \mu \frac{\partial \tilde{U}}{\partial y}$  with respect to  $y$ :

$$\tilde{U} = \frac{\tau_w y}{\mu} \quad (5.19)$$

In the outermost layer, the *logarithmic layer*, turbulence dominates the mixing process. The logarithmic nature gives rise to the “log law of the wall”. Its extent depends on the Reynolds

number. From experiments and dimensional analysis the general form of the relationship between the wall distance and the mean flow is defined by the “log law”:

$$\frac{\tilde{U}}{U_\tau} = 2.5 \ln\left(\frac{U_\tau y}{\nu}\right) + 5 \quad (5.20)$$

Where  $U_\tau = \sqrt{\frac{\tau_w}{\rho}}$  is the friction velocity or shear velocity. Experimental studies show that the log-law is valid in the region  $0.02 < \frac{y}{\delta} < 0.2$  [44].

Finally, there is a region between the viscous sub layer and the logarithmic layer called the *buffer layer*, where the effects of molecular viscosity and turbulence are of equal importance. The figure below illustrates these subdivisions of the *near wall region* in a little more detail than Figure 19:

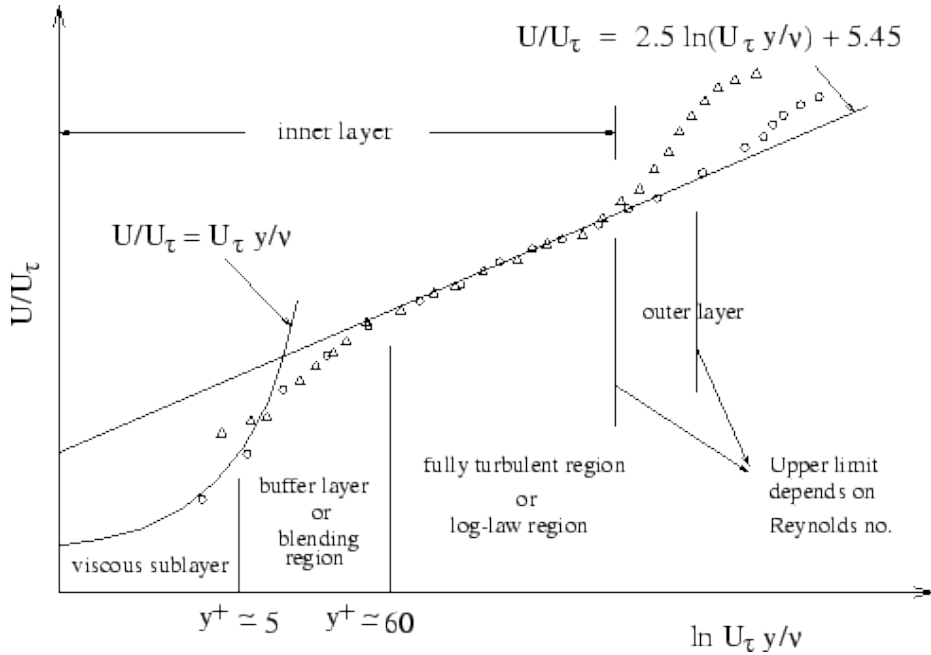


**Figure 20: A detailed description of the three regions of the near wall region [41].**

The distance from the wall boundary to the first cell in the mesh determines how the boundary layer is resolved by the turbulence model. This distance is defined by a  $y^+$  value and is given as

$$y^+ = \frac{y u^*}{\nu} \quad (5.21)$$

Here,  $y$  is the distance normal from the wall to the wall-cell,  $u^*$  is the reference velocity and  $\nu$  is the kinematic viscosity [41]. See chapter 5.3.4 for a more detailed description of how the  $y^+$  has been found in the present case.

### 5.3.2. Near wall meshing

In general, there are two approaches for modeling the near-wall region. One can use either *Turbulence models* which can resolve the flow all the way to the wall, including the viscous sub layer. Or semi-empirical formulas called *Wall functions* to account for the viscous presences of the wall can be used.

The mesh needs to be generated according to the approach used. According to Fluent and CFX, the placement of the grid nodes should follow these guidelines

- For standard or non-equilibrium wall functions, each wall adjacent cell centroid should be located within the log-law layer:  $y^+ \approx 30 - 300$ . Preferably at  $y^+ \approx 30$ .
- Placing the wall-adjacent nodes in the buffer layer  $5 < y^+ < 30$  should be avoided for all models.
- For near wall models, the wall-adjacent cell should be placed in the viscous sub layer  $y^+ < 5$ . Furthermore, at least ten cells should be placed within the boundary layer. In the thesis it will be attempted to achieve a  $y^+ < 5$  on most of the 10 MW blade.

How CFX calculates the distance from the wall to the first cell centroid will follow in chapter 5.3.4

### 5.3.3. Automated near-wall treatment for $\omega$ – based models [42].

Wall functions are one of the most popular ways to account for wall effects. In CFX, *Scalable Wall Functions* are used for all turbulence models based on the  $\varepsilon$ -equation. One of the advantages is that the high gradient shear layers near walls can be modeled with relatively coarse meshes, yielding substantial savings in CPU time and storage. It also avoids the need to account for viscous effects in the turbulence models. But, as mentioned before, turbulence models based on the  $\varepsilon$ -equation have some major disadvantages in regards to estimation of the onset of separation and its inability to handle low turbulent Reynolds number computations.

For  $k$ - $\omega$  based models (including the SST model), an automatic near-wall treatment method is applied. It automatically switches from wall-functions to a *low-Re* near wall as the mesh grows finer. Using a strict low-Reynolds number implementation of the model requires a near wall grid resolution of at least  $y^+ < 2$ . This cannot always be guaranteed. For this reason the *Automatic Near Wall Treatment* was made in CFX as default for all models based on the  $\omega$ -equation (standard  $k$ - $\omega$ , Baseline  $k$ - $\omega$ , *SST* and  $\omega$ -*Reynolds Stress*). It allows a smooth shift from a low-Reynolds number form to a wall function formulation [35]. Note that the “low-Re” method does NOT necessarily mean it only is suitable for low Reynolds numbers. The “low-Re” method refers to the turbulent Reynolds number, which is low in the viscous sub layer. This method can therefore be used even in simulations with very high Reynolds numbers, as long as the viscous sub layer has been resolved.

The “low-Re” approach requires a very fine mesh in the near wall region and thus a large number of nodes. Computer storage and runtime requirements are higher than those of the wall function approach and care must be taken to ensure good numerical resolution in the near wall region in order to capture the rapid variation in variables. To reduce the resolution requirements some, the automatic wall treatment will be used in the thesis.

### 5.3.4. How to determine a target $y^+$ in the CFX 12.1 mesher

The goal here is to determine the required near wall mesh spacing,  $\Delta y$ , in terms of Reynolds number, length of the plate and a  $y^+$  target value. This target value depends on the flow type and the turbulence model in use, or in other words the near wall treatment model. Generally speaking, the closer the  $y^+$  is to 1, the more accurate a solution one will get. The larger the  $y^+$ , the more of the turbulent boundary layer the computer needs to “guess” or model. This chapter is derived mostly from [35].

The estimates for the  $y^+$  value for the simulations of the wind turbine in question will be based on correlations for a flat plate with a Reynolds number of 14 million given by (4.33).

The correlation for the wall shear stress coefficient,  $c_f$ , is given by White [43]:

$$c_f = 0.027 \text{Re}_x^{-1/7} \quad (5.22)$$

where  $x$  is the distance along the plate from the leading edge.

The definition of  $\Delta y^+$  for this estimate is:

$$\Delta y^+ = \frac{\Delta y u_\tau}{\nu} \quad (5.23)$$

with  $\Delta y$  being the mesh spacing between the wall and the first node away from the wall.

Using the definition

$$c_f = 2 \frac{\rho u_\tau^2}{\rho U_\infty^2} = 2 \left( \frac{u_\tau}{U_\infty} \right)^2 \quad (5.24)$$

$u_\tau$  can be eliminated in eq. (5.23) and gives

$$\Delta y = \Delta y^+ \sqrt{\frac{2}{c_f}} \frac{\nu}{U_\infty} \quad (5.25)$$

$C_f$  can be eliminated using eq. (5.22) and will give

$$\Delta y = L \Delta y^+ \sqrt{74} \text{Re}_x^{1/14} \frac{1}{\text{Re}_L} \quad (5.26)$$

Further simplification can be made by assuming that

$$\text{Re}_x = C \text{Re}_L \quad (5.27)$$

where  $C$  is some fraction. Assuming that  $C^{1/14} \approx 1$ , then, except for very small  $\text{Re}_x$ , the result of

$$\Delta y = L \Delta y^+ \sqrt{74} \text{Re}_L^{-13/14} \quad (5.28)$$



is the equation that the CFX 12.1 mesher uses when it calculates the distance from the wall to the first cell centroid. The user feeds the wanted value of  $y^+$ ,  $Re_L$  and  $L$  (*chord length*). Seeing that the chord length varies from 0.9 m at the tip to 5 m at the broadest, the  $y^+$  value was calculated with an  $L$  of 1 m. The  $y^+$  might be a little small at the widest part of the blade and thus result in a  $y^+ < 1$ , but this is considered to be a better choice than calculating the  $\Delta y$  with a  $L$  of 5. This might have resulted in  $y^+$  values above 5 somewhere on the blade, but this is difficult to avoid. This would mean that the first cell centroid will be placed in the buffer layer. According to guidelines given by CFX this should be avoided.

**5.4. Discretization schemes**

A discretization scheme converts the differential equation into a set of algebraic equations, in other words it takes the continuous NS and turns the equations into discrete problems, both in time and space. A discretization scheme involves the breaking down of a geometry into smaller parts, such as elements, nodes or volumes. The resulting discretized geometry, which is now a group of several smaller computational regions, is termed a grid or a mesh.

For the time discretization there exists both explicit and implicit methods. This thesis will only run steady state flow, in other words there will be no calculations that are dependent on time. When it comes to space discretization, CFX uses finite elements, cell vertex numeric’s, similar to those used in structural Finite Element Method analysis, to discretize the domain. In CFX the schemes one can choose from are not as many as in Fluent. In this thesis the scheme called “Higher Resolution” is chosen. This is based on the fact that it has a higher accuracy than many other schemes even though it costs a little more in computational power.

CFX employs a vertex centered scheme for which the fluid flow variables are stored at the cell vertex, and the solver element or control volume as a “dual” of the mesh element. This means that the vertex of the mesh element is the center of the solver element [53].

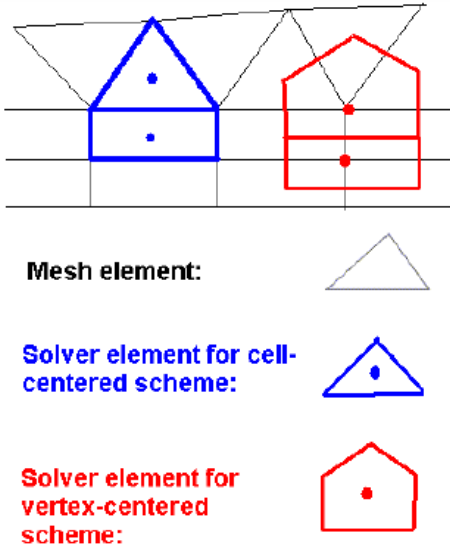


**Figure 21: Difference between cell centered- and vertex centered scheme [53].**

## 5.5. Meshing

A discretization scheme involves breaking down a geometry into smaller parts, such as elements, nodes or volumes. The resulting discretized geometry, which is now a group of several smaller computational regions, is termed a grid or a mesh. The approximate formulations of the governing equations, such as the NS, obtained through a discretization scheme are solved on the the discretized geometry or grid/mesh. This chapter is based on [41] and [53].

The accuracy of the simulation usually increases with increasing number of cells, i.e. with decreasing cell size. However, due to limitations imposed by the increased computer storage and run time some compromise in mesh size is nearly always inevitable.

How to best structure the grid depends on the type of flow, how it is modeled and the degree of resolution needed. A rule of thumb says the larger the number of elements, the better the solution accuracy will be, even though CPU effort and the total time of convergence will be higher as well. The resolution is limited by the user's available computer power. A best practice guideline for general meshing will not be given here; the mesh set up is a matter of experience and certain insight into CFD modeling. However, the final mesh set up used for the 10 MW blade is given in A.1. Each software producer provides users with documentation and some best practice guidelines, for example [53]. These guidelines will generally be followed.

There are five main types of 3D shapes a meshing program can choose from when making a mesh:

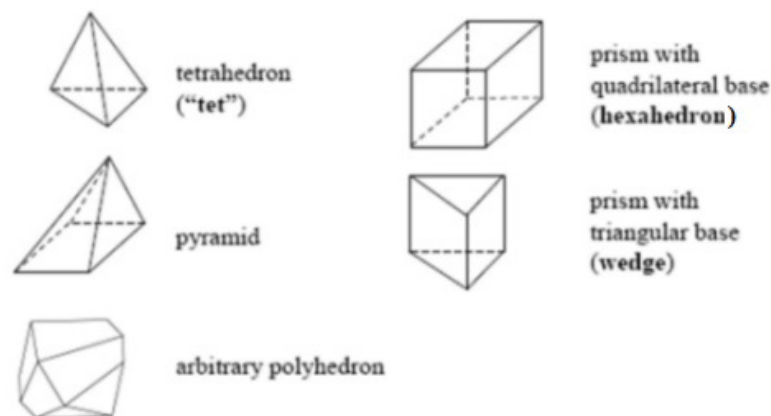
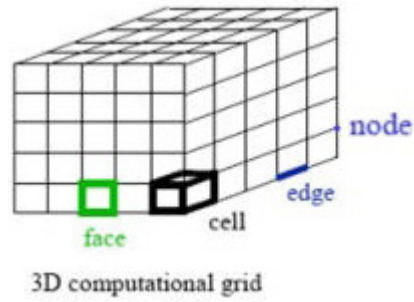


Figure 22: 3D shapes which a grid can contain [54].

CFX-Mesh creates linear tetrahedron, hexahedron and wedge/prism element shapes.



**Figure 23:** This figure shows the different entities associated with the grid [54].

### 5.6. Test cases

Three blades and two tunnels were attempted to run CFD on in the thesis; the 10 MW Offshore Wind Turbine case, case 1, the NREL Phase VI blade, case 2, and the tidal turbine case, case 3. For case 1 a blade was made by PhD Lars Frøynd in Matlab, and can be seen as a finished CAD model in Figure 24. The final version of all the models used can be viewed in the zip-file attachment to the thesis.

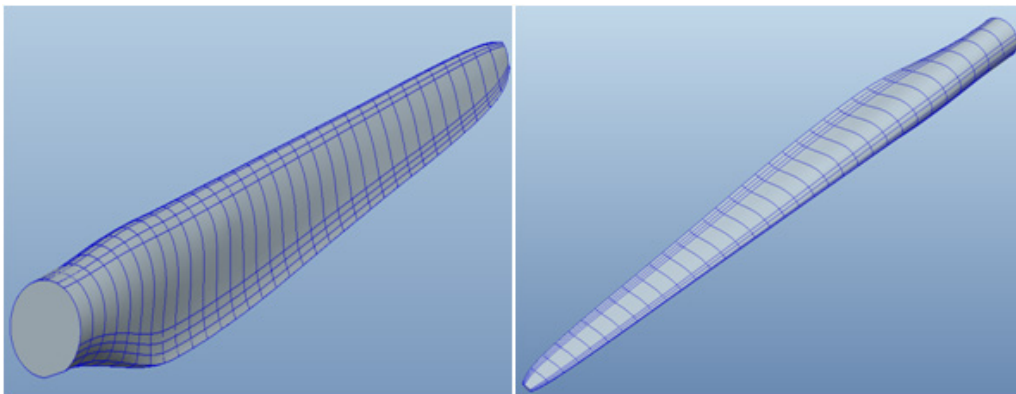


**Figure 24:** The blade for the 10 MW wind turbine. The blade to the right shows the pressure side, e.g. underside of the blade.

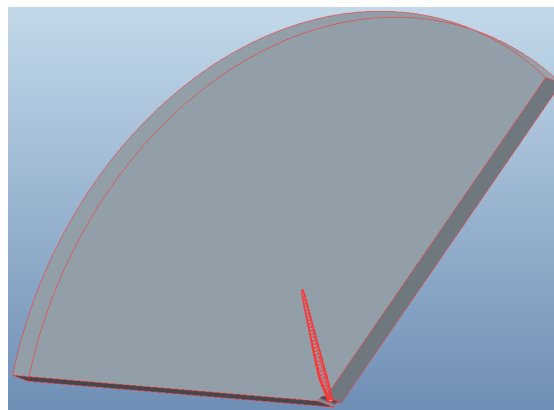


**Figure 25:** The cake in case 1 with the carved out 10 MW blade highlighted.

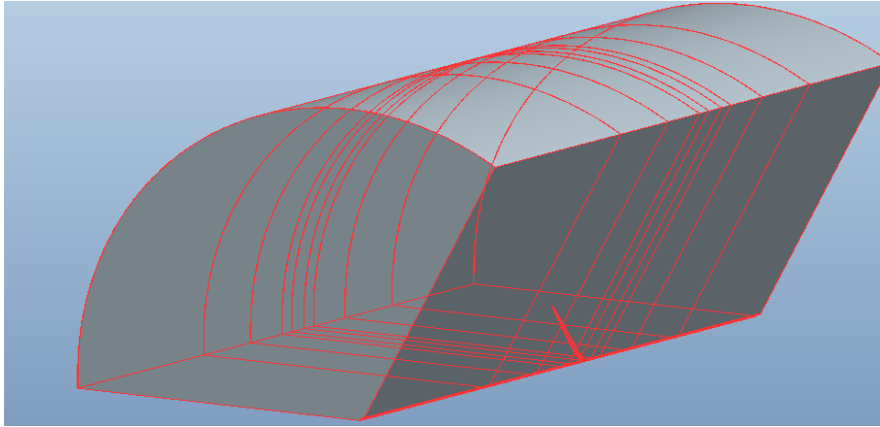


**Figure 26: The tunnel in case 1 resembling the surrounding of the wind turbine.**

Three different parts made by Pro Engineer for case 1, where the blade (Figure 24), the cake with the blade carved out (Figure 25) and the tunnel (Figure 26) demonstrates the construction parts of the system.

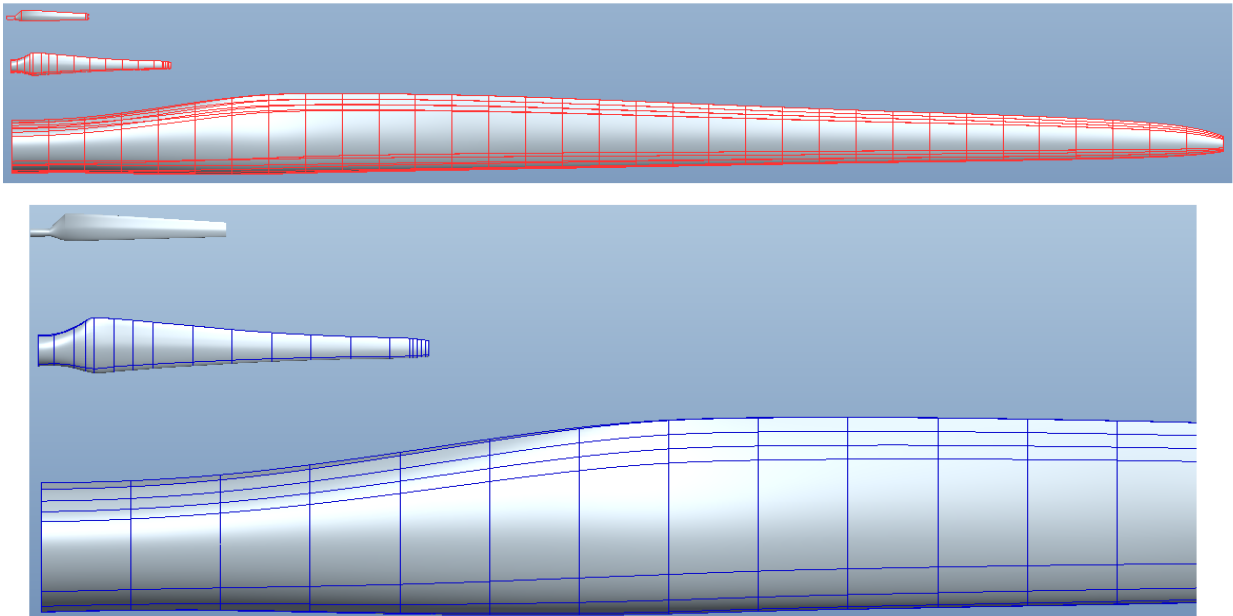


**Figure 27: Short blade, case 2, medium blade, case 3, large blade, case 1.**

There is a large difference in size between the cases in the thesis, with a close up at the bottom and a full size part at the top Figure 27. The NREL blade [14], the uppermost blade, is approximately 4.5 m long and the largest wind turbine blade in the world ever mounted on a wind turbine and used for experimental testing. Faudots [22] 1 MW tidal turbine blade, middle blade, is roughly 9 m long while Frøyds [40] 67.62 m long wind turbine blade (Figure 27, lower panel).

**Table 3: This table shows the dimensions of the different parts of each case.**

<b>Case 1</b>			
Dimensions [m]	Tunnel	Blade	Cake
Length	700	67,62	13
Width	-	5 max, 0,93 min	-
Radius	350	3,3 at root	210
<b>Case 2</b>			
Dimensions [m]	Tunnel	Blade	Cake
Length	-	4,58	-
Width	-	0,7 max, 0,36 min	-
Height	-	0,22 at root	-
<b>Case 3</b>			
Dimensions [m]	Tunnel	Blade	Cake
Length	500	8,92	4
Width	-	1,5 max, 0,35 min	-
Radius	90	0,8 at root	15

The tunnel for the tidal turbine can be seen (Figure 28) differs in lay out from the other figures in this chapter section because it was taken from ANSYS 12.1. The different colored sections represent different parts of the tunnel which will have different sizes of mesh elements. This was the final tunnel shape meshed after starting CFD calculations on tunnels not divided into any regions. After several runs it became clear that dividing the tunnel into multiple regions was necessary in order to save elements and therefore computer resources. Since all the actions occurs close to the blade it was not necessary to have the same fine mesh 300 m away from the blade as for 10 m away from the blade. Because this was discovered a bit late in the results from case 1 are with a tunnel of similar shape as Figure 26 but not divided in regions.

If one looks at the side view of the tidal turbine tunnel (Figure 28), the wind comes from the left into the tunnel and leaves to the right of the tunnel; this gives the wind a positive x direction. The lower part of the figure shows where the little cake piece in which the cake with the carved out blade is placed. A tunnel for case 2 was never made because a working mesh for the blade was never achieved.

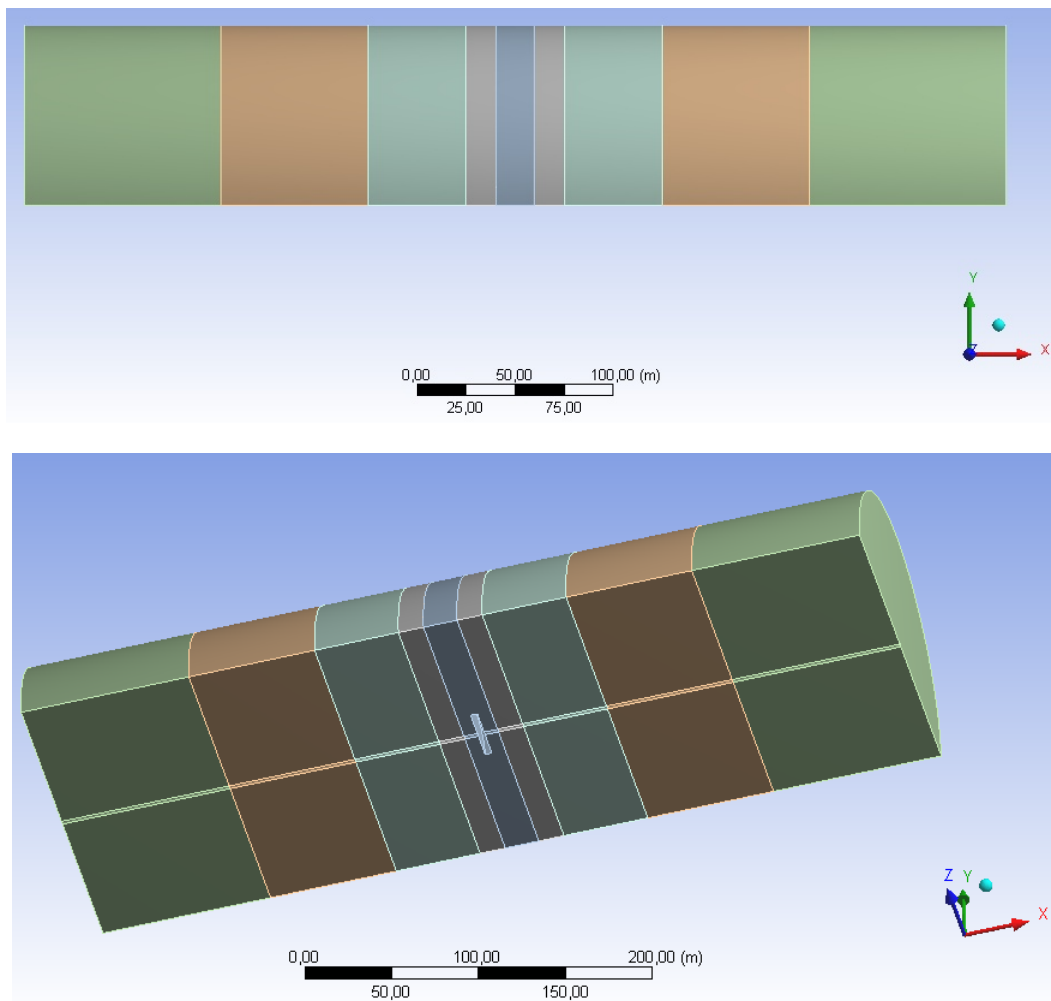


**Figure 28: Tunnel for the tidal turbine.**

Something worth mentioning in regards to CAD model drawing in Pro Engineer is that the program can automatically update coordinates for an object, and keep all its features, if the coordinate file does not exceed 650 points. The 10 MW blade as it is now is based on a coordinate file of 1223 points. Therefore a new three part CAD model of the blade should be made before further meshing is embarked on. It is suspected that one of the reasons why the author had difficulties achieving adequate meshes was that the smallest width of the trailing edge of the blade was 3 mm, while the length of the blade was 67.62 m. This means that both the CFX solver and meshing program had to resolve flows over an object that is almost 70 m long and has sides that are no wider than 3 mm. The author recommends that the blade in case 1 is constructed in such a way that the LE is no smaller than 1 – 1.5 cm long in order to minimize this difference.

### **5.6.1. Grid construction**

The CFX-mesher does not mesh directly on the blade, instead the blade needs to be carved out of a solid geometry which represents the surroundings. The main challenge of the present thesis was to achieve a mesh that is sufficiently fine close to the surface of the blade to detect the small fluctuations in the turbulence, and at the same time not ending up with an extreme

amount of elements that would exceed the computational resources available. In order to remedy these constraints, it was therefore decided to divide the process into two parts in order to provide a fine mesh close to the blade, and a coarser mesh further away from the blade. One part is consisting of a tunnel where the mesh cell length scale can vary in meters and another part, the cake with the carved out blade, where the mesh cell length scale can vary from millimeters close to the blade surface to centimeters a little further from the blade surface.

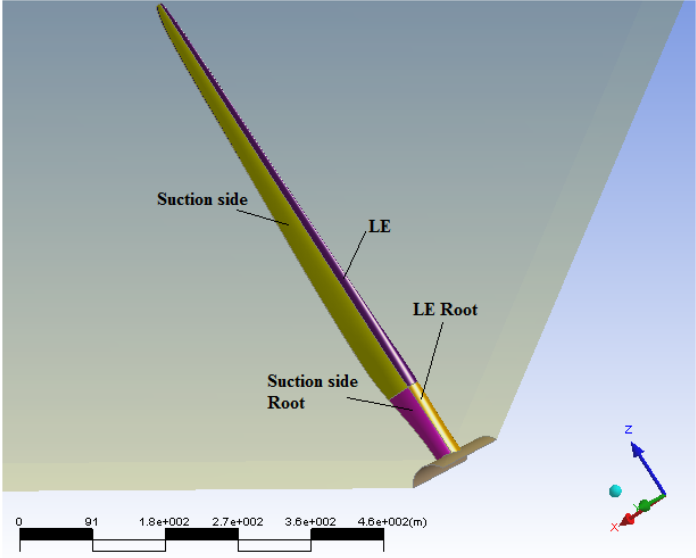


**Figure 29: Example of how the blade in case 1 is divided into regions.**

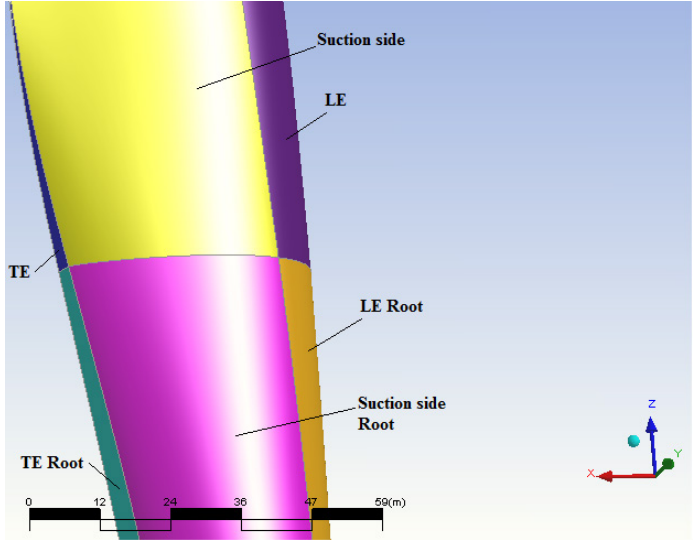


**Figure 30: Close up of blade in case 1 with regions marked.**

For both case 1 and 3 the blade was divided into different regions (Figure 29 and Figure 30). All the different regions had different cell size limits, these can be viewed in chapter 7. The blades were divided into 8 different regions; leading edge, LE, trailing edge, TE, suction side, pressure side, suction/pressure side for the root, LE and TE for the root and then the tip.



An example of a case 3 surface mesh can be seen in Figure 31. High velocity and pressure gradients close to the LE needs a finer mesh than the pressure or suction side of the blade. This jump in cell size from the LE area to the suction side can be a source of error in some cases, but since the CFD runs for case 3 both agreed with BEM results and experiments as we shall see later, this jump was accepted. A feature called inflation places layers on layers of the same grid very close to the surface of the blade to better resolve the boundary layer. All 8 regions of the blade shared the same inflation layers, see chapter 7.2.

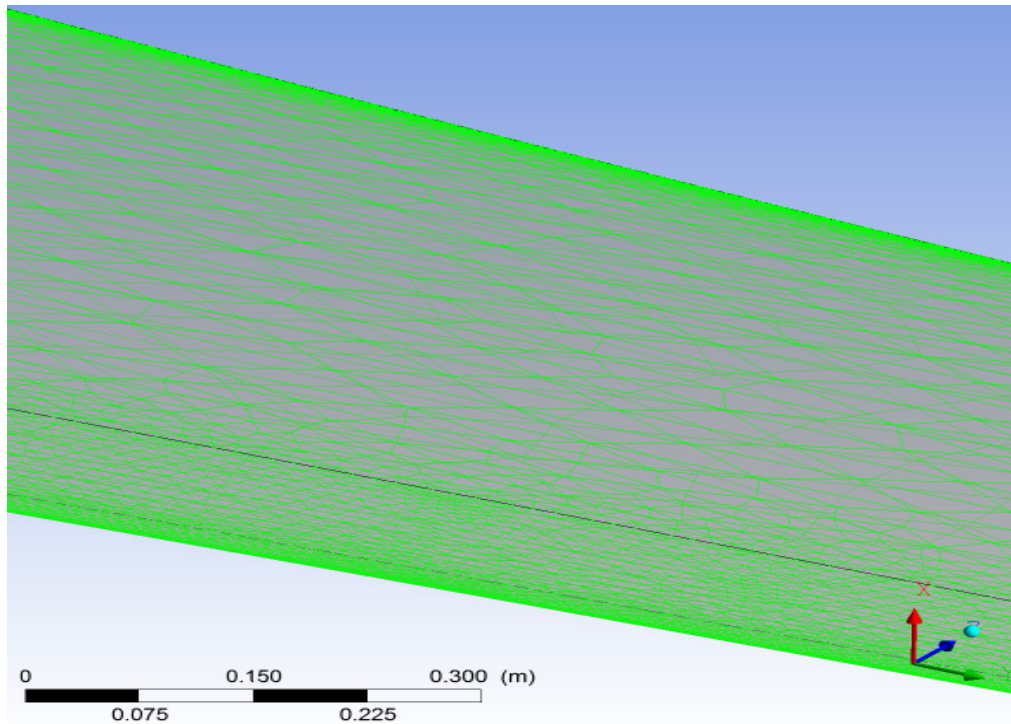


**Figure 31: Here the difference between in size of the surface mesh on the LE and the surface mesh on the suction side is visible.**

The tunnel in case 3 was first meshed with a feature in the CFX-mesher called “Sweep Method” [53]. This method was not successful in meshing the tunnel in case 1 so it was discarded in both cases due to the fact that it was desirable to use as identical methods as possible in case 1 and 3 for validation reasons.

### 5.6.2. Grid quality

The CFX solver calculates three important measures of mesh quality at the start of a run, these measures are *Mesh Orthogonality*, *Aspect Ratio* and *Expansion Factor* [53].

The Expansion Factor measures how poorly the nodal position corresponds to the control volume centroid, in other words it is the ratio of the largest to the smallest element volumes surrounding a node (Figure 32). A value less than 20 is desirable.



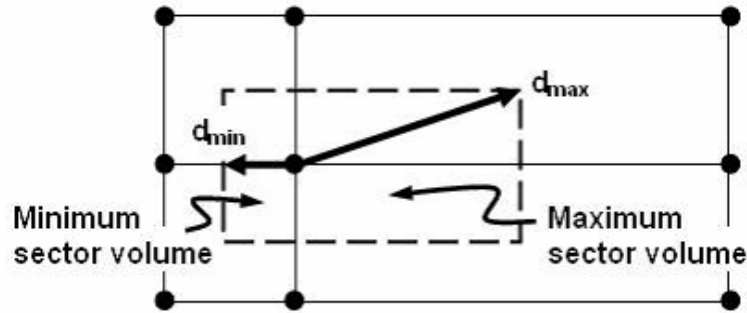


Figure 32: Example of *Expansion Factor* [55].

The aspect ratio is a measure of how stretched a control volume is (Figure 33). This ratio measures the maximum ratio of the largest to the smallest integration point,  $ip$ , areas for each element surrounding a node. A value less than 100 is desirable.

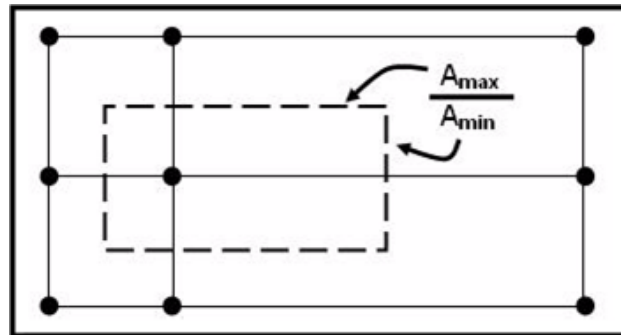


Figure 33: Example of *Aspect Ratio* [55].

Mesh Orthogonality measures alignment of the normal vector,  $n$ , of the  $ip$ -face and the node-to-node vector,  $s$ , (Figure 34). An orthogonality factor,  $n \cdot s$  of less than  $1/3$  is desirable and an orthogonality angle of  $90^\circ - \sin^{-1}(n \cdot s) > 20^\circ$  should be sought.

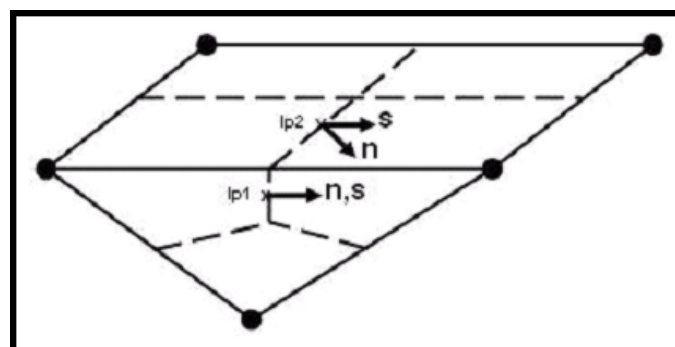


Figure 34: Example of *Orthogonality* [55].

The reason that the geometrical mesh quality is important is due to that a poor mesh can lead to sources of discretisation error, amplification of discretisation errors and difficulties solving linearised equations. All this can lead to convergence difficulties, unphysical influences and the runs may take longer time to finish.

# 6. Method

## 6.1. Wind turbine simulations/setup

The simulations all consists of the same two parts, one tunnel, with the cake carved out, called the *Stator* (Figure 35), and one cake with the blade carved out, called the Rotor (Figure 36). These two parts will be meshed separately in the CFX-mesher in ANSYS 12.1 before assembled in CFX-Pre. How CFX-Pre works is described in appendix A.2.10.

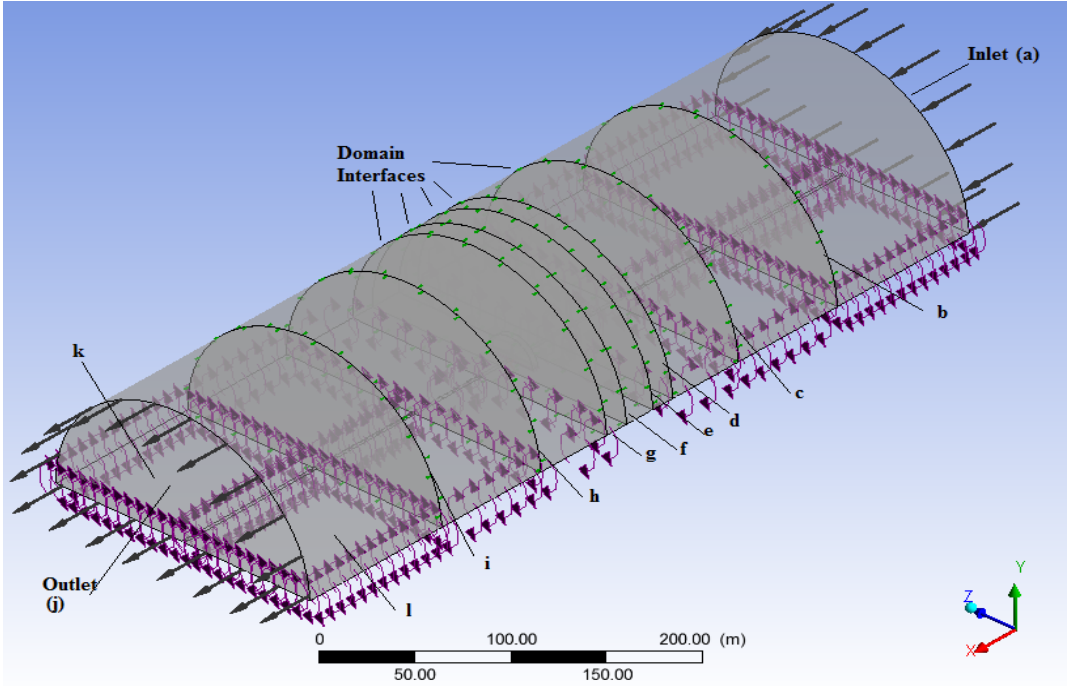


Figure 35: Different regions of stator in case 3.

Calculations in CFX showed that there were large jumps in cell size in the mesh close to the cut out part of the stator. Therefore the mesh had to be divided into smaller regions in the stator because large and abrupt changes in cell size can make it harder for the CFX run to converge and thereby give more inaccurate results. The tunnel was therefore divided into 9 different regions. See Table 8 in chapter 7.2 for the cell sizes of the different faces and regions.

The different interfaces between the regions in the stator and rotor, have been listed (Table 4). The interfaces between the 3D regions are called faces.

**Table 4: Different interfaces in stator and rotor.**

Face	Domain interface
a	Velocity inlet
b, c, d, e, f, g, h, i	General connection
j	Pressure outlet
k, l, m, n	Rotational periodicity
o, p, q	General connection

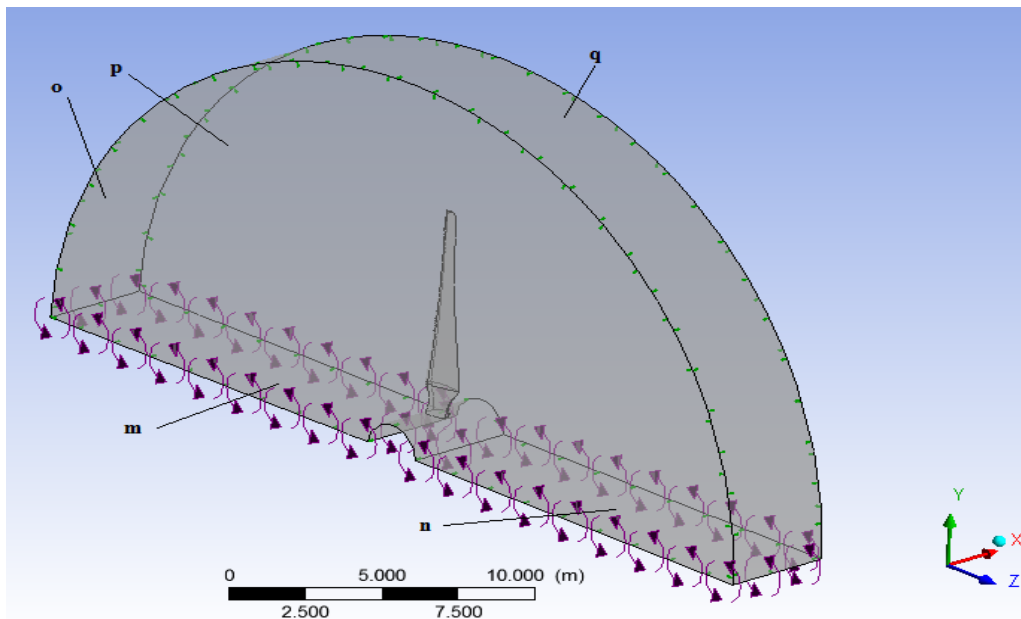


**Figure 36: Different regions of rotor in case 3.**

Domain *k* and *l* covers each half of the entire underside of the stator in all 9 regions. The rotational periodicity means that whatever comes out of domain *k* comes into domain *l*. This makes it possible to cut the domain in half and save many nodes in the mesh. In case 1 the stator and rotor domains are  $120^\circ$  degrees because we are operating with a 3 bladed turbine, see Figure 25 and Figure 26 on page 44, while in case 2 the stator and rotor are made for a 2 bladed turbine and therefore are  $180^\circ$ . The general connection which is most frequently used in Table 4 lets fluid pass from one region to another regardless direction and magnitude of velocity and pressure. At the velocity one specifies among other things the inlet velocity, turbulence intensity and pressure. In case 3 these settings are 2.5 m/s, 5% and 2.8 atm respectively. In case 1 these settings are 13.014 m/s, 7.4% and 1 atm.

See chapter A.2 for more details on the setup of the case 3.

In the simulations double precision is used due to the large difference in element size close to the blade compared to further away from the blade. For these large differences double precision is recommended instead of single precision [42].

## 7. Results and discussion

### 7.1. Validation

The performance of a wind turbine can be characterized by three main indicators, namely power, torque and thrust [6]. The power determines the amount of energy captured by the rotor. The torque determines the size of the gear box. The rotor thrust has great influence on the structural design of the tower. The most important of these three in regards to aerodynamics is power. Therefore this is the one of the key parameters that normally is compared between BEM calculations, experiments and CFD calculations. There are generally two ways of validating CFD calculations on wind turbine blades. The most secure way is to use a test rig for a wind turbine, then run experiments which measures the pressure distribution. From this pressure distribution lift can be calculated and torque and thrust can be found. Comparing these values to both the overall power production calculated in BEM and CFD results is considered the optimum way to validate CFD calculations. If no experiments are available, BEM results can be used to check if the CFD calculations can be trusted [19].

Due to the objectives outlined for the thesis, a plan was developed to make a mesh for a blade that already had been validated through both BEM and experiments and then adopt it, changing variables such as  $\Delta y$  to match our environment, to the 10 MW wind turbine. This method was assumed to give us a validated mesh and with further comparison to BEM results it was believed that the results obtained could be trusted.

The initial blade that was to be used for validation was the blade used in the NREL Phase VI campaign [14]. This blade had been used by a number of researchers around the world and there was a large amount of data available (chapter2).

Since the process of drawing a CAD model sufficient for CFD was time consuming the author tried to contact several international research groups that had used this NREL blade hoping to obtain a CAD model. Both NREL was contacted directly along with the authors of [10], [13], [16] and [17]. NREL did not have a CAD model of the blade, some were not willing to share their model and others had made their model with in-house software. The only who had a CAD model drawn in commercial available software and who was willing to contribute was Hansen [13].

Many of the researchers that had done CFD calculations on the NREL blade had used their own in house software in both the drawing process and the mesh generation. Hansen [13] had meshed the blade in a commercial available mesh program called CCM+ and found that a structured mesh of 14 million nodes was needed in order to obtain matching results to the experimental data of the NREL blade. A mesh this fine for a 5 meter blade could not be implemented on the 67.62 m long 10 MW blade because it would result in a mesh containing 189 million elements and would require immense computational power. Efforts were then made to start building a mesh for the NREL blade with CFX 12.1. After considerable efforts a mesh was not obtained for the NREL blade. According to Hansen many other researchers had also experienced difficulty in meshing the NREL blade and he estimated that close to 80% of his work load in his thesis was spent trying to achieve a working mesh. He recommended

trying to mesh in ICEM, a commercial meshing program which gives the user more control over certain aspects of the meshing process but has the disadvantage of having a higher user interface than the CFX-mesh method. This avenue was briefly pursued but was disregarded after some time due to the considerable effort it would take to master the software well enough to achieve a sufficient result.

Carcangiu [19] used BEM to validate his mesh and CFD calculations, and achieved good aerodynamic results with this GAMBIT produced grid. Gambit is also a commercially available meshing software. The next logical step for validation of the 10MW blade was to attempt to make a mesh with the CFX-Mesher method in ANSYS 12.1 and compare it to BEM results for validation. This mesh needed to be made only through trial and error. After much effort and time it became clear that due to the large size of the turbine the mesh became very large, in the order of 18 – 25 million elements. For every CFD run it could take up to 30 hours or more in order to achieve convergence. Many runs never achieved convergence and were terminated after two to three days. Also changing the parameters in the mesher and starting the mesh generation could take up to 8 hours because the CFX-Mesher only uses one logical entity, one core, of the computers 8 available to mesh. The best  $C_p$  obtained was 0.08 which was far too low compared to the  $C_p$  the turbine should have according to BEM, which was 0.49. It became obvious that this approach was not ideal and a new approach of validating the mesh needed to be found.

Based on the above a third validation path was chosen to consist of the in-house CFD calculations, BEM results and experiments by Faudot [22]. Since Faudots tidal turbine had rotor blades of 10 m it would take less time to test out different mesh configurations and find the ideal number and sizes of the different elements, instead of continuing with validation method two. This paper is based on a tidal turbine and not a wind turbine. In other words the mesh achieved would be validated for water and not for wind simulations. There was a question if a mesh made for an object in water would give accurate results for an object in air. The kinematic viscosity for water is 50 times higher than that of air, in other words air behaves like syrup compared to water. It was concluded that as long as the Reynolds number are comparable (Figure 37) this validation method would be applicable, because Reynolds number takes the kinematic viscosity into account (chapter 4.4.1). According to [32] flows over airfoils can be considered fully turbulent over  $2 - 5 \times 10^5$ , there will always be a small area at the leading edge where the Reynolds number is within the transition layer, but the larger the Reynolds number is, the smaller this area is. Both cases 1 and 3 are well above  $5 \times 10^5$  therefore the mesh in case 3 should work as a validated mesh for case 1 (Figure 37).

Since the CFD calculation, BEM and experiments of Faudot all matched well of each other (chapter 2.5), it was concluded that if the BEM calculations of case 1 matched the CFD calculations achieved with the tidal turbine mesh adapted to the 10MW wind turbine rotor, the results of the CFD in case 1 could be trusted. Several test cases of the tidal turbine were run in CFD in good agreement with both BEM results and the experimental results. In

Table 9 on page 61 the results of different grids can be viewed. The CAD model of the 1 MW tidal turbine was drawn in Pro Engineer following the same method as was applied when the

10 MW wind turbine CAD model was drawn. See A.1 for more details on the drawing process.

However, problems occurred when trying to implement the mesh achieved on the tidal turbine on the wind turbine. The meshing size parameters for the different regions of the blade did not adequately resolve the CAD model and therefore a mesh was not produced. Then the cell sizes were changed slightly so they still would be within a level that should produce a reasonable resemblance to BEM results but the mesher still refused to produce a grid. Changing the meshing parameters further would make the grid deviate too much from the idea behind the validation process so we would be back to the second validation method of trial and error meshing.

The computer used for the simulations was a Intel Xeon 2 x CPU E5440, 2.83GHz, 16 BG RAM, 64-bit operative system (Windows 7).

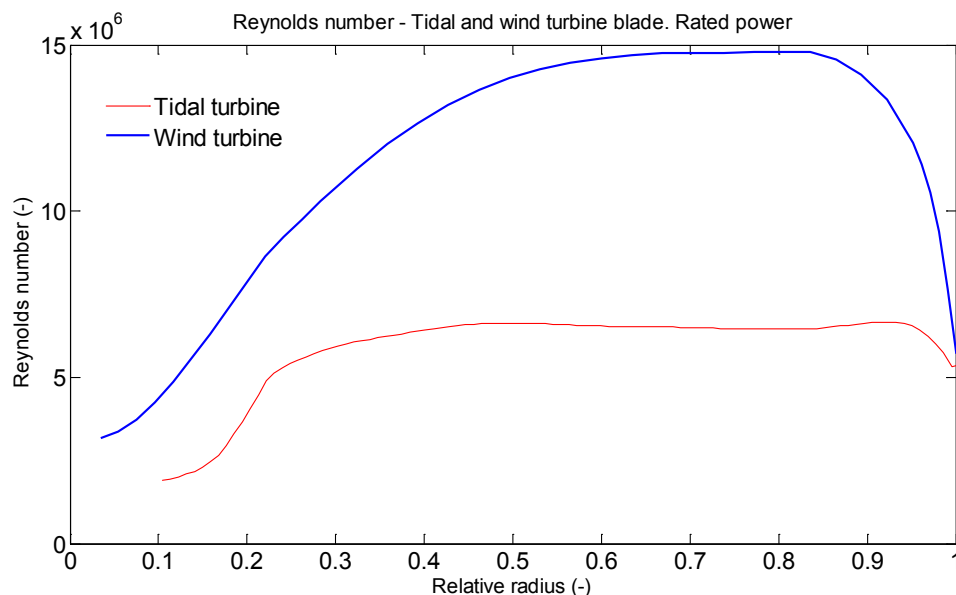


Figure 37: Reynolds number as a function of relative blade length for case 1 and case 3.

## 7.2. Validation runs

The first validation method did not produce any mesh; therefore the result from this method was that it was not possible to mesh the CAD model of the NREL blade at hand with the CFX-Mesher in ANSYS 12.1. If the results from the experiments of the NREL Phase VI campaigns still wants to be pursued as a validation method a new CAD model needs to be made and another mesh method should also be considered, the ICEM or the mesh generator in ANSYS 13 are recommended methods. ICEM is recommended because it offers the user more detail control in grid generation. The mesher in ANSYS 13 is recommended because it has the advantage of using more of the computers logical entities, partitions, in the process. It can therefore generate a mesh faster than the CFX-mesher in ANSYS 12.1, which is an advantage because of the number of elements involved. Meshing with multiple partitions can also be done in ICEM. Also EDR, ANSYS Customer support in Norway, can provide valuable help in both ANSYS 13 and ICEM.

The second validation method was disregarded due to the long time needed to produce and test a mesh. After many trials with different sizes of mesh the highest  $C_p$  achieved was 0.08, which is almost 80% below the estimated  $C_p$  of 0.49 given by the BEM. One of the problems with this mesh was large jumps in cell size in the transition between the tunnel and the cake. In the physical discussion following the mesh is assumed to be correct for case 1. The flow separated almost along the whole blade in case 1 (Figure 39 page 58). This run was done before the decision to divide the stator into regions to ensure a smoother transition in elements size closer to the blade. Only from 55 m to the tip the flow was attached. Therefore the low  $C_p$  was not a surprise when over 80% of the wing experiences separated flow. The  $y^+$  value was quite good, with a value of 2 – 4 along most of the blade with an average value of 3.89, so the SST  $k$ - $\omega$  model should here be able to calculate the flow directly and not through modeling. It has been seen in [20] by N.N. Sørensen that the  $k$ - $\omega$  SST model has had problems in predicting the onset of separation for Reynolds numbers under 3 million. This should not be a problem when we are operating at as high Reynolds numbers as we are, but close to the LE the Reynolds number will be low so a poor mesh combined with any problems the  $k$ - $\omega$  SST model might have with the onset of separation might contribute to the low  $C_p$  calculated.

The angle of attack given by the BEM and the angle of attack calculated by CFX simulations do not match well (Figure 38). Depending on the airfoil the flow normally separates between angles of attack between  $10^0 - 20^0$  [31]. From Figure 39 it is evident that the flow separates between 50 – 55 m, looking at Figure 38 the angle of attack in this area lays around  $15^0$  which would suggest that the air particles which have been slowed by the viscous forces cannot overcome the relatively large adverse pressure gradient, and the boundary layer separates. The separation always occurs first at the root because of the low Reynolds number regime in the area and spreads out towards the tip of the blade giving a three dimensional effect [32]. Since the angle of attack at rated conditions is too high and causes separation the induction factors,  $a$  and  $a'$ , have been calculated wrongfully in the BEM and as a result the design of the 10 MW blade is poor. In reality this might not be the case, but the author is here drawing conclusion with the assumption the mesh is correct and the results from the CFX calculations can be trusted.

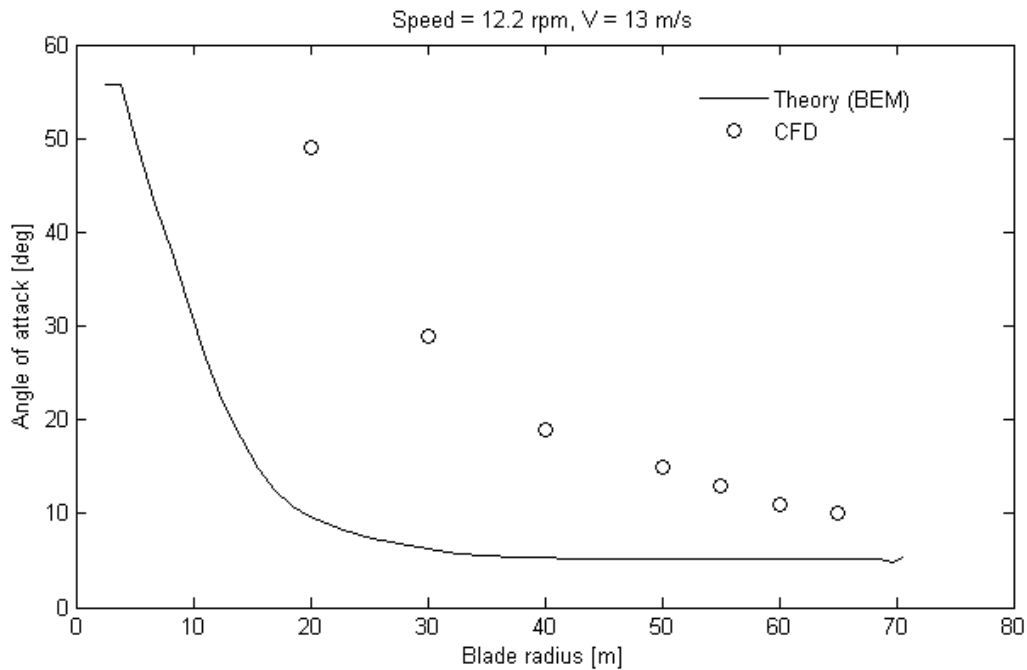


**Figure 38: Angle of attack from CFD and BEM.**

The root of a wind turbine experiences flow separation at much lower Reynolds numbers than an airfoil due to large adverse pressure gradient the flow encounters because of the blunt configuration of the cylinder. Seeing that the root for the 10 MW blade has both a large radius (3.3 m) and is very long (roughly 8 m to the first airfoil), the separated flow which is pushed outwards towards the tip due to centrifugal effects, might influence the flow further towards the tip in such a way that it separates more easily than it would on a smaller blade with a smaller root section. But this is only speculations from the author.

A mesh of 21 million for the cake and 8 million for the tunnel, with the tunnel now being divided into different regions was tried, run b (Table 6). Also the mesh in the cake had been refined so that there was a steady decrease in cell size close to the blade. This mesh was believed to provide a better  $C_p$ , but was not successfully run due to insufficient computer memory; the available memory at the time was 16 GB.



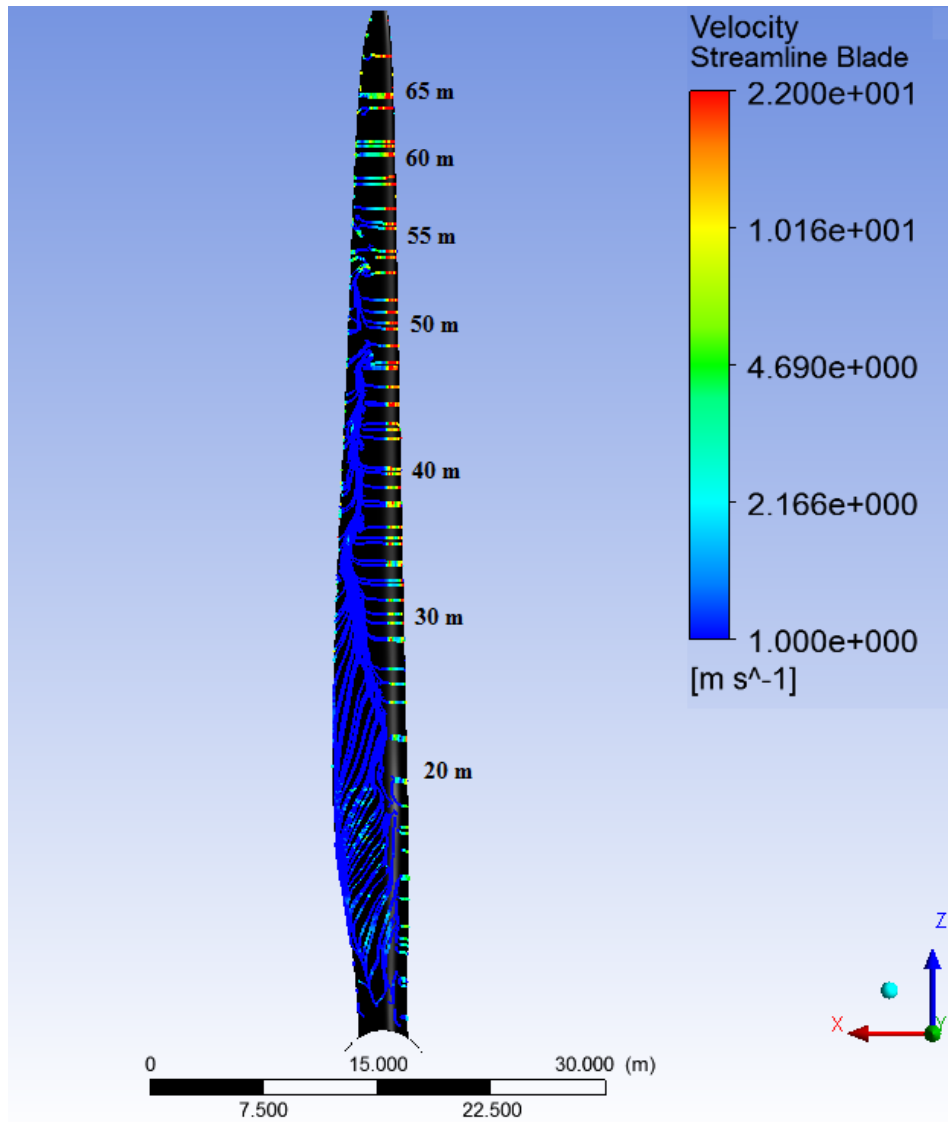


Figure 39: Streamlines for 10 MW wind turbine run a, suction side of blade.

Table 5: Parameters for the inflation layers of case 1 run a and run b.

Inflation Mesh 1		Inflation Mesh 2	
First Layer Thickness	yes	First Layer Thickness	yes
Layers	15	Layers	15
Expansion Factor	1,35	Expansion Factor	1,25
Defined by First Layer	y+	Defined by First Layer	y+
Reynolds number	$14 \times 10^6$	Reynolds number	$15 \times 10^6$
Reference length	1 m	Reference length	1 m
First Prism Height	$4,139 \times 10^{-6}$	First Prism Height	$3,882 \times 10^{-6}$
Reference length	1 m	Reference length	1 m

**Table 6: Meshes used in run a (mesh 1) and run b (mesh 2) of case 1.**

Dimension [m]	Mesh 1		Mesh 2		Radius of influence mesh 2 ; expansion factor
	Min	Max	Min	Max	
Default Body Spacing	5	-	1	-	-
Default Face Spacing	0,01	3	0,02	0,5	-
Root pressure/suction	0,03	0,1	0,03	0,1	No
Root LE	0,03	0,1	0,03	0,1	No
Root TE	0,01	0,05	0,01	0,05	No
Blade suction side	0,005	0,025	0,005	0,025	0,2 ; 1,2
Blade pressure side	0,0025	0,075	0,0025	0,075	0,2 ; 1,2
Tip	0,005	0,01	0,005	0,01	No
TE	0,005	0,03	0,0005	0,03	No
LE	0,005	0,05	0,005	0,05	0,2 ; 1,1
Faces cake suction/pressure	-	-	0,2	0,4	No
Outer edge cake (radius edges)	-	-	0,1	0,5	No
Hub	-	-	0,1	0,4	No
Edge spacing	0	-	0	-	No
Total number of elements	18846665		21283379		
Elements added compared to mesh 1	-		13 %		
Elements saved in %	-		-		
$C_p$	0,08		?		

The third validation method, case 3, seemed to be the most promising since a working mesh was achieved and many runs were possible. 7 meshes were made and run through CFX. Mesh 1b, 2, 3I and II and 4 (Table 9) were run with double precision; this enables the numerical solver to use more decimals in the calculations. This option takes more time but is recommended to use when the ratio between the smallest and largest element is large [35]. This option can provide more numerical stability and therefore easier convergence. To save time meshes 1a and 0 were run with single precision in the solver and it was found that double precision took up to 30 % more time and did not provide easier convergence nor any difference in the result.

In Table 7 the parameters for the inflation which determines  $y^+$  value in case 3 can be found. The  $y^+$  differed from 20 to 150 along the blade. This means that the SST  $k-\omega$  model models, or in other words guesses, how the two innermost layers behave according to the CFD theory in chapter 5. Faudot [22] ran a simulation with a  $y^+$  value varying from 2 to 5 on the blade, but the  $C_p$  obtained did not differ much from the calculations with a larger  $y^+$ .

The scaled down model used in the experiments used “trippers” close to the leading edge to ensure a fully turbulent boundary layer. Mesh 1a and 1b gave a  $C_p$  of 0.4273 which matches the experimental results obtained by Faudot perfectly. This is most likely due to sheer luck because the  $C_p$  in case 3 should be 1-2% lower than the BEM results due to the fact that CFD includes three dimensional results, while the BEM does not. In retrospect a mesh with element sizes between mesh 1a and mesh 0 could have been tested in order to achieve a  $C_p$  closer to 0.4 which would probably be a more realistic value for  $C_p$  than 0.4273.

**Table 7: Inflation parameters for case 3.**

Inflation	
First Layer Thickness	yes
First Prism Height	0.0007
Layers	10
Expansion Factor	1,4

**Table 8: Tunnel dimensions case 3.**

Dimension [m]	Tunnel 1		Tunnel 2	
	Min	Max	Min	Max
Default Face Spacing	1,3	25	1,755	33,75
Default Body Spacing	25	-	33,75	-
Side a, j	3,5	5	4,725	6,75
Side b, i	2,5	3,5	3,375	4,725
Side c, h	1,5	2,5	2,025	3,375
Side d, g	1	1,5	1,35	2,025
Side e, f	0,5	1	0,675	1,35
Sides of carved out cake	0,3	0,5	0,405	0,675
Top i-j, a-b	3	5	4,05	6,75
Top b-c, h-i	1,5	3	2,025	4,05
Top c-d, g-h	1	1,5	1,35	2,025
Top d-e, f-g	0,7	1	0,945	1,35
Top e-f	0,5	0,7	0,675	0,945
Top carved out cake	0,25	0,4	0,3375	0,54
Total number of elements	4432811		2294814	
Elements saved compared to tunnel 1			2137997	
Elements saved in %			48 %	
$C_p$	0,4327		0.391	

As a sensitivity test for tunnel mesh in case 3 (Table 8) two meshes were tested. As one can see 48% elements can be saved by choosing tunnel 2 instead of tunnel 1, with the  $C_p$  dropping to 0.391. The dimensions of tunnel 2 could therefore be tried out on case 1 because of the huge amount of elements that can be saved as a first test to see if the  $C_p$  is in the neighborhood of being correct. Then if a mesh starts to give a  $C_p$  in the vicinity of 0.4 a decrease in tunnel cell elements can be tested to see if the  $C_p$  matches the BEM results to a more realistic degree.

Table 9: The different meshes tested in case 3.

Dimension [m]	Mesh 0		Mesh 1a		Mesh 1b		Mesh 2		Mesh 3, I		Mesh 3, II		Mesh 4	
	Min	Max	Min	Max	Min	Max	Min	Max	Min	Max	Min	Max	Min	Max
Default Body Spacing	1,12	-	1,6	-	1,6	-	1,76	-	1,76	-	1,76	-	1,92	-
Default Face Spacing	0,0019	0,1	0,002	1	0,002	1	0,002	1,1	0,002	1,1	0,002	1,1	0,003	1,45
Root pressure/suction	0,014	0,0385	0,02	0,055	0,02	0,055	0,022	0,061	0,024	0,066	0,026	0,066	0,029	0,08
Root LE	0,007	0,028	0,01	0,005	0,01	0,005	0,011	0,044	0,012	0,048	0,013	0,052	0,015	0,058
Root TE	0,0056	0,016	0,008	0,02	0,008	0,02	0,009	0,022	0,01	0,024	0,01	0,026	0,012	0,029
Blade pressure/suction	0,007	0,028	0,01	0,04	0,01	0,04	0,011	0,044	0,012	0,048	0,013	0,052	0,015	0,06
Tip	0,0021	0,007	0,003	0,01	0,003	0,01	0,003	0,011	0,004	0,012	0,004	0,013	0,005	0,015
TE	0,00035	0,0014	0,0005	0,002	5E-04	0,002	6E-04	0,002	6E-04	0,002	7E-04	0,003	0,008	0,003
LE	0,0014	0,0035	0,002	0,005	0,002	0,005	0,002	0,006	0,002	0,006	0,002	0,007	0,003	0,008
Hub	0,07	0,28	0,1	0,4	0,1	0,4	0,11	0,44	0,12	0,48	0,13	0,52	0,145	0,58
Edge spacing	0,0035	-	0,005	-	0,005	-	0,006	-	0,006	-	0,006	-	0,007	-
Total number of elements	3240215		2512549	2512549	2512549		2356278		2349012		2122262		1845644	
Elements saved compared to mesh 1	(-)727666		-	-	-		156271		163537		390287		666905	
Elements saved in %	-28,9		-	-	-		6,219619995		6,508808385		15,533508		26,54296493	
C <sub>p</sub>	0,345		0,4273	0,4273	0,4273		0,4325		-		0,4422		0,46	

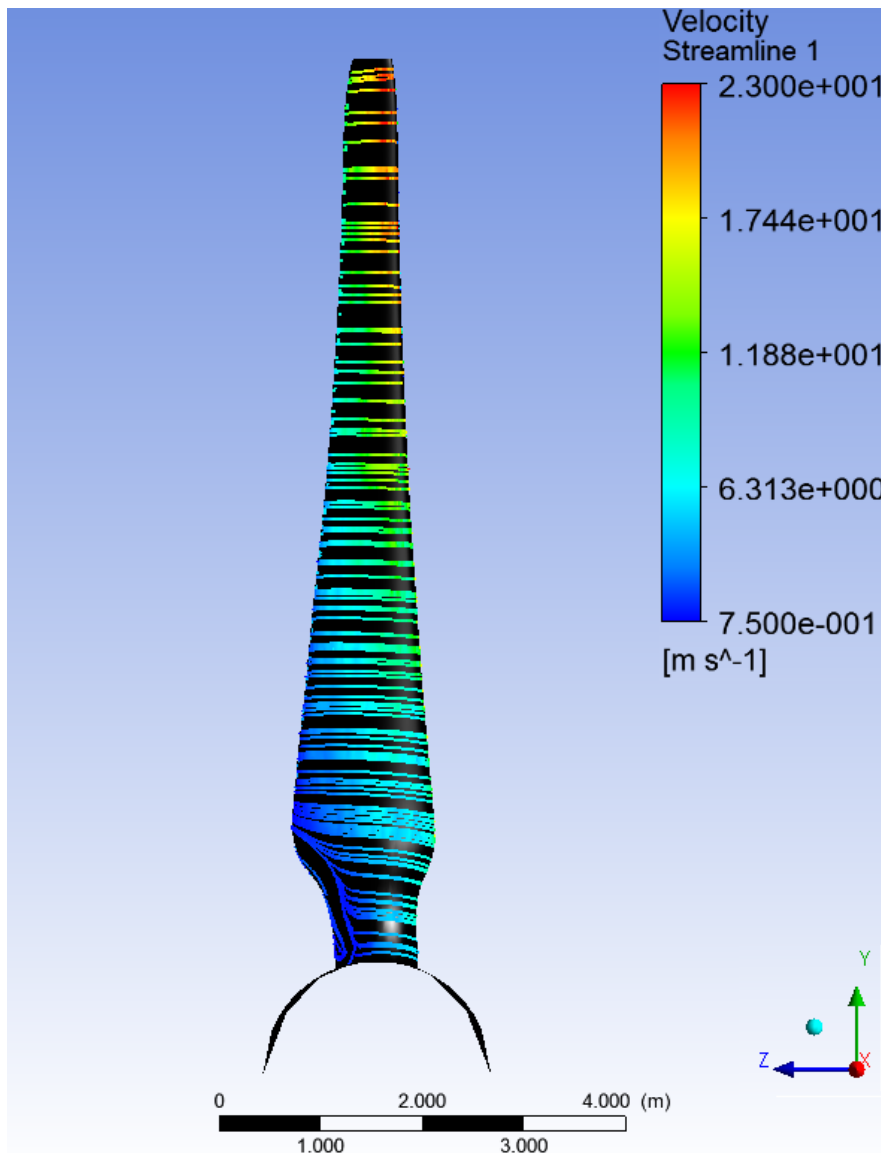


**Figure 40: Streamlines of rated power for 1 MW tidal turbine.**

Figure 40 serves as an example of how streamlines over a wind or tidal turbine should look like. Here one can observe that the flow is attached over the entire wing except close to the root, which is natural due to separation always occurs more easily close to the root due to the low Reynolds number in this region and the blunt shape of the cylinder.

### 7.2.1. Grid Quality case 3

The most important mesh metrics for the CFX solver were mentioned in chapter 5.6.2. In case 3 the values of Aspect Ratio, Mesh Expansion Factor and Mesh Orthogonality varied in quality but were overall quite good.

The “!” is used if the value is questionable, “ok” is considered acceptable and “OK” are good values (Table 10). This table shows that aspect ratios of both the Rotor and the Stator are good. The largest expansion factor is questionable for both domains while the minimum orthogonal angle is questionable the Rotor, but ok for the stator.

Table 10: Mesh statistics for case 3.

Mesh Statistics									
Domain Name	Orthog. Angle			Exp. Factor			Aspect Ratio		
	Minimum [deg]			Maximum			Maximum		
Rotor	6.3	!		882	!		375	OK	
Stator	33.7	ok		42	!		9	OK	
Global	6.3	!		882	!		375	OK	
	%!	%ok	%OK	%!	%ok	%OK	%!	%ok	%OK
Rotor	<1	85	15	2	21	77	0	0	100
Stator	0	1	99	<1	7	93	0	0	100
Global	<1	33	67	1	13	86	0	0	100

Domain Name : Rotor

```

Total Number of Nodes           =      511958
Total Number of Elements         =      2512860
  Total Number of Tetrahedrons    =      2325105
  Total Number of Prisms          =      158452
  Total Number of Pyramids        =       29303
Total Number of Faces           =      98081

```

Domain Name : Stator

```

Total Number of Nodes           =      835125
Total Number of Elements         =      4432811
  Total Number of Tetrahedrons    =      4432811
Total Number of Faces           =      304446

```

Global Statistics :

```

Global Number of Nodes           =      1347083
Global Number of Elements         =      6945671
  Total Number of Tetrahedrons    =      6757916
  Total Number of Prisms          =      158452
  Total Number of Pyramids        =       29303
Global Number of Faces           =      402527

```

The second part from the top down shows in percent how many of the nodes are questionable, ok or good. The expansion factor has globally, in both Rotor and Stator domain, over 86% good elements; they have together a total of 1% questionable elements with questionable expansion factor. The minimum orthogonal angle is questionable globally in less than 1% of the elements, while the aspect ratio is good in all elements for both rotor and stator. This mesh can be considered adequate and the results from the CFX runs can be trusted, especially since they have been validated against both experimental data and BEM results. The “Total Number

of Elements” is in the Rotor and Stator domain is approximately 6.9 million. The residuals in case 3 converged well and target value of  $1 \times 10^{-5}$  was achieved.

Since this mesh is considered adequate for CFD other aerodynamic effects like stall and tip loss, a three dimensional effect, can be investigated in case 3 along with the waves interaction with the turbine.

### 7.2.2. Grid Quality case 1

The mesh statistics for the run which gave the highest  $C_p$  value is shown in Table 11, the highest value obtained was 0.08. It was observed that abrupt changes in cell size occurred close to the blade so a radius of influence were added to the LE and the suction and pressure side of the blade in hope to minimize this abrupt cell size change. The mesh statistics for this grid can be viewed in Table 6. The aspect ratio of the rotor is questionable while this ratio is good for the stator. The largest expansion factor is questionable for both domains while the minimum orthogonal angle is questionable the Rotor, but ok for the stator. The expansion factor has globally over 86% good elements; they have together a total of 5% of the elements with a questionable expansion factor. The minimum orthogonal angle is questionable globally in less than 1% of the elements. The aspect ratio is questionable in 21% of the elements globally, it can be seen that all of these questionable elements lies in the rotor domain.

Case 1 run b did not produce any result file because of insufficient RAM, the runs were attempted on a computer of 16 GB RAM, 32 GB RAM is probably what is necessary in order to run this mesh. There were negative elements present in the mesh so it is possible this might have given convergence difficulties if enough RAM had been in place. Both the minimum orthogonal angle and the maximum expansion factor were slightly better in the mesh for run b (Table 12) while the aspect ratio had deteriorated. The residuals in this case did not converge to the target value of  $1 \times 10^{-5}$ .

One way to save node would have been to make the rotor in case 1 with a smaller radius,  $1.5R$ ,  $R$  being the length of the blade in case 1, instead of  $4R$ . Also the stator both in front and behind could have consisted of two parts, one inner tunnel with radii of  $1.5R$  and one outer part with a radius of  $4R$ . This would have opened the possibility for a finer grid from the inlet all the way to the outlet of the stator in  $1.5R$  tunnel, while in the outer parts of the stator the grid could have been coarser. This would likely have saved nodes in the grid with no negative effect on the result.

Table 11: Mesh statistics for case 1 run a.

Mesh Statistics										
Domain Name	Orthog. Angle			Exp. Factor			Aspect Ratio			
	Minimum [deg]			Maximum			Maximum			
Rotor	6.8	!	!	84402	!	!	125865	!	!	!
Stator	25.1	ok	!	93	!	!	8	OK	!	!
Global	6.8	!	!	84402	!	!	125865	!	!	!
	%!	%ok	%OK	%!	%ok	%OK	%!	%ok	%OK	
Rotor	<1	70	30	6	8	86	25	9	66	!
Stator	0	1	99	<1	11	89	0	0	100	!
Global	<1	59	41	5	9	86	21	8	71	!

Domain Name : Rotor

```

Total Number of Nodes           = 4118360
Total Number of Elements        = 18846665
  Total Number of Tetrahedrons   = 16393747
  Total Number of Prisms         = 2343508
  Total Number of Pyramids       = 109410

Total Number of Faces           = 365134

```

Domain Name : Stator

```

Total Number of Nodes           = 790185
Total Number of Elements        = 4341614
  Total Number of Tetrahedrons   = 4341614

Total Number of Faces           = 182902

```

Global Statistics :

```

Global Number of Nodes          = 4908545
Global Number of Elements       = 23188279
  Total Number of Tetrahedrons   = 20735361
  Total Number of Prisms         = 2343508
  Total Number of Pyramids       = 109410

Global Number of Faces          = 548036

```



Table 12: Mesh statistics for case 1 run b.

Mesh Statistics										
Domain Name	Orthog. Angle	Exp. Factor			Aspect Ratio					
	Minimum [deg]	Maximum			Maximum					
Rotor	8.2 !	590039 !			131707 !					
Stator	24.9 ok	72 !			9 OK					
Global	8.2 !	590039 !			131707 !					
	%!	%ok	%OK	%!	%ok	%OK	%!	%ok	%OK	
Rotor	<1	64	36	5	9	86	28	11	61	
Stator	0	1	99	<1	10	90	0	0	100	
Global	<1	53	47	4	9	87	23	9	68	

Domain Name : Rotor

Total Number of Nodes = 4768216

Total Number of Elements = 20334392

    Total Number of Tetrahedrons = 16897573

    Total Number of Prisms = 3315584

    Total Number of Pyramids = 121235

Total Number of Faces = 660341

Domain Name : Stator

Total Number of Nodes = 1048409

Total Number of Elements = 5842734

    Total Number of Tetrahedrons = 5842734

Total Number of Faces = 185976

Global Statistics :

Global Number of Nodes = 5816625

Global Number of Elements = 26177126

    Total Number of Tetrahedrons = 22740307

    Total Number of Prisms = 3315584

    Total Number of Pyramids = 121235

Global Number of Faces = 846317

## 8. Further strategy

Based on the present Master thesis, it appears that C CFD computations on the 10 MW offshore wind turbine is a daunting task. Future success will be dependent upon upgrading of infrastructure and strengthening of cooperation between the research environment at NTNU and the leading international research teams on CFD on wind turbines.

It would be of great value to students and researchers that further CFD computations (as on case 1) are being run on super computers. They are set up for CFD calculations. Alternatively this challenge could be met by upgrading some key computer equipment locally at the Water Power Lab of NTNU. Following is a set up of some computer hardware that may work:

The most expensive alternative (45 000 NOK) consists of

- CPU: 2 x Intel Xeon X5680 3.33 GHz LGA 1366, 4.8 GT/sec (6 core)
- RAM 72GB: 3 x DDR3 1333MHz 24 GB KIT ECC/REG
- Mother Board: 1 x ASUS Z8PE-D18, 2 x Socket - 1366
- Hard Drive: 1 x Solid State Drive, Intel SSD 510 Series 250GB 2.5"

The more inexpensive alternative (33 000) NOK consists of

- CPU: 2 x Intel Xenon X5650 2.66Hz LGA 1366, 4.8 GT/sec (6 core)
- RAM 48GB: 6 x DDR3 1333MHz 6 GB KIT REG/ECC
- Mother Board: 1 x ASUS z8PE-D18, 2 x Socket – 1366
- Hard Drive: 1 x Solid State Drive, Intel SSD 510 Series 250GB 2.5"

There are numerous scientific questions then opening up. When a validated mesh is achieved for the 10 MW blade, CFD can be used further to examine a non uniform vertical velocity profile. Naturally different parts of the blades see different wind, both in strength and direction. How much power is lost because of the increase in size and how do the waves change the vertical velocity profile are important questions to address?

After this has been investigated Fluid Structure Interaction studies, FSI, can be performed although it will be a costly operation with regards to computer resources. But one can firstly perform a modal analysis, less costly; to see which eigen frequencies are inclined to resonate. This will give us information on the eigen frequencies of the wind turbines and if any parts of the windmill will experience resonance. Combined with the Weibull Diagram these modal analyses can reveal areas of the turbine with frequencies that are inclined to resonate, FSI studies can be undertaken in order to see how large these resonating movements will be.

In order to ensure that there is not separation anywhere on the blade it might be wise to investigate the possibilities of the gamma-Re transition model. The papers by Suluksna, K. et al [56] and Sørensen [20] should be carefully examined before embarking on this task. This method needs a very small  $y^+$  preferably between 0.1 – 1, so it is demanding to run this model on the entire blade.

As the “UpWind” project concluded [7], the largest feasible future wind turbine would probably be of the magnitude 20 MW. Understanding and discovering the challenges of the

10 MW turbine in the present thesis is therefore important and will lay the ground pillars in a future attempt of building a 20 MW wind turbine. If CFD is to play an important role in the analyses of a turbine of this magnitude, CFD analyses of the 10 MW case must be carried out in great detail.

The author would recommend that further work on case 1 starts with a scaled down model of 1:10. Make a mesh for this model, run CFD and compare it to results from BEM and then scale up the model step by step, running new CFD calculations and checking them against BEM results each time a scale up is done. Eventually a full size model is reached and then implementing the found mesh parameters on a better CAD model of the NREL blade then used in this the present thesis would be recommended. If the CFD calculations with this grid matches those of Sørensen [17] it would serve as an even stronger validation and assurance that the results obtained with the grid parameters can be trusted.

## 9. References

- [1] Wind Energy Facts. (2011, April) Brief History of Wind Energy. [Online].  
<http://windenergyfacts.eu/brief-history-of-wind-energy.html>
- [2] J. F., McGowan, J., Rogers A. Manwell, *Wind Energy Explained - Theory, design and application, 2nd edition.*: John Wiley & Sons Ltd., 2009.
- [3] FOREWIND. (2011, May) FOREWIND, Delivering your energy future. [Online].  
<http://www.forewind.co.uk/dogger-bank/>
- [4] EU, "Functionalities of smart grids and smart meters," EU Commision Task Force for Smart Grids,  
[http://ec.europa.eu/energy/gas\\_electricity/smartgrids/doc/expert\\_group1.pdf](http://ec.europa.eu/energy/gas_electricity/smartgrids/doc/expert_group1.pdf), 2009.
- [5] World Wide Energy Association, "World Wide Energy Report 2010," in *10th World Wind Energy Conference & Renewable Energy Exhibition*, Cairo, Egypt, April 2010.
- [6] Tony Burton, David Sharpe, Nick Jenkins, and Ervin Bossanyi, *Wind Energy Handbook.*: John Wiley & Sons, 2001.
- [7] The European Wind Energy Association. (2011, April) [Online].  
<http://www.windfair.net/press/8967.html>
- [8] Research & Innovation European Commision. (2011, April) EU Energy Research. [Online]. [http://ec.europa.eu/research/energy/eu/research/wind/index\\_en.htm](http://ec.europa.eu/research/energy/eu/research/wind/index_en.htm)
- [9] Michael B. McElroy, and Juha Kiviluoma Xi Lu, "Global potential for wind-generated electricity," School of Engineering and Applied Science, Cruft Lab 211, and Department of Earth and Planetary Sciences, Harvard Univeristy, Paper 2008.
- [10] S. Gomez-Iradi, R. Steijl, and G. N. Barakos, "Development and Validation of a CFD Technique for the Aerodynamic Analysis of HAWT," *Journal of Solar Energy Engineering*, vol. 131, no. 3, p. 031009 (13 pages), August 2009.
- [11] Sørensen J.N. and Shen W.Z., "Numerical modeling of wind turbine wakes.," *Journal of Fluid Engineering*, no. 124, pp. 393-399, 2002.
- [12] M. S. Selig P. Giguère, "Design of a Tapered and Twisted Blade for the NREL Combined Experiment Rotor," NREL, SR-500-26173, 1999.
- [13] Thomas Hansen, "Wind Turbine Simulations Using Navier-Stokes CFD," Royal Institue fo Technology, Stockholm, Master Thesis 2010.
- [14] S. Scrheck et al., "Unsteady Aerodynamics Experiment Phase VI: Wind Tunnel Test Configurations and Available Data Campaigns," National Renewable Energy Laboratory,

Technical Report NREL/TP-500-29955, 2001.

- [15] H., Schepers, J. G., Montgomerie, B. Snel, "The MEXICO Project (Model Experiments in Controlled Conditions): The Database and First Results of Data Processing and Interpretation," Technical University of Denmark, Lyngby, 2007.
- [16] E. P. N., Burklund, M. D., and Johnson, W. Duque, "Navier-Stokes and Comprehensive Analysis Performance Predictions of the NREL Phase VI Experiment," *ASME J. Sol. Energy Eng.*, pp. 457-467, 2003.
- [17] N. N., Michelsen, J. A., and Screck, S. Sørensen, "Navier Stokes Predictions of the NREL Phase VI Rotor in the NASA AMES 80 ft x 120 ft Wind Tunnel," *Wind Energy*, pp. 151-169, 2002.
- [18] A., and Lecanu, J. Le Pape, "Navier-Stokes Computations of a Stall-Regulated Wind Turbine," *Wind Energy*, vol. III, pp. 309-324, 2004.
- [19] Carlo Enrico Carcangiu, "CFD-RANS Study of Horizontal Axis Wind Turbines," Dipartimento di Ingegneria Meccanica, DIMeCa, Cagliari, PhD Thesis 2008.
- [20] N. N. Sørensen, "CFD modeling of Laminar-Turbulent Transition for Airfoils and Rotors Using the Gamma - Reynolds Model.," *Wind Energy*, vol. doi:10.1115/we.325, 2009.
- [21] F.R. et al. Menter, "A Correlation-based Transition Model Using Local Variables Part 1 - Model Formulation," in *Proceedings of the SME Turbo Expo, Power for Land, Sea and Air*, ASME GT2004-53452, June 14-17, 2004, pp. ASME GT2004-53452.
- [22] C., Dahlhaug, O.G. Faudot, "Tidal Turbine Blades: Design and dynamic loads estimation using CFD and Blade Element Momentum Theory," in *30th International Conference on Ocean, Offshore and Arctic Engineering, June 19-24, Rotterdam, 2011*.
- [23] Olimpo Anaya-Lara et al., *Wind Power Integration - Connection and System Operational Aspects.*: Institution of Engineering and Technology, 2007.
- [24] NTNU, *Lecture notes in FY3490 Control theory on wind turbines, Specialization course Physics*. Trondheim: NTNU, 2010.
- [25] NTNU, *Lecture notes in TEP4545 Engineering Fluid Mechanics, Specialization*. Trondheim: NTNU, 2010.
- [26] (2011, April) The Encyclopedia of Alternative Energy and Sustainable Living. [Online]. [http://www.daviddarling.info/encyclopedia/H/AE\\_hub\\_height.html](http://www.daviddarling.info/encyclopedia/H/AE_hub_height.html)
- [27] J. V. Seguro and T. W. Lambert, *Modern estimation of the parameters of the Weibull wind speed distribution for wind energy analysis.*: Journal of Wind Engineering and

- Industrial Aerodynamics, Volume 85, Issue 1, pages 75-84, 2000.
- [28] (1992-2010) The weibull.com. [Online].  
[http://www.weibull.com/AccelTestWeb/weibull\\_distribution.htm](http://www.weibull.com/AccelTestWeb/weibull_distribution.htm)
- [29] H. Wayne Beaty and Donald G Fink, *Standard Handbook for Electrical Engineers (15th Edition)*.: McGraw-Hill, 2007.
- [30] *McGraw-Hill Encyclopedia of Science & Technology*, 5th ed.: McGraw-Hill Companies.
- [31] J. J., Cummings, R. M Dertin, *Aerodynamics for Engineers*, Fifth Edition ed., M. J. Horton, Ed.: PEARSON Prentice-Hall, 2009.
- [32] NTNU, *TEP4160 Aerodynamics*, Prof. Per Åge Krogstad, Ed. Trondheim, 2010.
- [33] Frank M. White, "Fluid Mechanics," 2008.
- [34] M., Emeis, S. Türk, "The dependence of offshore turbulence intensity on wind speed," *Journal of Wind Engineering and Industrial Aerodynamics*, no. 98, pp. 466-471, March 2010.
- [35] ANSYS CFX-Solver Theory Guide. (2009) ANSYS CFX-Solver Theory Guide. [Online]. <http://www1.ansys.com/customer/content/documentation/121/cfx/xthry.pdf>
- [36] N. N. Sørensen, "CFD Modelling of Laminar-Turbulent Transition for Airfoils and Rotors Using the Gamma - Reynolds Model.," in *Power Point Presentation, EWEC*, 2008.
- [37] J.P., van Wijk, A.J.M, Cleinje, J.W. and Pleune, R. Coelingh, "Description of the North Sea wind climate for wind energy applications," *Journal of Wind Engineering and Industrial Aerodynamics*, no. 39, pp. 221-232, 1992.
- [38] Martin O.L. Hansen, *Aerodynamics for Wind Turbines*.: Eartschan, 2008.
- [39] M. Drela, "XFOIL 6.5 User Primer," 1995.
- [40] L. , Dahlhaug, O.G. Frøyd, "Rotor Design for a 10 MW Offshore Wind Turbine," in *21st International Offshore (Ocean) and Polar Engineering Conference*, Maui, Hawaii, 2011.
- [41] Lars Erik Klemetsen, "An experimental and numerical study of the free surface Pelton bucket flow," Water Laboratory NTNU, Trondheim, Master Thesis 2010.
- [42] ANSYS Canada Ltd. (2004) CFX-5 Solver modelling. [Online].  
[http://iceberg2.shef.ac.uk/docs/cfx-pdf/printfiles/CFX5\\_Solver\\_Modelling.pdf](http://iceberg2.shef.ac.uk/docs/cfx-pdf/printfiles/CFX5_Solver_Modelling.pdf)
- [43] F. M. White, *Viscous Fluid Flow*, Second Edition ed.: McGraw-Hill, 1991.

- [44] H. K. and Malalasekera, W. Versteeg, *An introduction to computational fluid dynamics - The finite volume method*. Essex, England: Longman Scientific & Technical, 1995.
- [45] NTNU, *Lecture notes in TEP4112 Turbulent Flows*. Trondheim: NTNU, 2010.
- [46] (2010, December) www.CFD-Online.com. [Online]. [http://www.cfd-online.com/Wiki/Boussinesq\\_eddy\\_viscosity\\_assumption](http://www.cfd-online.com/Wiki/Boussinesq_eddy_viscosity_assumption)
- [47] N. N., Schreck, S., Michelsen, J. A. and Johansen, J. Sørensen, "Detached-Eddy Simulation of FLOW Around the NREL Phase VI Blade," *Wind Energy*, no. 5, pp. 185-197, 2002.
- [48] F. R. Menter, "Two-equation eddy viscosity turbulence models for engineering applications," *AIAA-Journal*, vol. 32(8), 1994.
- [49] CFD. (2011, February) CFD-Online. [Online]. [http://www.cfd-online.com/Wiki/SST\\_k-omega\\_model](http://www.cfd-online.com/Wiki/SST_k-omega_model)
- [50] G. et al. Kalitzin, "Near wall behavior of RANS turbulence models and implications for wall functions," *Journal of Computational Physics*, vol. 204, no. 1, pp. 265-291, March 2005.
- [51] F. R. et al. Menter, "Ten Years of Industrial Experience with the SST Turbulence Model," Software Development Department, ANSYS-CFA, Otterfing, Germany, 2003.
- [52] K., Schlichting, H. Gersten, *Boundary Layer Theory*, 8th ed. ISBN: 3-540-66270-7: Springer, 2003.
- [53] ANSYS Inc. (2011, March) Meshing Help. [Online]. [http://www1.ansys.com/customer/content/documentation/121/wb\\_msh.pdf](http://www1.ansys.com/customer/content/documentation/121/wb_msh.pdf)
- [54] CCTech. (2011, March) Centre for Computational Technologies. [Online]. <http://www.cctech.co.in/training/dacfd/ICEMCFDFluent-FAQs.htm>
- [55] ANSYS Inc. (2011, May) Ansys Mesh Introduction, Training Manual. [Online]. [http://www.cadfamily.com/download/CAE/ANSYS-MESH/AM\\_12\\_Appendix%20A.ppt](http://www.cadfamily.com/download/CAE/ANSYS-MESH/AM_12_Appendix%20A.ppt)
- [56] P. et al. Malan, "Calibrating the Gamma-Reynolds Transition Model for Commercial CFD," in *The 47th AIAA Aerospace Sciences Meeting*, Jan 2009.
- [57] T. J., Jespersen, D.C. Barth, "The Design and Application of Upwind Schemes on Unstructured Meshes," *AIAA, Paper 89-0366*, 1989.





## A.1. Appendix From Matlab through Pro Engineering.

### A.1.1. Introduction

This paper is ment to serve as a cookbook recipe for those who want to pursue the process of making an object of some sorts from a matlab script through Pro Engineering 4 and finally end up in a computational fluid program, i.g. CFX. I will use a blade for a 1 MW tidal turbine as an example for this process. The instruction found here are similar to how one can draw a wind turbine blade. Except that in this tutorial we make the tidal turbin 10 times bigger than it needs to be, this is not necessary for a wind turbine. In this paper the word ProE will be used as an abbreviation for Pro Engineering. ProE 4 and 5 are very similar with much the same functions, but the 5 version might have the functions placed elsewhere than ProE 4. Ansys is the name of the company that owns many different fluid computational programs, e.g. CFX, Fluent, etc.

I recommend you to go through each step in this tutorial, but for instance, the making of the blade could be a time consuming exercise, so you could perform the steps in the tutorial on a few sections of the blade, not the entire blade. This will save you some time. The sections for the blade that you will work with can be found here:

[http://www.ntnu.edu/c/document\\_library/get\\_file?uuid=ef661017-d0c1-41dc-b9df-2db5befacf68&groupId=948989](http://www.ntnu.edu/c/document_library/get_file?uuid=ef661017-d0c1-41dc-b9df-2db5befacf68&groupId=948989)

The finished tidal blade (wing4-3.prt.1), the tidal blade surroundings (cake4-3.prt.1), the tidal blade and surroundings ready to mesh (surr-4-3.prt.1), the surroundings to find the wake (big.surroundings.prt.1) and the blade for the 10 MW offshore wind turbine (kopi22juni.prt.9) can all be found here:

[http://www.ntnu.edu/c/document\\_library/get\\_file?uuid=669e492e-daba-4880-ab92-ac5f0de9365c&groupId=948989](http://www.ntnu.edu/c/document_library/get_file?uuid=669e492e-daba-4880-ab92-ac5f0de9365c&groupId=948989)

All the models we are making, except the tunnel for the wake, are going to be 10 times larger than they need to be in ProE. One of the reasons we do this is because it will ease the process of making a grid in ANSYS since we are dealing with small angles in regards to the trailing edge. When the grid is made we can scale down the models to real size inside ANSYS.

### A.1.2. From Matlab to Pro Engineering

In this chapter I will show how you can import coordinates from Matlab to ProE. If nothing else is specified, then whenever the phrases "click on", "push on" or "Press" objects on the screen are used, it is implied that you use the left mouse button on your mouse. The scroll button also works as an "ok" button. In ProE the mouse buttons have a somewhat different area of application then one might be used to.

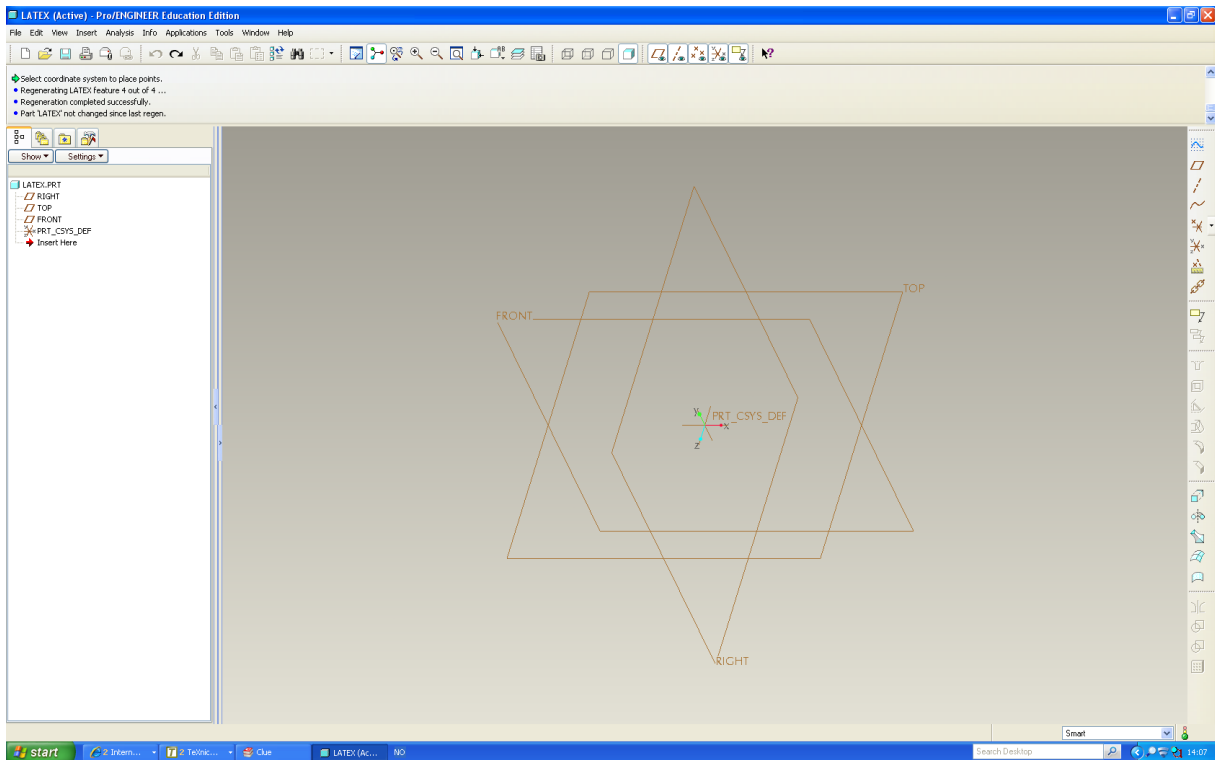


**Figure 1: Main window in Pro Engineering 4.0.**

Open ProE and create a new document. On the right side of your screen you will find a toolbar that shows a list of actions you can take such as "Sketch", "Plane", "Axis", "Curve", etc. On this list you find "Point", the fifth option on this menu (ProE version 4.0 Wildfire). Press this and choose "Offset Coordinate System". A box window will appear and you will be asked to choose a reference.

Here you click directly on 'PRT\_CSYS\_DEF' which you find in your main window in ProE, you do not have to click on anything in the box window that just opened. Further down in the box where you have chosen a reference, you press 'import'. Here you will import your coordinate files, they should be in the form of \*.pts or \*.ibl. Find the files you want to import and press "open" followed by pressing "ok". The files will be at the addresses given in the introduction.

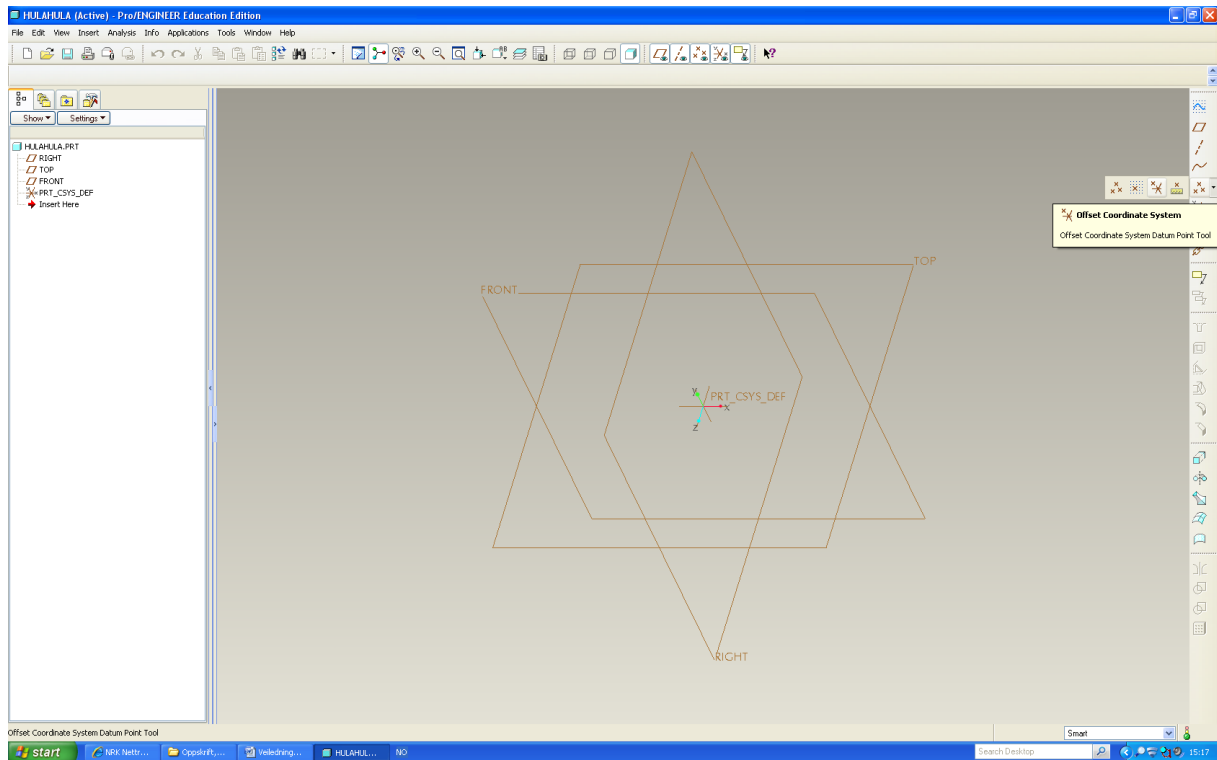


**Figure 2: Where to find offset Coordinate System button.**

### A.1.3. How to draw the object in Pro Engineer

Before one starts to draw lines between the points just imported some parameters must be set. On the upper toolbar click on “View”, “Display Settings” followed by “Display Model”. A box will appear, here click on ”Edge/Line”, set “Edge Quality” to “Very high”, then press “Shade” and set the “Quality” box to 10. This will make ProE visualize the model you are drawing as ANSYS will see it. If you do not perform these changes, ProE will use less computer power and show you a less detailed model of the blade you are drawing.

### A.1.4. Accuracy and units

There is a feature called accuracy, this needs to be as small as possible. To change the accuracy you click on “Edit”, “Setup”, “Accuracy” and finally click on “Absolute”. If you can’t find it you need to go to “Tools”, then press “Option”, find “absolute\_accuracy”, then enable this accuracy. Now go back to “Edit” and try the procedure again. Write a value very small, say 0.000001. ProE will automatically change this number to the smallest number in your design you can operate with. Now, press “Regenerate” and everything should be ok. There is a accuracy called “Relative” but from the authors experience the absolute accuracy will give the best result later on.

You also need to change the units to meters, this you can do by clicking on “Edit”, “Setup”, “Units” and change the units to “Meter Kilogram Seconds” and choose 1” to 1 mm.

### A.1.5. How to connect points

When you have imported your coordinates to ProE, your object will soon start to take shape. We need to draw lines between our coordinates. To do this you click on "Curve" on the

toolbar on the right side of your ProE window, see figure 3. Then you choose "Thru Points" and three boxes pop up. In the largest box named "Curve: Thru Points" the option "Curve Points" should have a mark to the left of it. Then you focus on the box called "Menu Manager", here the option "Spline" should be marked. In this box you also have two more options depending on what you want to draw:

Option 1) you can draw a line between each point you click on by choosing "Single Point". You will then have to click on every coordinate you want to draw lines between.

Option 2) you can connect all your imported points at once by choosing "Whole Array". Be aware that this action will draw a line between all points from the first point to the last point and you will not be able to divide your object into any sections or form any other borders if that is wanted.

In the case of the example model of a turbine blade for a 1 MW tidal turbine you can't choose option 2 because the blade will have to be divided into three separate parts due to issues that will arise when one attempts to use a computational fluid dynamics program on the object. As we see the way one connects the coordinates is based on what one wishes to use the object for further on.

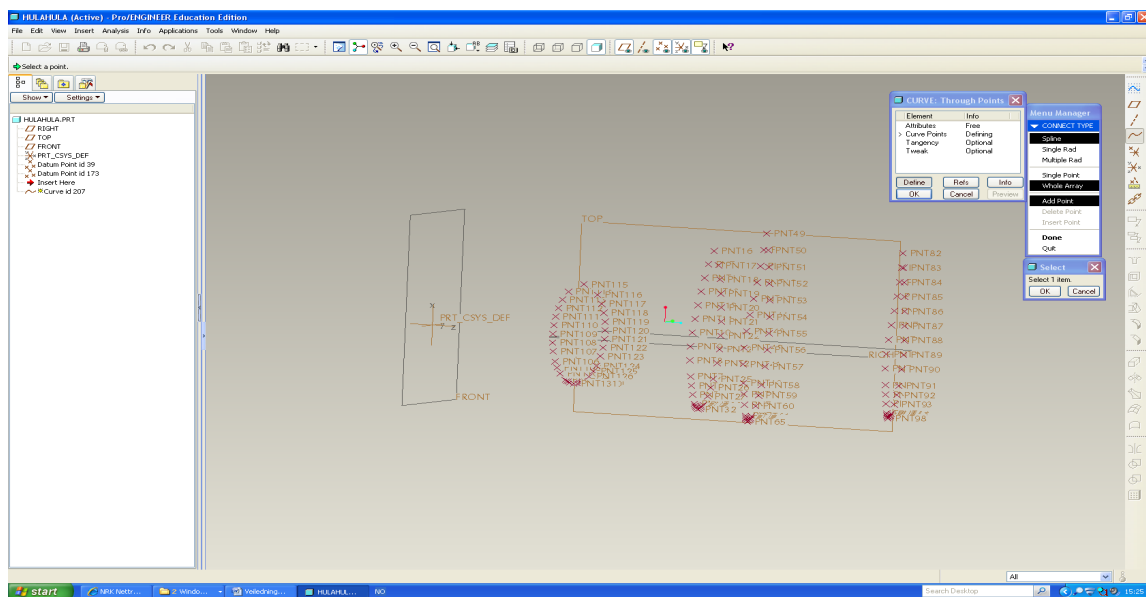


**Figure 3: First step of drawing lines between the coordinates.**

You can delete points by changing from "Add Point" to "Delete Point" in the "Menu Manager".

### Leading and trailing edge

Our blade needs to have a leading edge, upper section, lower section and a trailing edge. The leading edge starts in the point just before the points starts to cluster together. The leading edge will consist of 12 points. This width in points stays constant throughout the wing. The upper and lower sections begin at each end of the leading edge, and they go all the way back

to the points just before the last point. Do not include the last coordinate when you draw the sections, this because the trailing edge will become too thin for ANSYS do compute on it.

As we see in figure 4 there is a point which is left out when the sections are drawn. You only connect the upper and lower side of the blade at the root and tip. You need to draw a line between the root and tip, following both sides of the trailing edge as it is shown in figure 4 as a rigde. You can do this process for some sections at the root or tip just for the sake of ProE training, if you feel it is too time consuming to draw all the sections needed and then use the finished blade for CFX calculations later on. But go through all the steps in this tutorial, it is valuable training.

If you wish to draw the entire wing remember to have root trailing edge, root leading edge, upper and lower side of the blade, upper and lower side of root, a leading edge for the blade and a trailing edge for the blade.

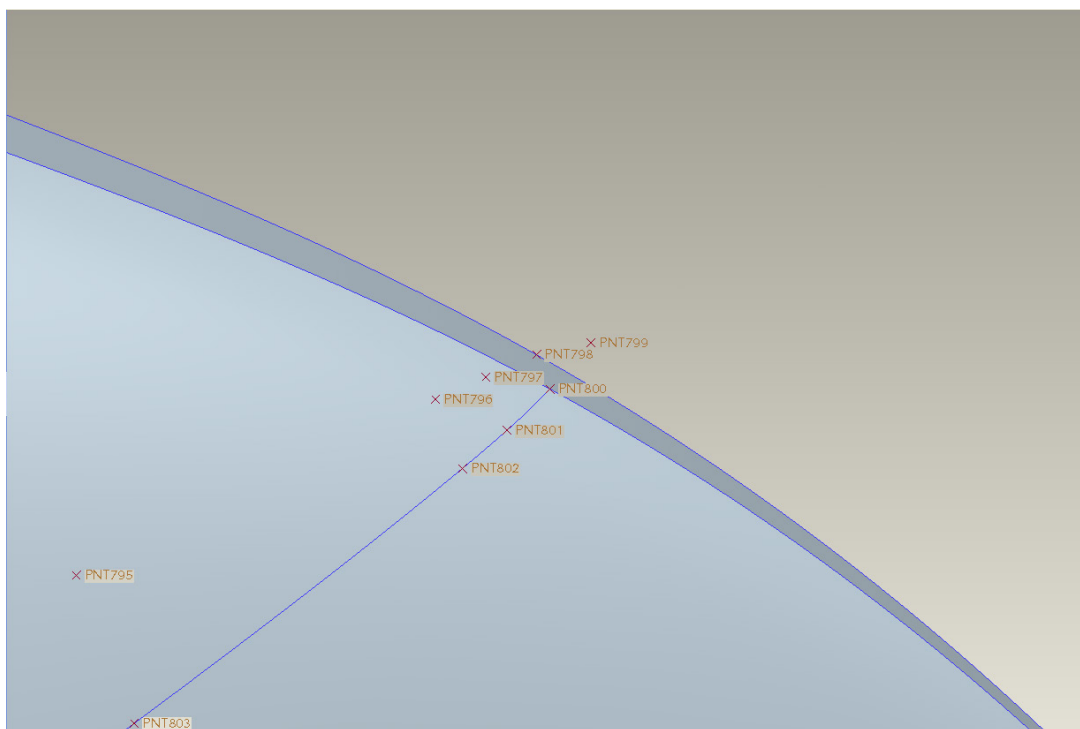


**Figure 4: Traling edge.**

#### **A.1.6. Tangency for two meeting lines**

You can constrain your lines, leading edge and trailing edge. This can often ease the process you need to take your geometry through in CFX in order to perform fluid calculations on it. You need to add a constrain of tangency between the leading edge and the upper and lower side of the blade. Because this tangency function is sensitive to the chronological order of the lines made out of the sections, we need to choose the first last made out of a section from the left menu window. Right click on the first line of a section, regardless if it's the leading edge

or the upper or lower side of the blade. Choose “Edit Definition”, click on “Tangency” in the box that pops up and press “Define”. A “Menu Manager” will appear, here you can first choose if it should be tangent at the start or the end. In the example case use “Start”. Now click on the line it should be tangent to. Press “ok” and zoom in on the junction where the two lines meet. If they connect to each other on a fairly straight line everything is okay, if there is some strange curvature where they meet, repeat the procedure and click on “Flip” as a last step before pressing “Okay” and ending the tangency process. The two lines are now tangent to each other in the meeting point.

Draw all the sections given or just a couple of them, either at the end or at the front.

#### A.1.7. Splitting lines using “Trim tool”.

If you have made one whole line out of one section of coordinates you can cut the line and divide it into smaller lines. Since we need a leading edge, a upper side and a lower side we divide the section into three parts. Be aware that the line can’t be a closed curve. When you connect the points on a section, connect everybody at once but skip the last point at the trailing edge and don’t let the upper and lower side of the blade meet. Click on the line that goes through all the points on your section, choose “Trim Tool” in the lower part of the right toolbar then click on the point where you want to cut the line and press “ok”. Now you will see that there is a line called “Trim” which has been added to your left menu which shows all the pieces of your blade so far. Now click, in the left menu, on the line you have cut and choose “Trim” from the right menu again. Choose the same point as last time, but change the direction of the yellow arrow that points out what is cut. This you do by clicking on the last option on the upper function toolbar, see figure 5.

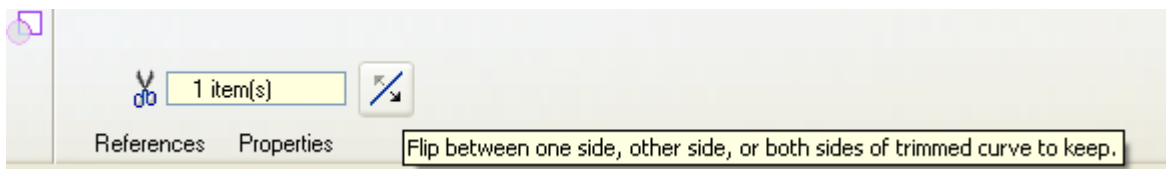


**Figure 5: Function toolbar for "Trim" tool**

#### A.1.8. Boundary blend

Now, you might like to make sections of solid material between the lines between your coordinates. To do this you click on "Boundary Blend" towards the bottom of the right toolbar. Hold in "Ctrl" on your keyboard and click on all the lines you want to draw solid sections between, remember that you have to click on the lines in the right order or the computer will draw undesirable solid sections.

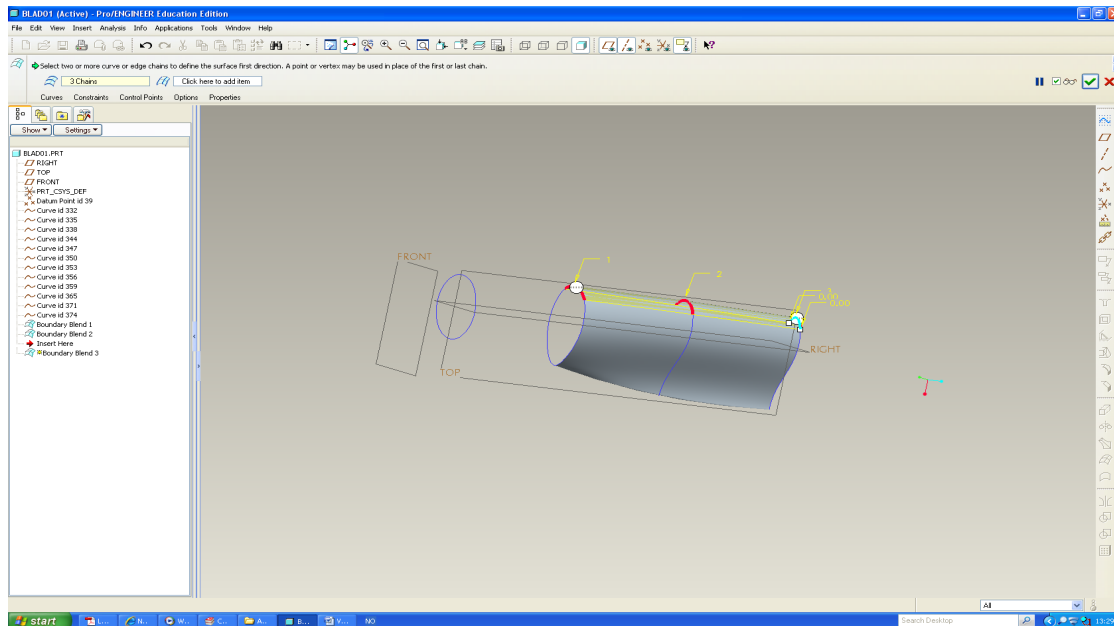


**Figure 6: Boundary blend**

In order to use the blade in our example case in any meaningful way all the sides of the object needs to be one continuous solid surface including the tip and root of the blade.

When you want to make surfaces you click on boundary blend in the left toolbar then choose the sections you want to merge, hold down “Ctrl” in order to choose multiple sections. In the upper toolbar click on the thin and elongated box to the right that popped when you chose “Boundary Blend”. Now click on the sides of longitude sides of the section you want to merge, while holding down “Ctrl”. This constrain will make the merge more solid when you take it into CFX.

### A.1.9. Solid ends

The next step in the process of constructing our blade in ProE is to make it have solid ends at the bottom and tip; this is essential for calculations in CFX and also if one wishes to send the blade to some manufacturer for production. To do this you first choose “Create Datum Plane”, 2<sup>nd</sup> option from the top in your right toolbar. Here you will be asked to choose a reference frame. Choose one of the lines on the root and press “ok”. You should now have made a plane you can use to sketch on.

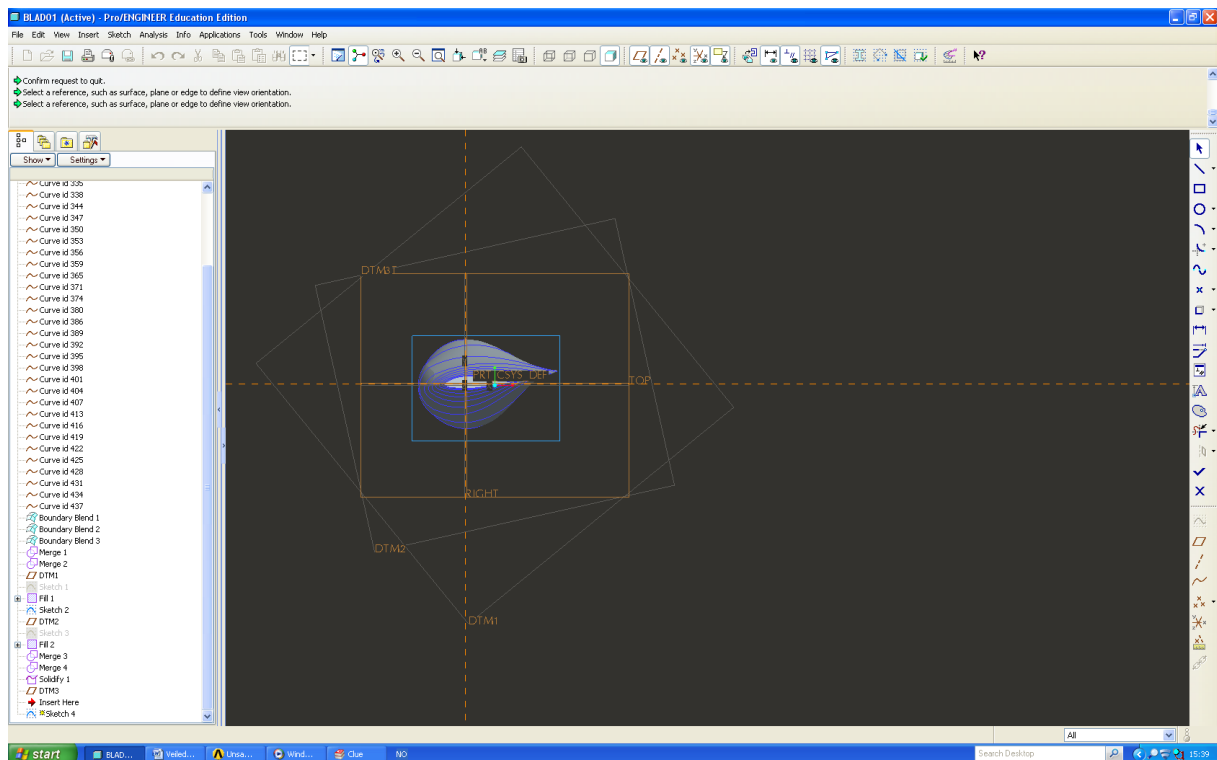


**Figure 7: Pro Engineering main window in sketch mode**

Find the function “Sketch” in the right toolbar. The sketch window will open and you will be asked to choose a reference axis, we choose the “Right axis” in our example. In sketch mode you can only make changes to planes or lines you have chosen as references. When you have chosen a plane and a reference the sketch work window will open. Here you can add all the objects you want to alter by clicking on “Sketch” in the upper toolbar followed by “References”. By clicking on “Rectangle” in the right toolbar you can draw a rectangle around the end you wish to fill with solid material. After the rectangle is made, click on “Done”, it can be found in the right toolbar.

ProE should have brought you back to the main work window now. In the upper toolbar there is an option called “edit”, click on this and scroll down to the option “Fill”. This function fills your rectangle with solid material.

Do the same for the tip of the wing.

#### **A.1.10. Merge**

The next function in ProE we will use is a tool called “Merge”. This allows you to merge two solids together so when you click on either one of the two solids the computer will treat the solids as one. This you do by choosing the two surfaces you want to merge. First of you need to merge all the sections on your blade before you can merge the blade and its end sections. You choose one section on the blade; you hold down “Ctrl” and choose another section on the blade. Then you press “Merge” which you will find in the toolbar to the right on your work window, in this version of ProE it is the 3<sup>rd</sup> option from the bottom. A yellow grid should appear on the selected sections, click ok. If the yellow grid does not appear, then try again.



When you have done this on all the sections on the blade you will then be able to choose the whole blade when you click anywhere on the blade. Now follow the same procedure, but choose the blade and the newly sketched solid plane. A yellow arrow should appear inside the root or tip; this should point inwards since this will decide what part of the plates at the end will be kept.

#### **A.1.11. Smoothing of surfaces**

If you want to insert more sections to your object to smooth out curves or bends, you can do this easily by importing \*.pts files. Instead of having to make a new trailing edge, leading edge or any other line to implement this new section to and its points; you can add this section to the already existing lines you've drawn by clicking on the line you want to alter, right click, choose "Edit Definition", then choose "Curve Points" in the box that opens and press on the option "Define". As "Connect type", you want to highlight the option "Spline", click on "Single Point" in the next list and then choose "Insert Point". Just under the upper toolbar there is an information toolbar that contains information on what you have done or sometimes on what you should do when you choose certain function. Now, for example, this window/bar tells you to choose the point on the curve in front of the point you wish to add, this is used as a reference point. When you have performed this task it tells you to choose the point you wish to add. When this is done properly you will see the line change. If the line doesn't behave as you wish, try to choose your reference point on the opposite side of the point in your newly imported section. A general rule is that the more sections you have, the more accurate the CAD model will be and it will be less likely that you experience meshing problems due to a bad CAD model.

#### **A.1.12. Solidify**

Solidity is the final step in making a solid object from the imported coordinates. Click on the object you want to make an entire solid of. If all the steps until now have been executed properly, then when you click anywhere on your object, the whole object and all its sides should be highlighted. Now you click on "Edit" in the upper toolbar on your work window. On the list that pops up you will find "Solidify" approximately in the middle of the list, press this option and your object becomes a solid. If the program does not let you choose "Solidify" there is some form of discontinuity somewhere on your object. If so you have to check that all your surfaces are merged properly and that any ends on your object has been filled with solid material. If you can't solidify your object it's normally because your sections are not accurate enough so when they meet, there are air gaps that will influence a meshing process in CFX.

Congratulations, you finally have created a solid object from your imported coordinates. But, if your goal is to implement this object in CFX and perform fluid flow calculations on it, you're not at the finish line just yet. We now need to make a cake. From the cake we will curve our blade and it is this geometry we will upload to CFX.

#### **A.1.13. Cutting of sharp edges**

The coordinates you work with have already been cut 2% at the trailing edge. So this next task is not necessary to do for you. But it still a smart way of reducing a sharp edge on an

object if you for some reason need to do so on a future object, so it's recommended you take the time to go through the process of cutting off 2% of the trailing edge. Because the end of the trailing edge is so thin compared to the rest of the wing, CFX might not be able to make a mesh fine enough to calculate the flow at the end. It could be possible but one will need an unnecessary large number of nodes to perform this task and the total amount of computational power needed will be needlessly large. So in order to make our engineering life a little simpler we cut off 2% of the trailing edge. This will not make our flow calculations significantly inaccurate.

You will use another blade to perform the cutting of the edge, since the blade you are making already has the end cut off correctly. Open the file "kopi22juni.prt.9" from the zip file you downloaded earlier, this is the blade for a 10 MW offshore wind turbine. One way to do make this cut successfully is to mark points in sketch mode on every section we have imported, one at the front and one at the end of each section. Then we will draw a line between the endpoints which will have a length of: "new point = 0.02\*end point".

Click on the "Extrude" function in the right toolbar, press on placement in the upper toolbar that appears and click on define, choose "Top" as your plane and "Right" as the reference. When the "Sketch" window opens click on "Sketch" in the upper toolbar menu, it should be between "Insert" and "Analysis", then choose "References". You now need to click on every section you want to work with, so click on every section of the lower OR upper part. Also click on every leading edge, for this it's useful to zoom in on the wing. You do not need to cut 2% of the root section.

Choose the "Point" function from the right toolbar and mark one point at each end of every section and then a third point somewhere between the two end points. Then choose the "Normal" function from the right toolbar; this will make you able to define dimensions. Now click on the extremity points and press on your scroll button on the mouse. In the box that now pops up, choose "Dim>Ref".

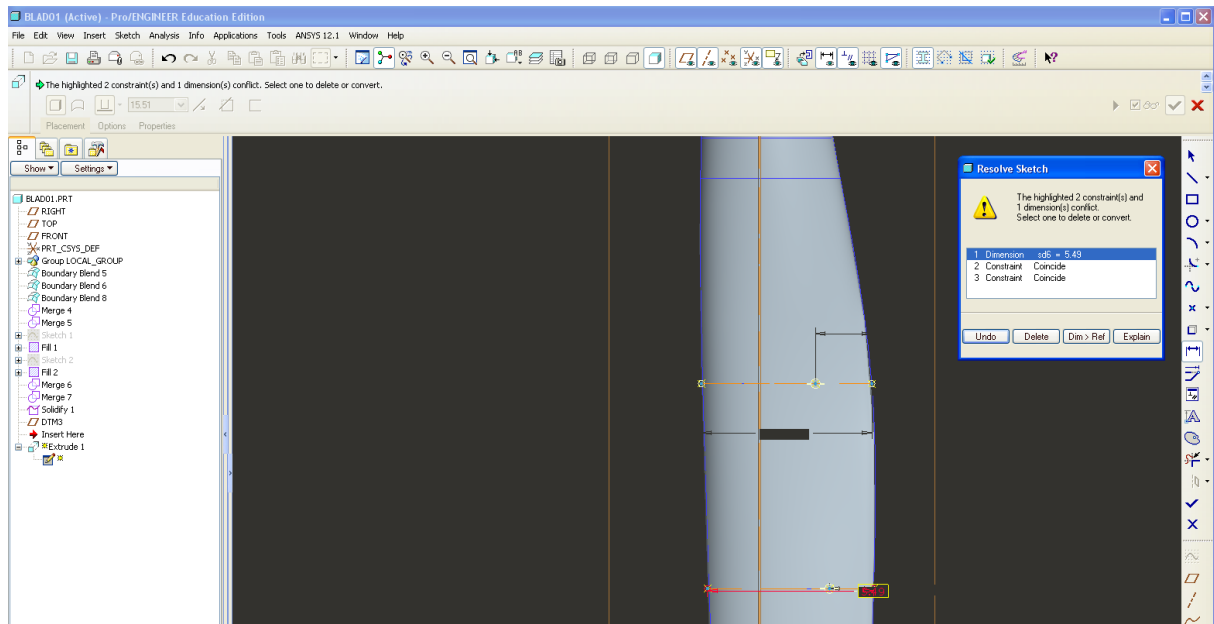


**Figure 8: Marking points on chosen sections.**

Now click on the end point and the third point which is in between the end points, press scroll button. The length between these points should appear. Find “Tools” in the upper toolbar, click on this and choose “Relations”. A box should pop up, here you choose the point that is not an endpoint, the name of this point will now appear in the box. Behind the name of the box you write “=0.02\*endpoint”. Instead of writing “endpoint” you need to click on the end point of the section you are working with. You need to write this equation for all the sections of the blade. When you press on “ok” all the middle points you have chosen will now be at 2% of the chord length compared to the leading edge.

You now need to make a spline between the points. Click on “Spline” in the right toolbar and choose the points you have made, scroll click to end action when you have your mouse pointer just over the last chosen point or else you will make a spline that bends undesirable, this is easily seen on the screen if you try to move your mouse after choosing the last point. After making a spline between all the cutting points you make a three more splines, two short ones at the top and the bottom of your first spline. You want to create something that compares to a rectangle, now make a last spline to close the rectangle.

Press “Done” in the left toolbar and the “Sketch” mode will end. Choose “Extrude” from the right menu and concentrate on the upper toolbar that pops up. Change the depth value to 1 and press the 2<sup>nd</sup> option from the right which is “Remove Material”. The cutting should now be visible. Leave the menu by clicking on the green checkmark to the right in the upper toolbar.

#### **A.1.14. Making the cake**

CFX does not calculate directly on any object, you need to “carve” out the object in a greater solid. This solid will be imported to CFX for meshing and fluid calculations. If you have a two bladed wind turbine you need a cake of 180<sup>0</sup> and if you have a three bladed wind turbine you need a 120<sup>0</sup> cake.

## 180° cake

Make a new part. Press “Revolve” from the right menu. In the upper menu that opens, click on “Placement” and then “Define”. Choose the “Right” plane as your plane and the “Top” plane as your reference. Z direction needs to point upwards, if it doesn’t click on “flip”. Make a rectangle by choosing the 3<sup>rd</sup> option from the top on the right toolbar. Press “Defining dimensions” on the right menu. The long sides should be 300 m, the short sides should be 40 m and you need a distance of 11.24 m from one of the short ends of the rectangle to the center axis on your screen. You do not want to lie any of your rectangle sides on the center axis’ because this will give you unnecessary restrains. See figure 10 for visual aid.

Press ok and leave the sketch. You now need to tell the program what axis you want to revolve the cake around. This is done by clicking on the empty box in the upper menu that appeared when you opened the “Revolve” function. You want to revolve the cake around the y-axis. Look at figure 6, you need to change the box where it says “360” to “180”.

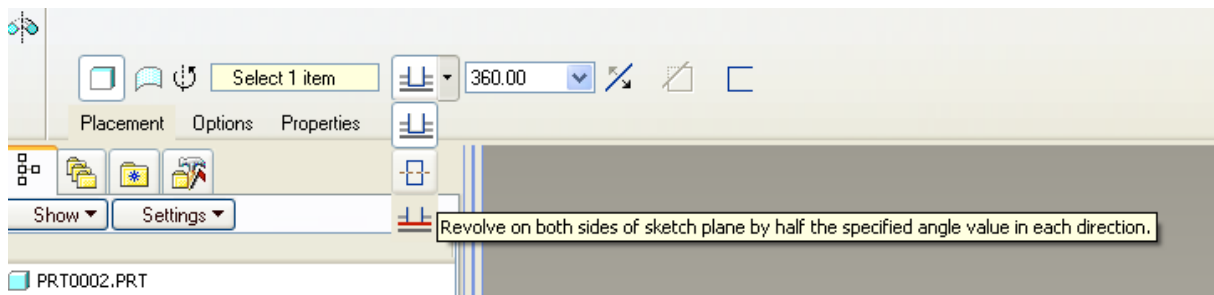


**Figure 9: Function toolbar for "Revolve".**

Select the “revolve on both sides of sketch plane by half the specified angle value in each direction” as shown in figure 9. Press then on “Select 1 item”, this is the axis you want to revolve around, choose the y-direction.

Click on the green checkmark to the right in the upper function toolbar. The function will close and you should now have a solid 180° cake with a depth of 40 m.

## 120° cake

Make a new part. We are going to follow much of the same procedure as for the 180°. Choosing the same references as for the 180° cake should give us an x-z orientation in 2D instead of the regular x-y orientation. Just to be precise, the z-axis is pointing upwards on the screen. If your z-axis is pointing downwards, click on “Flip” in the box window that popped

up when you pressed “Sketch”.

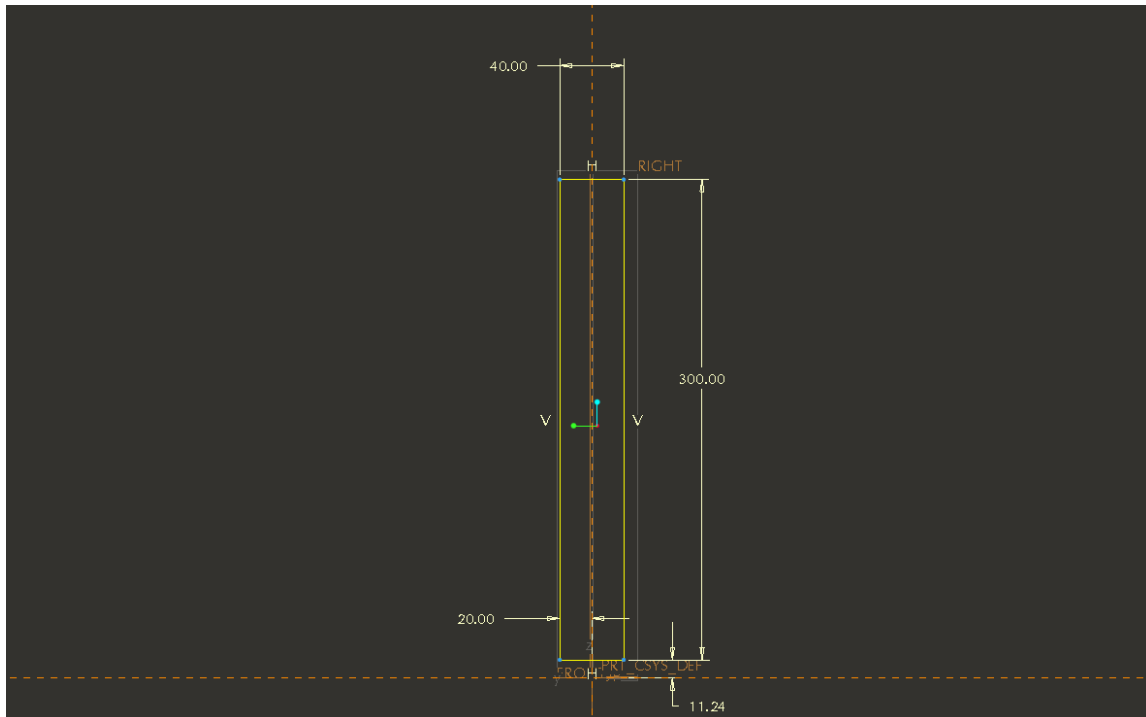


**Figure 10: Window appearance when you have drawn the rectangle along the z-axis.**

We want to produce a cake piece of 120 degrees, our blade is oriented along the z-axis and we need 60 degrees on each side of the z-axis. Make a rectangle with the same dimensions as for the previous cake, but this time, make the rectangle point upwards along the z-axis. Press ok and leave the “Sketch” mode. Look at figure 9, you need to change “360” to “120”, change the rest of the options in the same way as in the previous cake.

In order to split the tunnel into different regions you need to make a new plane where you want a region to start, then extrude the rest of the tunnel so you only are left with the region you want a certain mesh size in. Copy this part and go back to the original tunnel, do the same procedure, but make the plane sketch where you want the new area and make a copy with a new name. The mirror function can be used after the extrude function to save time, mirror the extruded part of the tunnel with the origo plane as the reference plane. When you have divided the tunnel into all the necessary regions, make an assembly and join all the parts together.

#### **A.1.15. Assembling cake and blade**

To connect the blade and the cake you have to open a new file, an assembly file. Press “File” in the upper toolbar and then click on “New” in the list that shows up. In the box window that opens click on the option “assembly”. A new working window opens up, press on “Insert” in upper toolbar and choose “Component” or “Assemble”, then choose which part you want to import and click on “ok”.

Now you need to constrain the newly imported component. This is done by choosing “Placement” which is found in upper toolbar that appeared when the part was imported to the

working window. In our example we choose “TOP” and “ASM\_TOP”, and then press “New Set”. Same procedure two more times with the constraints “FRONT” and “ASM\_FRONT” and “RIGHT” and “ASM\_RIGHT”. In the second constraint you might have to look in the “Offset” box, and change the content to coincident. If the planes don’t match try the “Flip” switch. The same procedure must be followed for the blade. You will clearly see if the two imported elements match or how they do not match if they have not been constraint in the same planes.

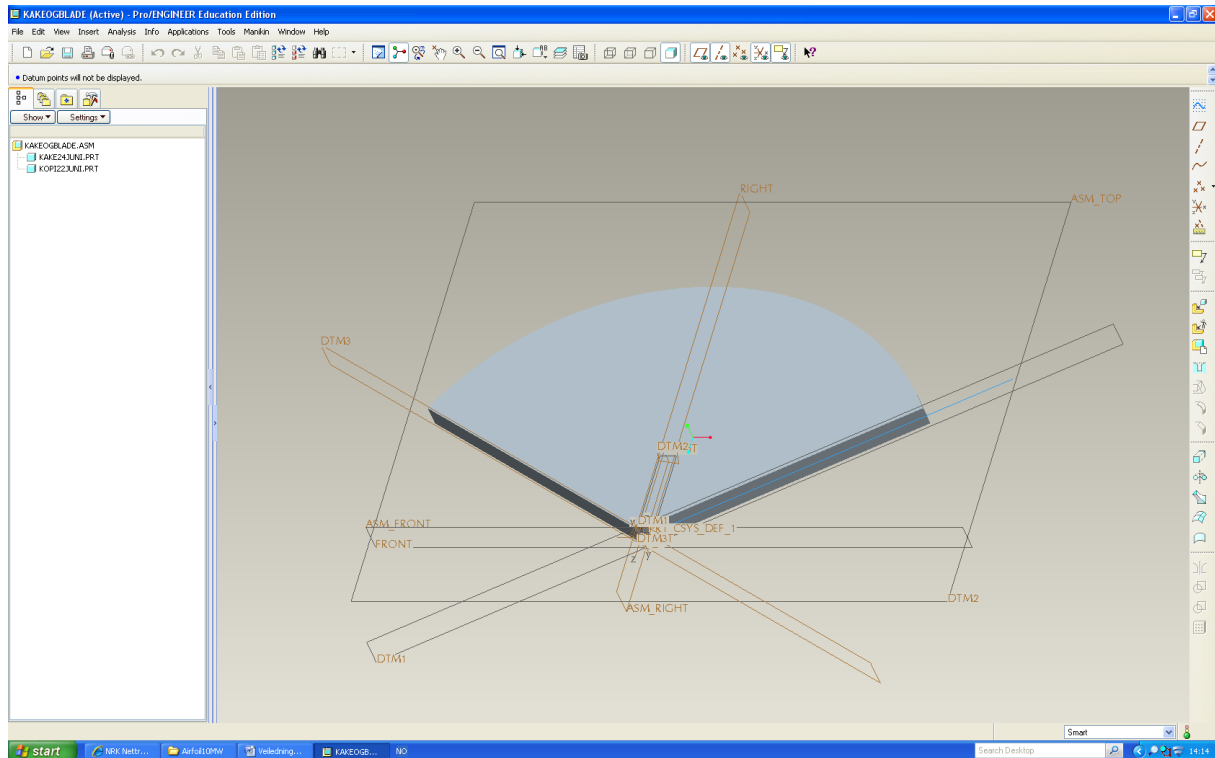


**Figure 11: Connection between the larger cake piece of a 120° and the smaller blade. You should use the cake of a 180° for this task.**

To carve the blade from inside the cake you must choose “Edit”, then “component operation” followed by “cut out”. Remember to have a window with your cake open on your computer. You will not see the cut out in the \*.asm file but in the \*.prt file of the cake instead. Now you click on the cake, click “ok” then click on the blade and finish off by clicking on “ok” and “Done”. This should carve the shape of the blade into the cake. Remember to save this file when you are done.

#### A.1.16. Tunnel

This tunnel is where you will monitor the wake. Make a cake of 180° as you have done before, but use 1000 m as the longest side and use a radius of 600m. The 1000 m side is divided into 300 m in front of the blade and 700 m behind the blade. The hub radius, i.e. the inner radius of the cake is 2.97 m. You need to carve out the little cake around the blade from this larger tunnel; the little cake should be carved out at the middle of the tunnel. The finished tunnel is found in the files you can download for this tutorial as “big-surrounding.prt.1”. You need to cut the cake out of the tunnel, but you need to delete the blade from the cake before

you do this. If you don't you will have a mould of the blade in your tunnel; this is not desirable.

## A.2. Appendix From Pro Engineer to CFX

### A.2.1. Workflow in a CFX analysis

Workflow in performing a CFX analysis on a object:

1. Import geometry
2. Use Geometry to generate mesh
3. Setup the physics of the problem
4. Run problem to create solution
5. Post process solution to see results

### A.2.2. Importing objects to ANSYS from ProE

In order to ease the process of importing drawings from ProE, there is a quick button that needs to be installed in ProE which enables to easily open ProE files in Ansys. This you do by going in to “start” menu in your left lower part of your screen, go to “All Programs”, then find ANSYS 12.1 (or other versions), find “Utilities” and open the “CAD Configuration Manager”. Here you choose the boxes “Workbench” and “Pro/Engineering”. Then click on “Next”. You will now have to find the address of where your ProE software is placed on your computer, then press on “Next”. After choosing “Config CAD Interfaces” your computer will make the necessary quick buttons on the upper toolbar in ProE. Exit the program.

Now, import your cake into ANSYS, open the file you want to work with in ProE. Do not use the \*.asm file, use instead the \*.prt file! The name of the cake file is “surr-4-3.prt.1”. In the upper toolbar in ProE there should be a quick button for ANSYS, press this and select “Workbench”. In the window that now opens you click on “Mesh” in the left menu and drag it over to the “Project Schematic” window. Do not open double click on this geometry or try to view it in any other way, because small surfaces might be compromised if this geometry is opened from this stage of the process.

### A.2.3. Installing quick buttons in your work window

You need to have some quick buttons to a few functions in the “Component Systems” on the left of your screen, see figure 12 for an idea of how your workbench should look like. In order to achieve the menu to the left called “Component Systems” you need to open “Toolbox Customization”, mark what functions you want under “Component Systems”, then press “Tools” followed by “License Preferences”. Then under “Global Settings” click on “Academic Licences”, press “Apply” and “Ok”, close the program.

If you have a green “check mark” behind “Geometry” In workbench, you can proceed to the next step which will be to connect the geometry to the meshing function as shown in figure 12. When you have a working cell it will have a green checkmark behind it and you may proceed to the next step. If you do not have this checkmark you will not be able to go on. Right click anywhere in your Project Schematic window in your Workbench and choose “New Component Systems”. Here choose “Mesh”. In the new little box that pops up right click on geometry and choose the cake file you have in ProE. Next, click on “Mesh” and choose “Edit”.



You will now be taken to a window. There will also be a window to the left which asks you to state some “Meshing Options”, choose “CFD”, “CFX” and let the rest be default. In the “Outline” box which is situated to the left, you need to click on the “Mesh” function and then find “Edit in CFX-Mesh”. You should now have a working window that looks like figure 13 and 14. Now it is time to start meshing! The Mesh is a grid of points where CFX will perform its calculations. It’s crucial to have a good mesh in order to achieve good results from the simulations.

In the new window that opens there is a smaller window to the left of your command window that gives you a few meshing options. Here you need to choose CFD as your Physical preference, the “Default method” has to be CFX and leave the rest as they are, i.e. default mode. If you can’t find this window then you can go into “Tools”, “Option” and “Mesh”. In these menus you should find your physical preferences and a lot of other applications you can alter.

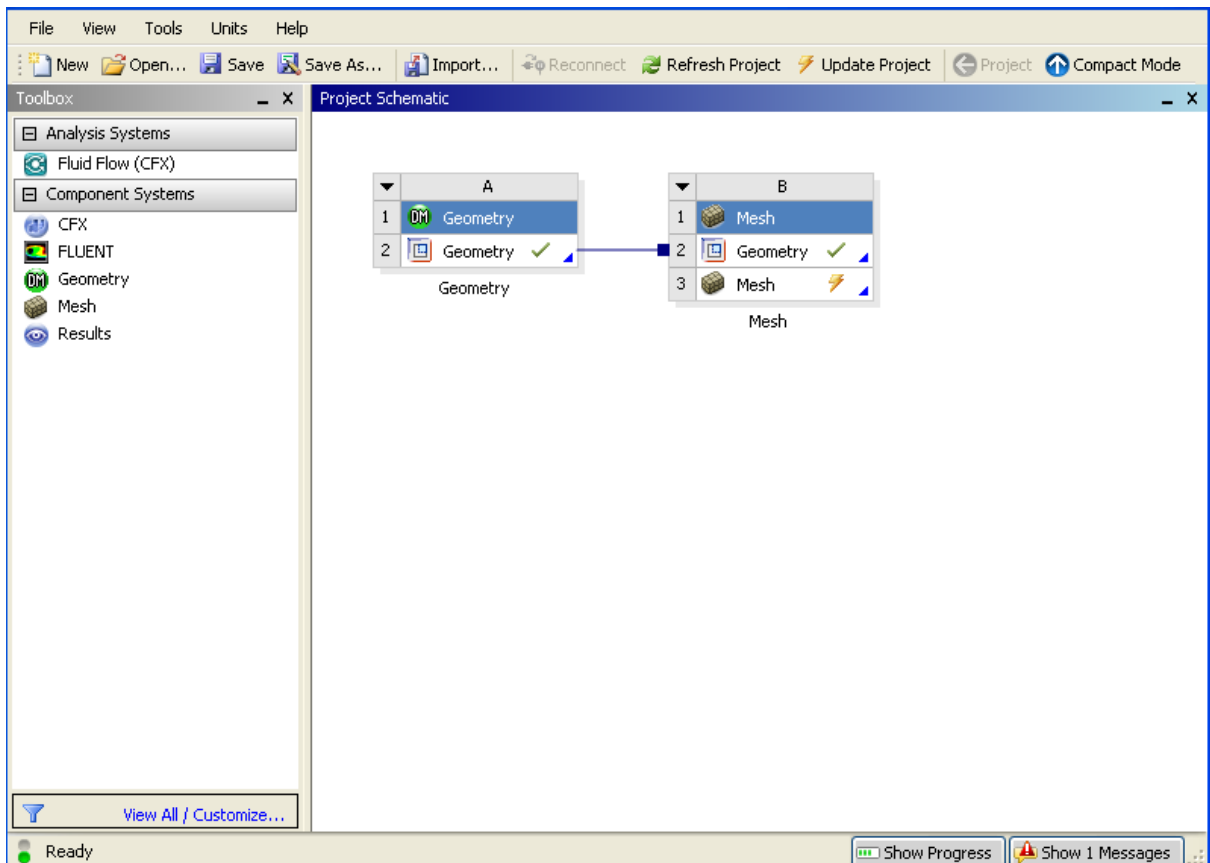


**Figure 12: Workbench lay out.**

Remember to save your work in both the working window you have done changes in and in the ”Workbench”.

You want to mesh cake with the cut out blade; you then need to import the “surr-4-3.prt.1” file from the links you were given in the start of this tutorial.

## A.2.4. Regions

Focus your attention on the left top menu called “Tree view”. This is your main command window in the meshing process. You need to divide your object into different regions, this will ease your meshing process and the analyzing of the results of a run.

To create regions right click on the option “Regions” and choose “Composite 2D Region”, then choose one of the large sides of the cake. In the lower left command window you have menu called “Details view”, here you will have to press “Apply” or else ANSYS will not be make the region you have told it to make. Do the same for the other large side of the cake and rename the regions “Upper cake” and “Lower cake”. To get back to normal view of the object you press the magnifying glass with the blue circle in it on the upper toolbar.

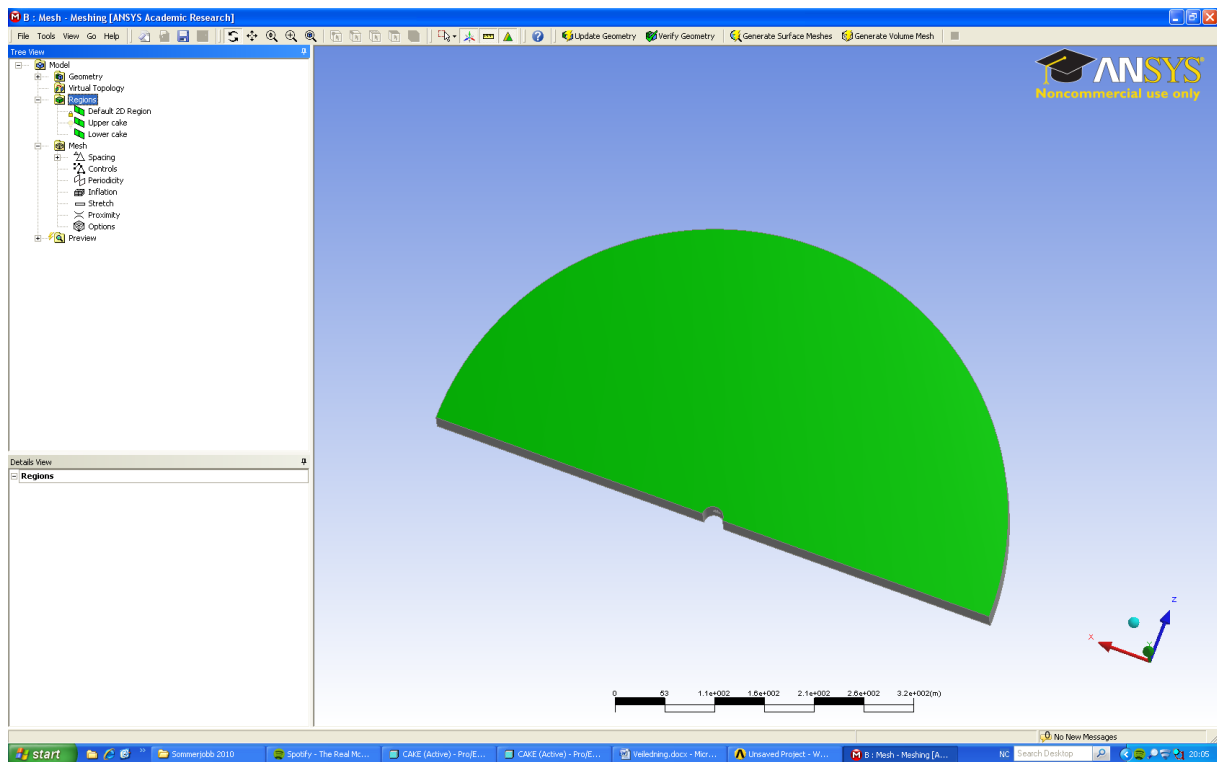
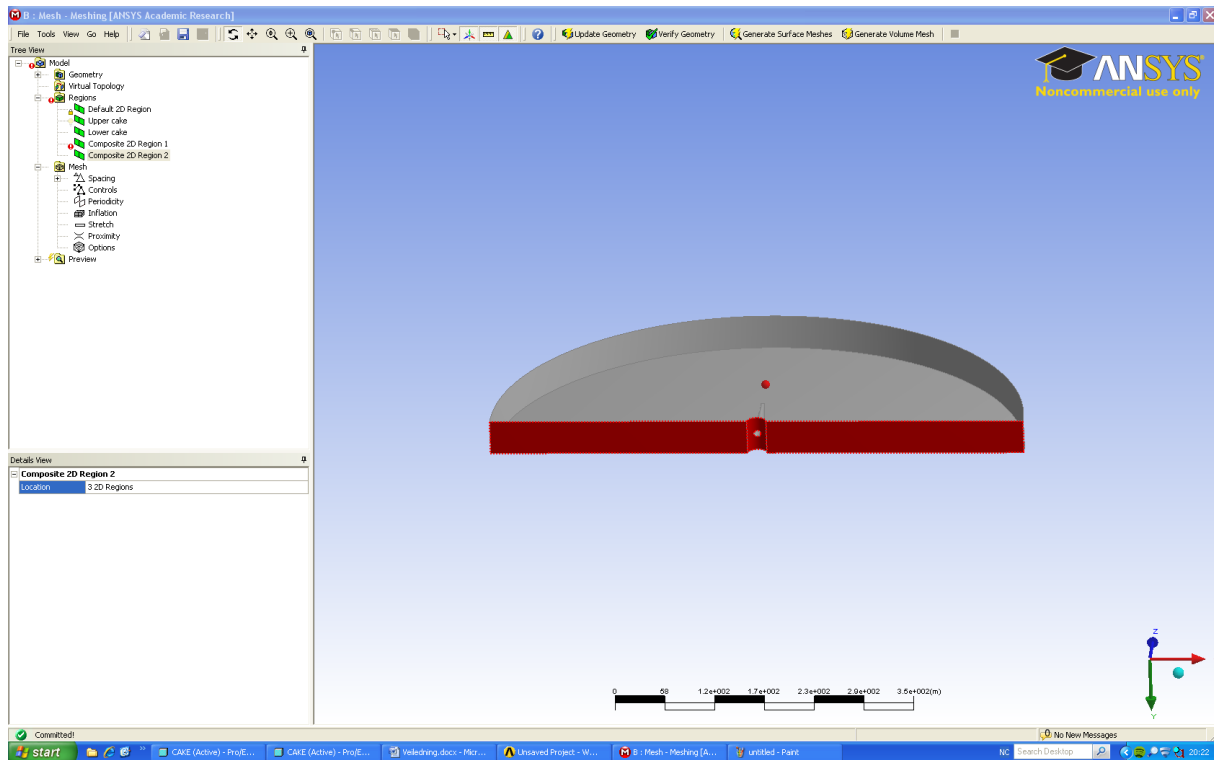


Figure 13: Work window when meshing.



**Figure 14: Underside of cake.**

Right click on the Upper cake and choose “Hide”, this allows you to see the blade and divide the blade into regions. You need to look closely on the wing inside the cake to see which side is the lower one and which is the upper one. To zoom in on different areas of the wing, right click and drag a small box on the area you want to zoom in on. Check if you named the upper and lower side correctly by looking closely at the wing.

Now make three regions out of the underside of the cake, hub and the two long under sides see figure 14. You should create a region for the upper and lower side of the blade, one for the tip, one for the lower and upper side of the root, one for the leading edge on the root, one for the leading edge of the main wing, one for the trailing edge on the main wing and one for the trailing edge of the root. You will use all of these regions later on. Hold down “Ctrl” when you try to choose multiple sides of the blade.

One annoying aspect of this program is that every time you start up the program you have to define the regions on your object again. In the “Tree view” menu the regions will have a small yellow check mark to the left of the regions which need to be redefined. Luckily this is done rather quickly, just by clicking on the region you want to redefine in the “Tree view” menu followed by clicking on the now yellow “2D region” in the lower left menu called “Detailed view”. Check that the highlighted region on the plane is the correct region and press “Apply”. Also when if you have closed the program and want to reopen it and continue your meshing work you need to right click on “Mesh” in “Tree View” and choose “Edit in CFX mesh”.

### A.2.5. Face spacing and Edge spacing

Next step is to make something called “face spacing”. Here you will decide which areas of the blade will have what dimensions of grid spacing. Look at ”Tree view”, right click on “Spacing”, choose “insert” and then “face spacing”. In the “Details View”, left lower window, you will have a list of options, change “Minimum Edge Length” to 0.25 and “Maximum Edge Length” to 0.75, leave the rest of the settings as they are (default mode) and click on the box to the right of the “Location”, then choose the regions you want to use this spacing on, it is the upper and lower side of the root. Then press “Apply”. Now you need to do the same for the upper and lower side of the wing, use 0.15 as minimum edge length and 0.5 as maximum edge length, leave the rest as default. For the trailing edge use 0.01 and 0.02. For the tip use 0.03 and 0.1, the leading edge needs 0.04 (min) and 0.08 (max) and finally the leading edge root needs 0.05 and 0.5. All other options you leave at default.

You need to make one last face spacing for the hub. Look closer on figure below if you wonder what the hub on this model may be. The hub needs to have a “Minimum Edge Length” of 1 and a maximum one of 4.

When you make mesh grids for other objects you will have to choose your own dimensions. If the lengths are too small the time a computation will take could be enormous, so the trick here is to have a mesh that is fine enough so it gives you accurate results, but not so detailed that a calculation will take a week. It is always smart to start with a small grid and end up with a large number of nodes, then work your way towards fewer nodes with the help of larger mesh sizes. ANSYS will tell you when the mesh sizes are too large because you will get fault messages like “overlapping geometry” when mesh or the geometry is inaccurate.

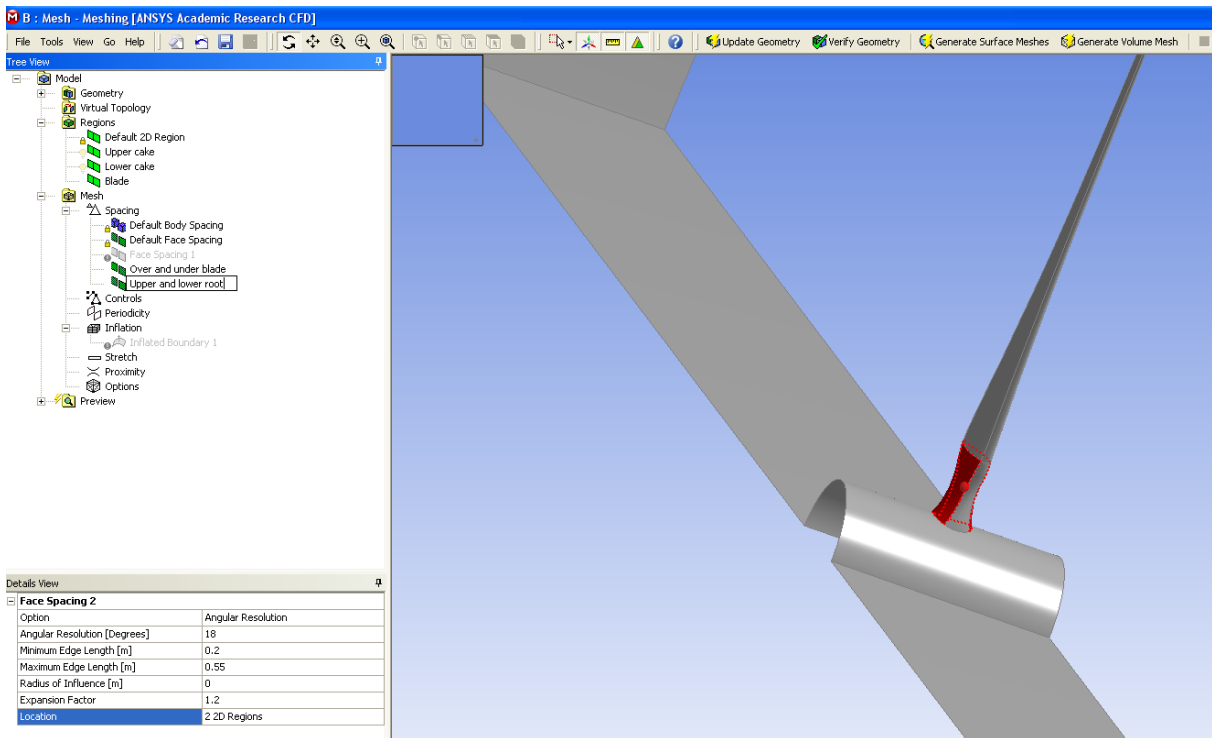


**Figure 15: How you work window when making face spacing for upper and lower side of blade.**

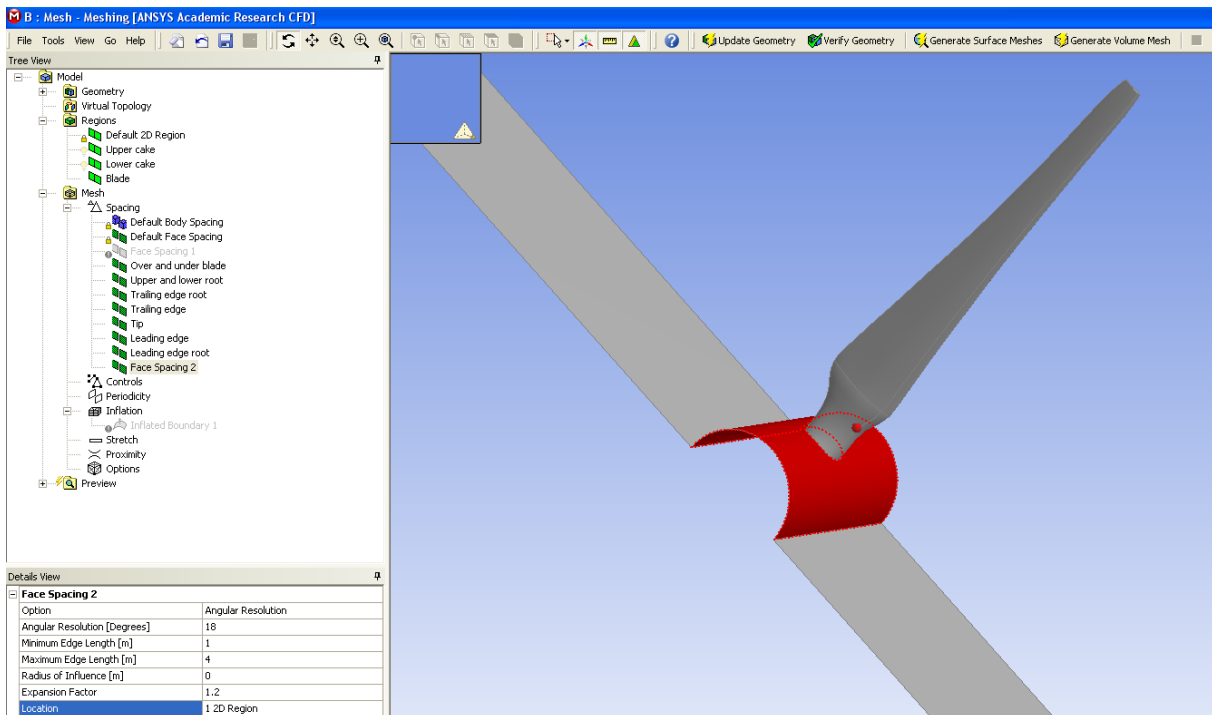


**Figure 16: The hub.**

You are now done with the face spacing. Edge spacing is the next step. Right click on “Spacing”, then “Insert” followed by “Edge spacing”. Set the “Constant Edge Length” to 0.005, the “Radius of Influence” to 0, the “Expansion Factor” to 1.2. Apply this to the two leading edge lines and the two trailing edge lines.

### A.2.6. Inflation

Next step is to use a function called inflation. This is a layer function that you use to create a web of grid points which internal length between the layers will augment exponentially. “Inflation” you only use close to areas of special interests where you know there will be a lot of fluid motion. You find the function in the “Tree View”, right click on this option, choose “insert”, “Inflated Boundary” and then mark all nine sections of the blade and press “Apply”. Now click on “Inflation” with your left mouse button, you will now see a list in the “Details View” in the lower left corner of your screen. Change the number of inflated layers to 10, change the expansion factor to 1.4 and the minimum internal angle should be 15 degrees. Click on “Inflation Option” and choose “First layer Thickness” in the box “Option”. “Define First Layer By” will need to have “First Prism Height” behind it. It should be 0.007 m high. Leave the rest of the options as default. Now, look at the “Tree View”, click on “Stretch” and change the stretch factor in z direction to 0.3, leave the rest in default mode.

The last step you need to execute before you can let the computer make the surface mesh is to change some settings in the “Default Face Spacing” option in the “Tree view” menu. Click on “Default Face Spacing” and in “Details View” change the “Minimum Edge Length” to 0.02 and the “Maximum Edge Length” to 12.

Now you are ready to start “Generate Surface Mesh”, press this option in the upper toolbar. This operation might take everything from 5 minutes to 20 minutes depending on how powerful your computer is and if the mesh is approved or not. If the surface mesh is okay, which it should be if every step in this tutorial has been followed to the point, you can try to generate a volume mesh, this might take everything from 15 minutes to 1 hour or so. This function you will also find in the upper toolbar.

### A.2.7. Meshing the tunnel

The tunnel we are about to mesh we use because we want to see the wake after the turbine. This part of the model set up will give you valuable training in how to use multiple objects in CFX and how they interact with each other, so it would be wise to also perform this task.

Go to the “Workbench”, from the “Toolbox” you drag “Mesh” over to the “Project Schematic”. Now you right click on the second option on the newly added box in “Project Schematic” and find the ProE file of the object you want to upload, then right click on the “Mesh” option and choose edit. The “Meshing” window will now be opened. You should see your object in the large “Graphics” window. You might want to change the name of your newly added “Workbench” box so the computer program does not confuse the two Mesh boxes on your “Project Schematic”.

### A.2.8. Sweep

An important difference in meshing of this tunnel compared to the cake is that we are going to use a “Sweep” method of meshing instead of a “CFX-mesh”. To make this change in the program you need to go to the newly opened ANSYS window and look at your “Tree view”, click on “Mesh” or “CFX-mesh”, whichever works, and the lower left window should now contain an option which you can change from “CFX-MESH” to “Sweep”.

### A.2.9. Edge sizing

Now you will add something called “edge sizing”. Right click on the “Mesh” option in the upper left window, now called “Outline”, choose “Insert”, then “Sizing”. In the upper toolbar in the middle there will be an option called “Edge”, choose this. Mark the two long sides of the tunnel. In the lower left window called “Details” you now have to do some adjustment. First press the “Geometry” option and click on “Apply”. Then change the option “Type” to “Number of Divisions”, then below that option, you need to change the “Number of Divisions” to 210. The “Behavior” needs to be “Soft”, the “Bias type” needs for these edges to be small in the middle and long at the edges and finally the “Bias factor” needs to be 15. The edges you have marked should now have yellow small figures on them, see figure 15.

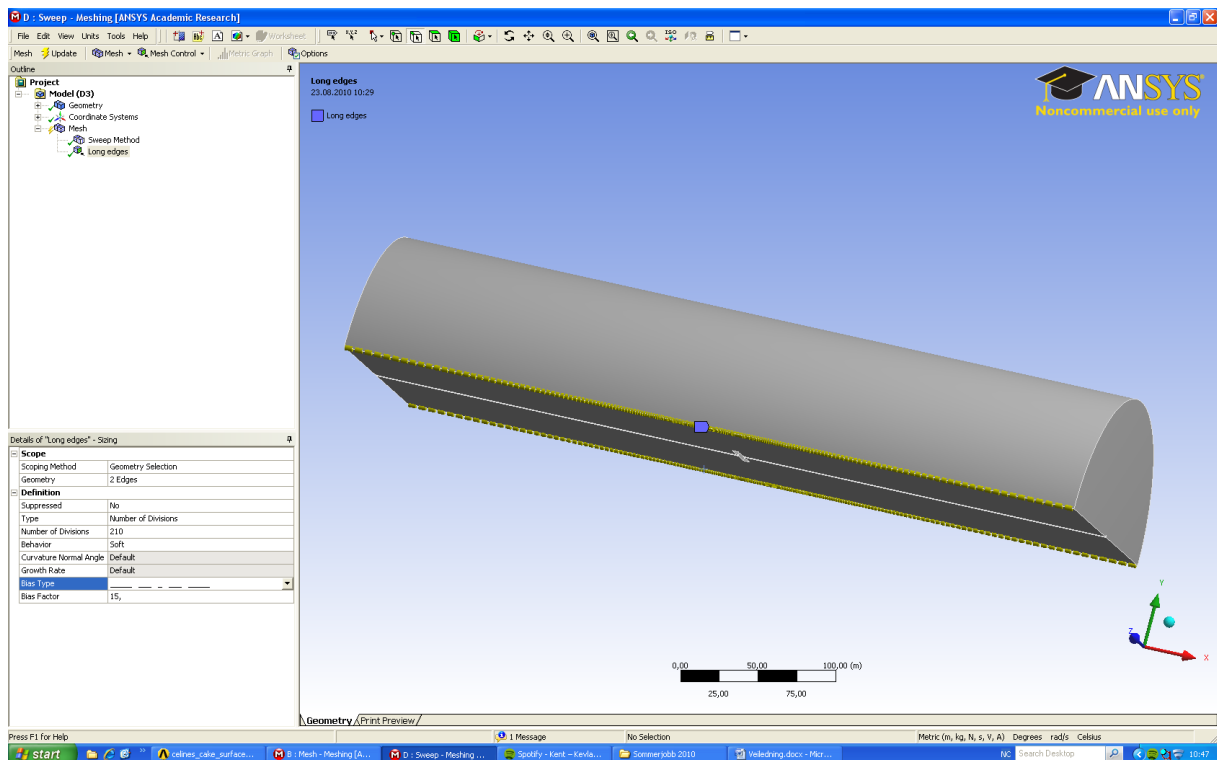


**Figure 17: Edge sizing**

Mark the two edges at each end of the tunnel, in total 4 edges. Here the “Number of Divisions” should be 30 and the “Bias Type” should be the second option “short-short-longer-long”. Set the “Bias factor” to 10.

On figure 18 you see what part I call “Short end of inner cake”, mark both ends. Here you use a number of divisions of 10 and no bias.

For the long sides of the inner cake you use a number of divisions of 15, with a bias factor of 7 and a bias type of short – short – longer – long. When I say long sides of inner cake I do not mean the curved sides, only the base lines. For the long edges of the inner side of the tunnel you use a number of divisions of 100, with a bias type as the one before and a bias factor of 15. Do the same on the other side of the carved out cake. You should now have made edge boundaries for all edges on the bottom of the tunnel, when you now press on “Update” in the

upper toolbar, the “Sweep” function previously chosen will mesh the entire tunnel based upon the edge boundaries you have made.

For mesh parameters used in the thesis for case 1, the 10 MW offshore wind turbine blade, and case 3, the 1 MW tidal turbine see chapter 7.

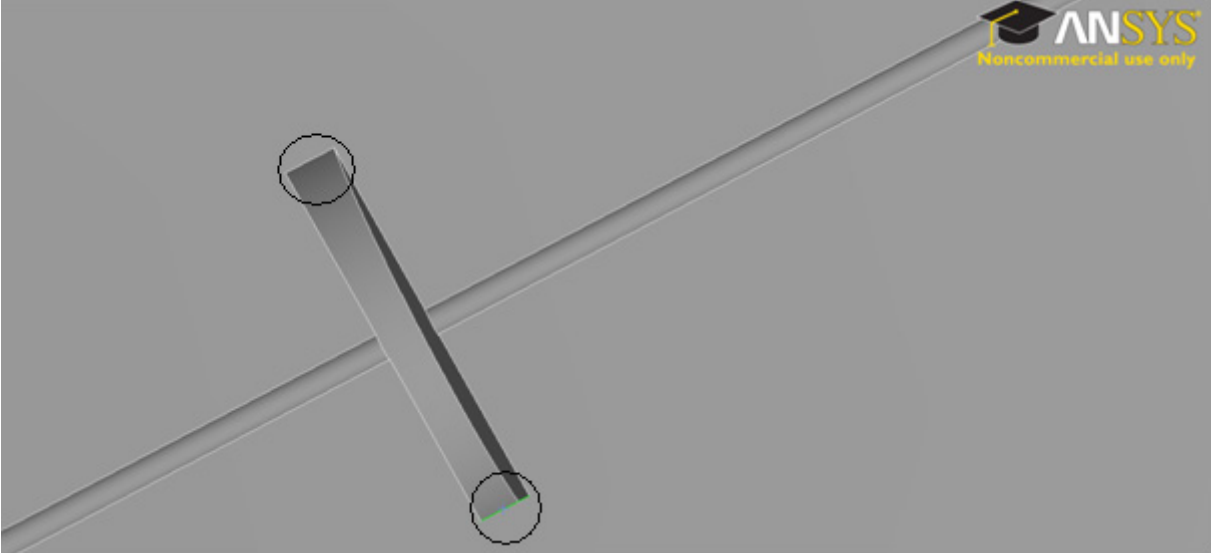


Figure 18: Depth of inner cake

A.2.10. CFX Pre

We have now meshed all the objects we need, the next step is to set some basic settings for the environment we want the objects to experience. Go to the Workbench in ANSYS and drag a CFX function from the left menu called “Component Systems” to the “Project Schematic”. You now need to link the two meshes of the tunnel and cake to the new box, see figure 19 for how it should look like.

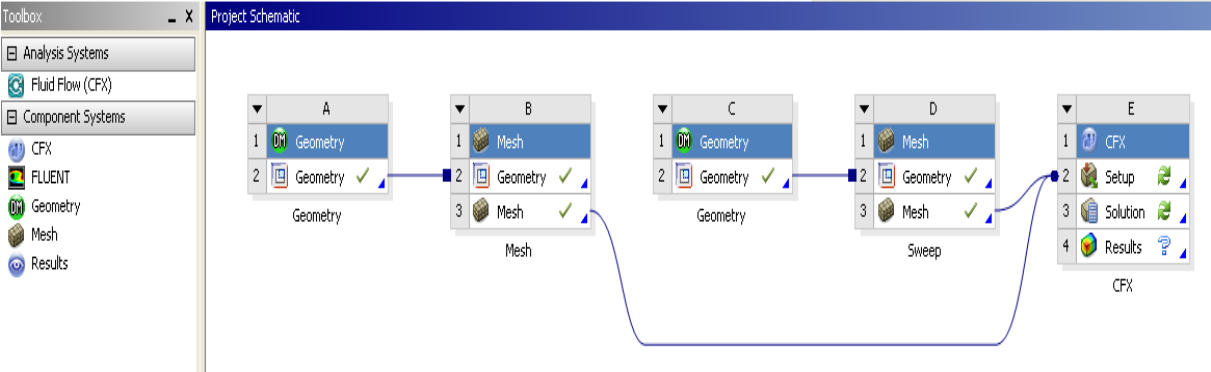


Figure 19: Project Schematic including CFX Pre

Double click on the setup option in the new box. A new window will open and you will see your tunnel and the cake. Your cake is much larger than it should be; this is because it was made too large on purpose in ProE, this to make the meshing easier. You need to scale the cake and probably twist it in some direction so it fits the tunnel. Right click on “SYS.cmdb” and choose transform mesh, a window will be opened in which you will choose twist



direction and scaling factor. You can measure the width of the cake and that of the tunnel in ProE. The cake should be 10 times bigger than it's supposed to be. Play around with the settings in order to make the cake fit the tunnel.

#### **A.2.11. Rotor Domain – tidal turbin**

The tunnel and the cake is one domain, you need to create a new domain in order to separate the cake from the tunnel. You do this by clicking on the blue box in the upper toolbar, if you hold the mouse over it, a small box stating that you are looking at the “Domain” function will appear. Call the new domain the “Rotor”. A menu resembling figure 20 on the next page will appear on the left of your screen.

In this new menu, click on “Basic Settings” then you need to change the “Location”, choose the cake inside the tunnel. “Domain type” is “Fluid Domain”. Change the “Material” to “Water”. The “Reference Pressure” needs to be 2.8 atm, which resembles the depth of the tidal turbine. Change the “Buoyancy” to “Non Buoyant”. The “Domain Motion” needs to be stationary for 25 iterations and then we will make the further calculations run with rotating rotor. CFX has trouble starting iterations with a rotating rotor, that is why we first do some calculations in a static rotor. Leave the rest of the settings in “Basic settings” as default.

Now click on “Fluid Models”, change the “Turbulence” to “Shear Stress Transport” and have no heat transfer, leave the rest as default. Click on “Initialization”, here you only need to change “Turbulence” to “Medium Intensity and Eddy Viscosity Ratio”. Click on “Apply” and “Close”.

#### **A.2.12. Rotor Domain – wind turbine**

Much the same settings as for the tidal turbine except inlet velocity, turbulence intensity and pressure as in case 3, but in case 1 these settings are 13.014 m/s, 7.4% and 1 atm respectively.

#### **A.2.13. Stator Domain – tidal turbine**

Make a new domain and call it “Stator”, choose the tunnel as its location. In “Basic settings” use the same settings as for the rotor, except in “Initialization”, set the speed in U-direction to -2.5 m/s. Otherwise use the same settings as for the “Rotor” Press “Apply” and “Close”.

#### **A.2.14. Stator domain – wind turbine**

Inlet speed of 13.014 m/s and turbulence intensity og 7.4%

#### **A.2.15. Inlet and Outlet**

Now click on the object to the right of “Domain” in the upper toolbar and create a “Boundary”. Create it in the Stator and choose the inlet of the large tunnel, i.e. the underside of the wing, as its location. In “Boundary Details” choose a speed of 2.5 m/s. Create a new boundary at the outlet. In “Boundary Details” the “Mass and Momentum” option needs to be “Total Pressure (stable)” with a 0 Pa “Relative Pressure”, “Flow Direction” should be “Normal to Boundary Condition”, the “Turbulence” should be set to “Medium (Intensity = 5%)”. Press “Apply” and “Close”.

Because the rotor will at some point in the calculation be rotating, you need to set a coordinate frame. Right click on “Coordinate Frames”, choose “Insert” and then “Coordinate Frame”. Look at “Basic Settings”, choose “Axis Points” in the “Option” frame. The “Origin” needs to be [0, 0, 0], the “z-axis” should be [0, 0, 1] and finally the “x-z Plane” should be [1, 0, 0]. Press “Apply” and “Close”.

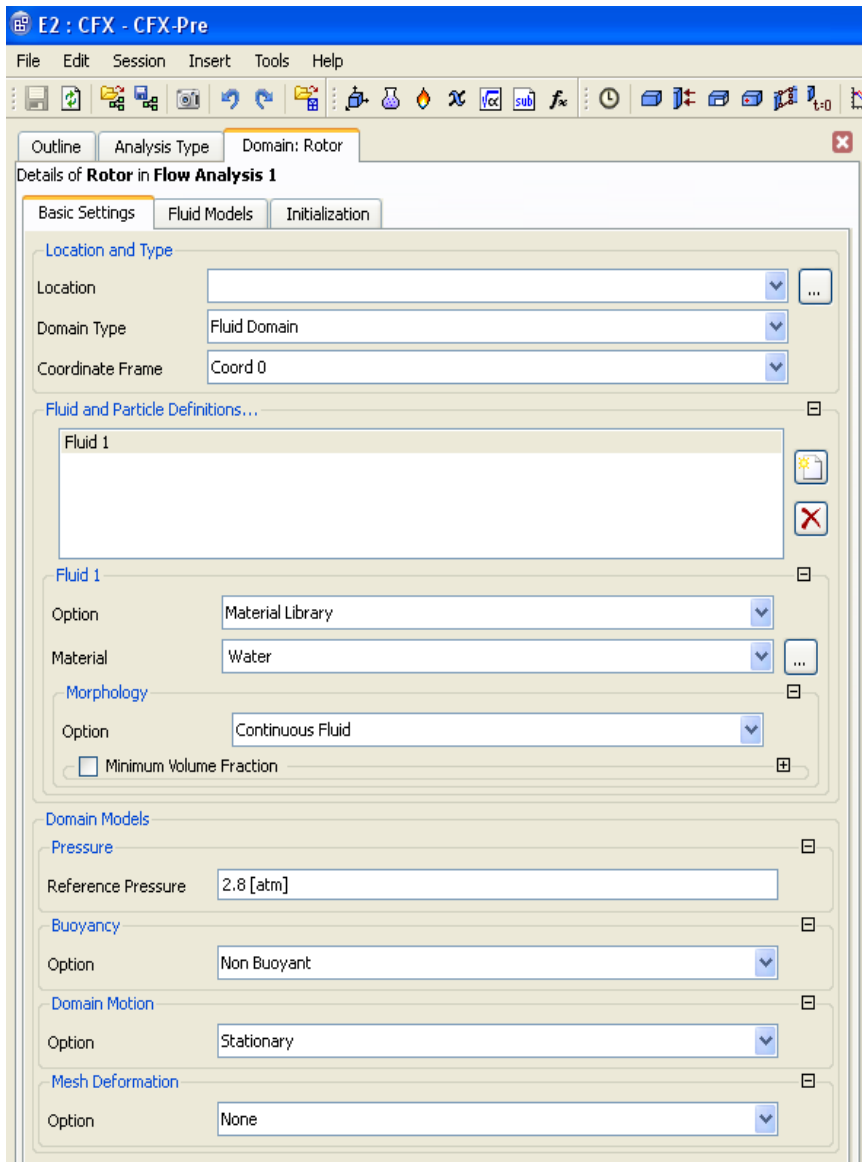


**Figure 20: Menu to left of the screen when you have created a new domain.**

### A.2.16. Domain Interface

Now click on “Domain interface” on the upper toolbar, call it “Front Part”. “Interface Side 1” should be the Rotor and “Interface Side 2” should be the Stator. In “Region List” the interfaces needs to have the same sides, namely the back of the cake. For the Stator use “F156.139” as the “Region list” and for the Rotor use “Front”. These numbers in the “Region List” will most likely not fit with the numbers you get up on your screen. The general idea

here is that one face or side of the tunnel should correspond to the correct face or side of the cake. As “Interface Models” you set it to “General connection”. The “Frame Change/Mixing Model” at this stage set to “None”. The first time you run the calculations you will run the program without a rotating Rotor for the first 25 iterations. Then you will run the simulations with a “Frozen Rotor”. Create a second “Domain Interface” for the back. Same “Basic Settings” but for the Stator use “F158.139” in the “Region list” and “Back” for the Rotor. Leave the rest of the options as default. You need one last interface for “Ryggen” to you cake, call it “Rygg”. “Interface Side 1” needs “Domain – Rotor” and the “Region List” as F304.218. For “Interface Side 2” you need the “Domain (Filter)” to be “Stator” and “Region List” F157.139.

### A.2.17. Periodicity, only in the rotational run

You need to add two domain interfaces you call “Periodicity Rotor” and “Periodicity Stator”. Because you only have a cake of  $180^{\circ}$ , if you do not add these domains the fluid will act as if it hits a wall when it has done a rotation of  $180^{\circ}$  i.e. comes to bottom end of the cake. With this function you allow the fluid that is pushed down in one end by the blade, come up through the other side of the cake.

Click on “Domain Interface” on the upper toolbar, call it “Periodicity Rotor”. “Interface Side 1” needs to be the Rotor, the “Region List” should be one of the cakes bottom sides, in this example case it should be “F290.218”. For side 2 you choose Rotor and “F295.218” as the other side of the bottom of the cake. For the “Interface Models” use “Rotational Periodicity” and “rotor.1” for the “Rotation Axis”.

Do the same for the “Periodicity Stator”, but choose Stator for the interface sides and “F177.139” and “F173.139” for the “Region Lists”. For the “Interface Models” use “Rotational Periodicity” and “rotor.1” for the “Rotation Axis”.

### A.2.18. The run

#### Without rotation

Now find “Solver Control”, right click on this and let the “Min. Iterations” be 1 and the “Max. Iterations” be 25. For “Timescale control” use “Local Timescale Factor” and set the factor to 5. Use a “Residual Target” of 0.00001. Leave the rest of the options as default.

Now, right click on “Rotor” in the “Outline” menu to the left. Go into “Basic Settings” and make sure the “Coordinate Frame” is the “Rotor”. In the “Initialization” let it “Velocity Type” be “Cylindrical”. The “Rotor Default” contains all the surfaces you don't use anywhere else. Here, you need “Free Slip Wall” as a condition in “Boundary Details”, but when the run with rotation starts you need this option to say “Smooth Wall”.

Go to “Stator”, you need to have the same “Coordinate Frame” as “Rotor Default”, that is “Rotor”. In the “Initialization” you need -2.5 m/s in the U-direction, this because of how the coordinate system is orientated. In the Stator you need the “Fluid Models” to have “Isothermal” as the “Heat Transfer” and have a temperature of 10 degrees.

Refresh the box in workbench where you have the CFX mesh and open the solver and press the "Run" button. This might take 1 hour or so.

If something happens and the simulation stops, you will find a “ \*.out file ” in the directory where you have told ANSYS to save your work that will tell what went wrong. The filename could look something like this, “...your\_work\_files\dpo\CFX\CFX\CFX\_002.out”.

### **With rotation**

Go to the Workbench and duplicate the CFX component of the steady flow conditions. Call this new component “Transient”. Make connections between the geometry boxes and the new “Transient” CFX box. Click on “Solution” in the “Steady flow” box which is already there and drag, while holding mouse button down, it over to “Solution” in the “Transient” box. When you run the new CFX it will

use the older CFX runs as initial boundaries for the new run. Go into the setup of this new box and change the “Domain Motion” of the Rotor to “Rotating”. Set the angular velocity to 15.9 rev/min. Change the “Mixing Model” of the “Back Part” to “Frozen Rotor”, do this for “Front” and “Rygg” also. In “Rotor Default” changes the “Mass And Momentum” to “No Slip Wall” with “Smooth Wall” as the “Wall Roughness”. Do the same for “Stator Default”. In both Rotor and Stator you need to change the rotation axis to “rotor.1”. Refresh the box in workbench where you have the CFX mesh and open the solver and press the "Run" button. This might take up to 10 hours depending on you're the computational power available.

### **A.2.19. Post Processing**

For Post-Processing I encourage you to go the homepage of ANSYS and do some of their tutorials on Post-Processing CFX results. How you Post-Process these results will depend entirely on what you want to investigate.

### A.3. Appendix Different formulas used in the thesis

$$\text{chord}(\text{position}) \cdot \sqrt{(\omega \cdot r)^2 + U_\infty^2} \cdot \frac{1}{V_{kin}} = \text{Re} \quad (2.1)$$

Equation (3.1) is the equation used in order to find the Reynolds numbers at different lengths of the blades given in Figure 37.

=areaAve(Yplus)@User Surface 30m , a “User Surface” was made by boundary intersection of the blade at x meters. This equation gives us the  $y^+$  value at 30 m of the blade.

=atan(areaAve(Velocity v)@Alpha 30m /areaAve(Velocity u)@Alpha 30m ) = angle of attack, alpha 30 m is the “Plane” function in CFX post. This just to have a point just before the wing in order to have a reference when calculating the angle of attack.